AD-A166 419 MAGNETO-OPTIC STUDIES OF SEMICONDUCTOR STRUCTURES AT HYDROSTATIC PRESSURE..(U) AIR FORCE INST OF TECH WRIGHT-PATTERSON AFB OH H ACKERMANN DEC 85 1/2

UNCLASSIFIED AFIT/CI/NR-86-25D F/G 20/12 NL

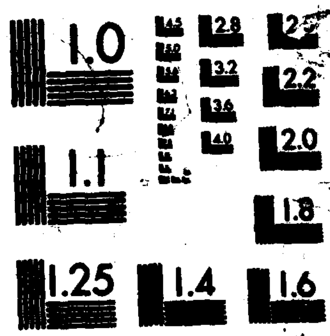

MICROCOP' CHART

SECURITY CLASSIFICATION OF THIS PAGE (When Data Entered)

REPORT DOCUMENTATION PAGE		READ INSTRUCTIONS BEFORE COMPLETING FORM
1. REPORT NUMBER AFIT/CI/NR-86-25D	2. GOVT ACCESSION NO.	3. RECIPIENT'S CATALOG NUMBER
4. TITLE (and Subtitle) Magneto-Optic Studies of Semiconductors Structures At hydrostatic Pressure and Low Temperature		5. TYPE OF REPORT & PERIOD COVERED ~~THESIS~~/DISSERTATION
		6. PERFORMING ORG. REPORT NUMBER
7. AUTHOR(s) Harro Ackermann		8. CONTRACT OR GRANT NUMBER(s)
9. PERFORMING ORGANIZATION NAME AND ADDRESS AFIT STUDENT AT: University of New Mexico		10. PROGRAM ELEMENT, PROJECT, TASK AREA & WORK UNIT NUMBERS
11. CONTROLLING OFFICE NAME AND ADDRESS AFIT/NR WPAFB OH 45433-6583		12. REPORT DATE 1985
		13. NUMBER OF PAGES 128
14. MONITORING AGENCY NAME & ADDRESS(if different from Controlling Office)		15. SECURITY CLASS. (of this report) UNCLASS
		15a. DECLASSIFICATION/DOWNGRADING SCHEDULE

16. DISTRIBUTION STATEMENT (of this Report)

APPROVED FOR PUBLIC RELEASE; DISTRIBUTION UNLIMITED

17. DISTRIBUTION STATEMENT (of the abstract entered in Block 20, if different from Report)

18. SUPPLEMENTARY NOTES

APPROVED FOR PUBLIC RELEASE: IAW AFR 190-1

Lynn Wolaver 22 April 86

LYNN E. WOLAVER
Dean for Research and Professional Development
AFIT/NR, WPAFB OH 45433-6583

19. KEY WORDS (Continue on reverse side if necessary and identify by block number)

20. ABSTRACT (Continue on reverse side if necessary and identify by block number)

DTIC
ELECTE
APR 0 9 1986
S D
D

AD-A166 419

DTIC FILE COPY

DD FORM 1 JAN 73 1473 EDITION OF 1 NOV 65 IS OBSOLETE

SECURITY CLASSIFICATION OF THIS PAGE (When Data Entered)

25

MAGNETO-OPTIC STUDIES OF SEMICONDUCTOR STRUCTURES AT HYDROSTATIC PRESSURE AND LOW TEMPERATURE

Harro Ackermann
B.S., Physics, University of Missouri at Rolla, 1966
M.S., Physics, Air Force Institute of Technology, 1977
Ph.D., Optical Sciences, University of New Mexico, 1985

We developed an unique experimental system to perform optical investigations of semiconductor materials in environments generally beyond the capability of other techniques. Using the solid helium pressure generating method and a superconducting magnet, we performed laser induced luminescence studies on a variety of structures at low temperature ($\leq$ 4K), high hydrostatic pressure, and high magnetic field. A quartz fiber was utilized to provide an optical path to and from a sample subjected to values of the external parameters. The use of the fiber alleviated the need for pressure chamber windows and concern for the transmissivity of the pressure medium, and allowed investigations over a frequency range limited only by the optical properties of the fiber.

Our investigation concentrated on the effects of hydrostatic pressure and magnetic field on strained layer superlattices, specifically on $In_xGa_{1-x}As$ / GaAs structures. In these structures the value of x, the

fraction of In present, affects the amount of lattice mismatch. If the layers are sufficiently thin, the mismatch is accomodated by strain and does not result in dislocations. The biaxial components of the strain remove the degeneracy of the valence band, resulting, in effect, in a simple band situation.

This interpretation was corroborated by our magneto-optic data which showed that the Landau level energies followed the well known relation, and yielded a value for the hole effective mass of $m_h^* \approx 0.16m_0$. This value was consistent with the results obtained from magneto-resistance measurements ($0.13 - 0.17m_0$) and indicated a conduction band to light hole band transition. The data also yielded values for the bandgap energy and, with the application of hydrostatic pressure, the pressure coefficient was determined to be ~12.2 meV/kbar, in good agreement with the values reported for III-V materials in general (~12 ± 2 meV/kbar). The pressure dependence of the reduced effective mass in this sample was found to be 1.2%/kbar, comparing favorably with the calculated value of 0.8%/kbar.

FOLD DOWN ON OUTSIDE - SEAL WITH TAPE

AFIT/NR
WRIGHT-PATTERSON AFB OH 45433

OFFICIAL BUSINESS
PENALTY FOR PRIVATE USE, $300

NO POSTAGE
NECESSARY
IF MAILED
IN THE
UNITED STATES

BUSINESS REPLY MAIL
FIRST CLASS PERMIT NO. 73236 WASHINGTON D.C.

POSTAGE WILL BE PAID BY ADDRESSEE

AFIT/ DAA
Wright-Patterson AFB OH 45433

FOLD IN

AFIT RESEARCH ASSESSMENT

The purpose of this questionnaire is to ascertain the value and/or contribution of research accomplished by students or faculty of the Air Force Institute of Technology (AU). It would be greatly appreciated if you would complete the following questionnaire and return it to:

AFIT/NR
Wright-Patterson AFB OH 45433

RESEARCH TITLE: ____

____

AUTHOR: ____

RESEARCH ASSESSMENT QUESTIONS:

1. Did this research contribute to a current Air Force project?

( ) a. YES ( ) b. NO

2. Do you believe this research topic is significant enough that it would have been researched (or contracted) by your organization or another agency if AFIT had not?

( ) a. YES ( ) b. NO

3. The benefits of AFIT research can often be expressed by the equivalent value that your agency achieved/received by virtue of AFIT performing the research. Can you estimate what this research would have cost if it had been accomplished under contract or if it had been done in-house in terms of manpower and/or dollars?

( ) a. MAN-YEARS __________ ( ) b. $__________

4. Often it is not possible to attach equivalent dollar values to research, although the results of the research may, in fact, be important. Whether or not you were able to establish an equivalent value for this research (3. above), what is your estimate of its significance?

( ) a. HIGHLY SIGNIFICANT ( ) b. SIGNIFICANT ( ) c. SLIGHTLY SIGNIFICANT ( ) d. OF NO SIGNIFICANCE

5. AFIT welcomes any further comments you may have on the above questions, or any additional details concerning the current application, future potential, or other value of this research. Please use the bottom part of this questionnaire for your statement(s).

____

NAME GRADE POSITION

____

ORGANIZATION LOCATION

STATEMENT(s):

25

THE UNIVERSITY OF NEW MEXICO
OFFICE OF GRADUATE STUDIES
ALBUQUERQUE, NEW MEXICO 87131

December 16, 1985
Date of Completion

CERTIFICATE OF COMPLETION

For

HARRO ACKERMANN

This is to certify that the above candidate completed all requirements for the doctoral degree in

PHYSICS
OPTICAL SCIENCES

at

THE UNIVERSITY OF NEW MEXICO

on the above date. With the approval of the Faculty and the Regents, the degree will be conferred December 21, 1985.

Decmeber 20, 1985
Date

107 Humanities Building Telephone 505: 277-2711

25

MAGNETO-OPTIC STUDIES OF SEMICONDUCTOR STRUCTURES AT HYDROSTATIC PRESSURE AND LOW TEMPERATURE

BY

HARRO ACKERMANN

B.S., University of Missouri at Rolla, 1966

M.S., Air Force Institute of Technology, 1977

DISSERTATION

Submitted in Partial Fulfillment of the
Requirements for the Degree of

Doctor of Philosophy in Optical Sciences

The University of New Mexico
Albuquerque, New Mexico

December, 1985

ACKNOWLEDGMENTS

As in many endeavors of this nature, the assistance of various organizations and individuals contributed to its completion. The support I received from the United States Air Force, the University of New Mexico, and Sandia National Laboratory is gratefully acknowledged.

I am indebted to the many individuals who helped me by providing encouragement, advice, and technical direction throughout this effort. Foremost among these is Dr. Eric Jones in whose laboratory I had the privilege to work and who became my mentor and friend. Dr. James Schirber was always available for discussions and provided critical technical guidance during times of experimental difficulties. The chairman of the committee, Dr. Marlan Scully, without whom this project would not have been completed, was an inspiration when the problems seemed insurmountable. Drs. Kevin Cahill and Kenneth Jungling provided welcome encouragement from the beginning.

I received excellent technical assistance from Mr. Gregory Wickstrom and appreciate his efforts in supporting the experiment.

MAGNETO-OPTICS STUDIES OF SEMICONDUCTOR STRUCTURES AT HYDROSTATIC PRESSURE AND LOW TEMPERATURE

BY

HARRO ACKERMANN

ABSTRACT OF DISSERTATION

Submitted in Partial Fulfillment of the
Requirements for the Degree of

Doctor of Philosophy in Optical Sciences

The University of New Mexico
Albuquerque, New Mexico

December, 1985

MAGNETO-OPTIC STUDIES OF SEMICONDUCTOR STRUCTURES AT HYDROSTATIC PRESSURE AND LOW TEMPERATURE

Harro Ackermann
B.S., Physics, University of Missouri at Rolla, 1966
M.S., Physics, Air Force Institute of Technology, 1977
Ph.D., Optical Sciences, University of New Mexico, 1985

We developed an unique experimental system to perform optical investigations of semiconductor materials in environments generally beyond the capability of other techniques. Using the solid helium pressure generating method and a superconducting magnet, we performed laser induced luminescence studies on a variety of structures at low temperature ($\leq$ 4K), high hydrostatic pressure, and high magnetic field. A quartz fiber was utilized to provide an optical path to and from a sample subjected to values of the external parameters. The use of the fiber alleviated the need for pressure chamber windows and concern for the transmissivity of the pressure medium, and allowed investigations over a frequency range limited only by the optical properties of the fiber.

Our investigation concentrated on the effects of hydrostatic pressure and magnetic field on strained layer superlattices, specifically on $In_xGa_{1-x}As$ / GaAs structures. In these structures the value of x, the

fraction of In present, affects the amount of lattice mismatch. If the layers are sufficiently thin, the mismatch is accomodated by strain and does not result in dislocations. The biaxial components of the strain remove the degeneracy of the valence band, resulting, in effect, in a simple band situation.

This interpretation was corroborated by our magneto-optic data which showed that the Landau level energies followed the well known relation, and yielded a value for the hole effective mass of $m_h^* \approx 0.16m_0$. This value was consistent with the results obtained from magneto-resistance measurements ($0.13 - 0.17m_0$) and indicated a conduction band to light hole band .. ansition. The data also yielded values for the bandgap energy and, with the application of hydrostatic pressure, the pressure coefficient was determined to be ~12.2 meV/kbar, in good agreement with the values reported for III-V materials in general (~12 ± 2 meV/kbar). The pressure dependence of the reduced effective mass in this sample was found to be 1.2%/kbar, comparing favorably with the calculated value of 0.8%/kbar.

CONTENTS

LIST OF FIGURES

I. INTRODUCTION

Experiments involving the variation of external parameters, e.g. pressure, temperature, magnetic field, have long been used to determine optical properties of solids. We have developed a method allowing the simultaneous low-temperature optical investigation of hydrostatic pressure and magnetic field effects on semiconductor materials, while avoiding many of the problems usually associated with experiments of this type. By attaching the sample directly to an optical fiber, we are able to illuminate the sample without having to be concerned with pressure chamber and Dewar windows, or with the transmissivity of the pressure medium. The luminescence signal from the sample returns through the same fiber and is processed. This method differs from more standard pressure experiments where hydrostatic pressure is usually applied by immersing the sample in a compressing medium -gas, liquid, or soft solid- and optical access to the sample is through this medium and a window. The physical properties of the medium and window limit the range of pressure, temperature, and frequency at which optical information can be obtained. The application of pressure to a semiconductor alters the lattice spacing and changes the energy levels, increasing or decreasing the energy gap

depending on material. Since the electronic properties of semiconductors depend strongly on the band structure and the value of the forbidden gap, marked effects are expected when pressure is applied. In zincblende compounds, for example, the direct gap increases with pressure, although GaAs, beyond a certain pressure, becomes an indirect gap material.

Subjecting a semiconductor to a magnetic field causes periodic carrier motion in the transverse direction and results in quantized orbits. This raises the bottom of the conduction band and lowers the top of the valence band for positive effective masses. This quantization of energy in the transverse direction changes the density of states from its zero-field parabolic configuration to discrete (sub) bands, or Landau levels.

The semiconductor samples we investigated were quantum well and superlattice structures. The term superlattice is applied to a periodic heterostructure of, in this experiment, Group III-V materials. These structures are grown by a process known as molecular beam epitaxy, which allows accurate control of layer width and composition. Thus, as the number of layers gets large, a band-like condition analogous to the Kronig-Penney one-dimensional crystal is approached. This impresses a periodic potential on the structure that is considerably larger than atomic

dimensions. Since the bandgap of the barrier can be significantly larger than the gap of the well material, the forbidden gap between the valence and conduction band edges will exhibit a step at each interface.

For barriers of sufficient height and width, an electronic carrier can be considered as confined to a three-dimensional potential well. If the width of the well is much smaller than the other dimensions, then particle motion in that direction is quantized, as opposed to the unquantized motion in the transverse directions. Thus, in the heterostructure, eigenvalues for bound states can be found. If barrier thickness however is reduced to the point that carriers can penetrate the barriers, then the coupled - well superlattice regime is reached. When the wells are brought together, an interaction between the degenerate band states occurs, causing a splitting of the the well levels. This splitting is a function of barrier height and width.

In direct-gap materials band-to-band transitions between states of the same k-value conserve momentum and result in a spectrum given by $L(\nu)=K(h\nu - E_0)^{1/2}$, where K is a constant depending on the reduced effective mass. Emission therefore has a low-energy threshold at $h\nu = E_0$ and a high energy tail. In addition to the band-band transitions, electron-hole pairs,

or excitons, may also contribute to the emission spectrum. Excitonic spectra are characterized by an energy below E_0 and a narrow linewidth.

In Section II we develop the **k**·**p** method (bold face symbols denote vectors, except $\hbar \equiv h/2\pi$) and expressions for the energy values of the bands at Γ for the face centered cubic lattice. These expressions are used in Section III to determine the direct absorption coefficient in the <100> direction. We also discuss the matrix elements and constants and address the exciton contribution to the absorption coefficient.

In Section IV, the effect of hydrostatic pressure is discussed and the absorption coefficient is modified to include the pressure dependence. The magnetic field effects are discussed in Section V and expressions yielding the Landau levels and also exciton effects are presented.

The experimental configuration and method are described in Section VI, along with some of the samples used, and results are presented in Section VII. Concluding remarks are contained in Section VIII.

II. THE k · p METHOD

The **k** · **p** method provides a powerful tool for investigating the band structure of semiconductors near high symmetry points in **k**-space. Its advantage lies in the fact that, by use of the symmetry properties of the crystal, the band structure at a point k depends only on a few parameters which may be determined experimentally. An early use of the method was to find an expression for the effective mass and to develop the "f-sum" rule.[1] Subsequent development included the extension to degenerate bands[2] and consideration of spin-orbit interaction.[3-5] Although the **k**·**p** method allows calculation of band structure throughout the Brillouin zone, it is most readily applied at selected symmetry points. The configuration of the empty lattice is developed and shown in Appendix A.

In order to develop the theory of the **k** · **p** method, we start with the one-electron Hartree Hamiltonian,

$$\mathcal{H}\,\Psi(\mathbf{r}) = [(-\hbar^2/2m)\,\nabla^2 + U(\mathbf{r})]\,\Psi(\mathbf{r}) = \epsilon\,\Psi(\mathbf{r}), \tag{1}$$

where U(r) represents a periodic potential. The eigenfunctions of the Schroedinger equation are Bloch functions and may be written as

$$\Psi_{n\mathbf{k}}(r) = e^{i\mathbf{k}\cdot\mathbf{r}}\,u_{n\mathbf{k}}(\mathbf{r}), \tag{2}$$

where n represents the band index, $u_{nk}(r)$ has the periodicity of the potential $U(r)$, and k lies in the first Brillouin zone.

Substituting Eq. (2) into Eq. (1) and performing the indicated operation, we obtain

$$[(-\hbar^2/2m)\nabla^2 + U(r)]e^{ik\cdot r}u_{nk}(r) = \epsilon_n(k)e^{ik\cdot r}u_{nk}(r), \tag{3}$$

or,

$$\mathcal{H}_k u_{nk}(r)=[(p^2/2m)+(\hbar/m)(k\cdot p)+(\hbar^2k^2/2m)+U(r)]u_{nk}(r) = \epsilon_n(k)u_{nk}(r). \tag{4}$$

Introducing k_0, we can rewrite Eq. (4) for a symmetry point,

$$[(p^2/2m) + (\hbar/m)(k + k_0 - k_0)\cdot p + (\hbar^2/2m)(k^2+k_0{}^2-k_0{}^2) + U(r)]u_{nk}(r)$$
$$= \epsilon_n(k)u_{nk}(r),$$

and separating,

$$[(p^2/2m) + (\hbar/m)(k_0\cdot p) + (\hbar^2k_0{}^2/2m) + U(r) + (\hbar/m)(k-k_0)\cdot p$$
$$+(\hbar^2/2m)(k^2 - k_0{}^2)]u_{nk}(r) = \epsilon_n(k)u_{nk}(r).$$

We now define $\mathcal{H}_{k_0} \equiv (p^2/2m) + (\hbar/m)(k_0\cdot p) + (\hbar^2k_0{}^2/2m) + U(r)$, and, since $\mathcal{H}_{k_0}u_{nk}(r) = \epsilon_n(k_0)u_{nk}(r)$, we have

$$[\mathcal{H}_{k_0} + (\hbar/m)(k-k_0)\cdot p + (\hbar^2/2m)(k^2-k_0^2)]u_{nk}(r) = \epsilon_n(k)u_{nk}(r). \quad (5)$$

Writing the wavefunction for any k in terms of k_0,

$$u_{nk}(r) = \sum_{n'} A_{nn'}(k-k_0)u_{n'k}(r), \quad (6)$$

and multiplying both sides of Eq. (5) by $u^*_{nk_0}(r)$ and then integrating over the unit cell, we get

$$\sum_{n'}\int_{\Omega_0} u^*_{nk_0}(r)[\mathcal{H}_{k_0} + (\hbar/m)(k-k_0)\cdot p + (\hbar^2/2m)(k^2-k_0^2)]A_{nn'}(k-k_0)$$

$$\times u_{n'k_0}(r)dr = \sum_{n'}\int_{\Omega_0} u^*_{nk_0}(r)E_n(k)A_{nn'}(k-k_0)u_{n'k_0}(r)dr$$

$$= \epsilon_n(k)A_{nn'}(k-k_0). \quad (7)$$

Performing the indicated operations results in

$$\sum_{n'}\epsilon_n(k_0)\delta_{nn'}A_{nn'}(k-k_0)+\sum_{n'}(\hbar^2/2m)(k^2-k_0^2)\delta_{nn'}A_{nn'}(k-k_0)$$

$$+\sum_{n'}\int_{\Omega_0}(\hbar/m)(k-k_0)\cdot u^*_{nk}(r)pu_{nk}(r)A_{nn'}(k-k_0)dr = \epsilon_n(k)A_{nn'}(k-k_0) \quad (8)$$

Rearranging and defining $p_{nn'}(k_0) \equiv \int_{\Omega_0} u^*_{nk_0}(r)pu_{nk_0}(r)dr$,

we obtain

$$\sum_{n'}\{[\epsilon_n(k_0) + (\hbar^2/2m)(k^2 - k_0^2)]\delta_{nn'} + (\hbar/m)(k - k_0)\cdot p_{nn'}(k_0)\}A_{nn'}(k - k_0)$$

$$= \epsilon_n(k)A_{nn'}(k - k_0). \qquad (9)$$

Equation (9) is the eigenvalue equation in the k_0 representation for the point k. This system of equations can be solved if the determinant is equal to zero. For example, in the case of a simple band, index n, second order perturbation theory yields

$$\epsilon_n(k) = \epsilon_n(k_0) + (\hbar^2/2m)(k^2 - k_0^2) + (\hbar/m)(k - k_0)\cdot p_{nn'}(k_0)$$

$$+ (\hbar/m)^2\sum_{n\neq n'}[(k - k_0)\cdot p_{nn'}(k_0)\,(k - k_0)\cdot p_{n'n}(k_0)]/[\epsilon_n(k_0) - \epsilon_{n'}(k_0)] \qquad (10)$$

As a further example, two strongly interacting non-degenerate bands result in the matrix

$$\begin{bmatrix} \epsilon_n(k_0) + (\hbar^2/2m)(k^2 - k_0^2) - \epsilon_n(k) & (\hbar/m)(k - k_0)\cdot p_{n'n}(k_0) \\ (\hbar/m)(k - k_0)\cdot p_{nn'}(k_0) & \epsilon_n(k_0) + (\hbar^2/2m)(k^2 - k_0^2) - \epsilon_n(k) \end{bmatrix} = 0, \qquad (11)$$

which is readily solved for $\epsilon_n(k)$.

The extension of the $k \cdot p$ method to degenerate bands is developed below. We assume an s-fold degeneracy at k = 0. The set of functions

$u_{10}(r)$, $u_{20}(r)$, $u_{30}(r)$,...., $u_{s0}(r)$ satisfying $\mathcal{H}_0 u_{j0}(r) = \epsilon_0 u_{j0}(r)$, where $\mathcal{H}_0 = (p^2/2m) + U(r)$, the unperturbed Hamiltonian, belong to the same energy ϵ_0. The k p method can be used to find the eigenfunctions, $u_{jk}(r)$, and eigenvalues, $\epsilon_j(k)$, for points $k \neq 0$. As a zeroth order approximation we let

$$u_{jk}(r) = \sum^{s}_{j=1} A_j(k) u_{j0}(r). \tag{12}$$

Substituting Eq. (12) into Eq. (5) and proceeding as before, i.e. multiplying by $u^*_{j'0}(r)$ and integrating over the unit cell, we have

$$\sum_j \int_{\Omega_0} u^*_{j'0}(r) \mathcal{H}_{k_0} A_j(k) u_{j0}(r) dr + \sum_j \int_{\Omega_0} u^*_{j'0}(r)(\hbar/m)(k - k_0)\cdot p A_j(k) u_{j0}(r) dr$$

$$+ \sum_j \int_{\Omega_0} u^*_{j'0}(r)(\hbar^2/2m)(k^2 - k_0^2) A_j(k) u_{j0}(r) dr$$

$$= \sum_j \int_{\Omega_0} u^*_{j'0}(r) \epsilon_j(k) A_j(k) u_{j0}(r) dr. \tag{13}$$

Upon separating the second and third terms and integrating, we obtain the following expression

$$\sum_j \epsilon_{j'}(k_0)A_j(k)\delta_{jj'} + \sum_j(\hbar/m)(k\cdot p_{jj'})A_j(k) - \sum_j(\hbar/m)(k_0\cdot p_{jj'})A_j(k) +$$

$$\sum_j(\hbar^2k^2/2m)A_j(k)\delta_{jj'} - \sum_j(\hbar^2k_0^2/2m)A_j(k)\delta_{jj'} = \epsilon_{j'}(k)A_j(k). \qquad (14)$$

Rearranging Eq. (14),

$$\sum_j[\epsilon_{j'}(k_0)\delta_{jj'} - (\hbar^2k_0^2/2m)\delta_{jj'} - (\hbar/m)(k_0\cdot p_{jj'})]A_j(k)$$

$$+ \sum_j[(\hbar^2k^2/2m)\delta_{jj'} + (\hbar/m)(k\cdot p_{jj'})]A_j(k) = \epsilon_{j'}(k)A_j(k). \qquad (15)$$

The bracketed [ ] term of the first summation in Eq. (15) is defined as ϵ_0. We can then write

$$\sum^s{}_{j=1} \{(\hbar/m)(k\cdot p_{jj'}) - [\epsilon_{j'}(k) - \epsilon_0 - (\hbar^2k^2/2m)]\delta_{jj'}\}A_j(k) = 0,$$

or simplifying further,

$$\sum^s{}_{j=1} [(\hbar/m)(k\cdot p_{jj'}) - E'(k)\delta_{jj'}]A_j(k) = 0, \qquad (16)$$

where $E'(k) \equiv \epsilon_{j'}(k) - \epsilon_0 - (\hbar^2k^2/2m)$, and solutions are obtained when the determinant of the system of equations (order s) is equal to zero.

If this approximation yields zero, it becomes necessary to go to the next order approximation. This is accomplished by including in the zeroth approximation not only the functions of the degenerate band, but also others at $k = 0$. Using, therefore,

$$u_k(r) = \sum^{s}_{j=1} A_j(k)u_{j0}(r) + \sum^{\infty}_{i\neq j} A_i(k)u_{j0}(r), \qquad (17)$$

and proceeding as before we get, for second order perturbation,

$$\sum^{s}_{j'=1} [(\hbar^2/m^2)\sum_i(k\cdot p_{ji})(k\cdot p_{ij'})/(\epsilon_0 - \epsilon_i) - E''(k)\delta_{jj'}]A_{j'}(k) = 0, \qquad (18)$$

where $E''(k) = \epsilon''(k) - \epsilon_0 - (\hbar^2k^2/2m)$, and $\epsilon(k) = \epsilon_0 + \epsilon''(k)$. Solutions again are obtained when the dzterminant of the system of equations is equal to zero.

As an illustrative example we determine the perturbation matrix $D^{\alpha\beta}_{jj'}$ for a crystal of cubic symmetry with the edges of the cube oriented along the x, y, z axes. We have,

$$\sum^{s}_{j=1} [D^{\alpha\beta}_{jj'} k_\alpha k_\beta - \epsilon(k)\delta_{jj'}]A_{j'}(k) = 0, \qquad (19)$$

where $$D^{\alpha\beta}_{jj'} \equiv (\hbar^2/2m)\delta_{jj'}\delta_{\alpha\beta} + (\hbar/m)^2\sum_i p^{\alpha}_{ji} p^{\beta}_{ij'}/(\epsilon_0 - \epsilon i), \qquad (20)$$

with α, β = x, y, z and ϵ_0 the origin of energy. We let the functions Φ_1, Φ_2, Φ_3 form the basis of representation Γ_{15} for k = 0, which transforms under the elements of the point group of the cube as $\Phi_1 \sim xf(r)$, $\Phi_2 \sim yf(r)$, and $\Phi_3 \sim zf(r)$.

Then, $D^{xx}_{jj'} \equiv (\hbar^2/2m)\delta_{jj'} + (\hbar/m)^2\sum_i p^x_{ji} p^x_{ij'}/(\epsilon_0 - \epsilon i)$, and

$$D^{xy}_{jj'} \equiv (\hbar/m)^2 \sum_i p^x_{ji}\, p^y_{ij'} / (\epsilon_0 - \epsilon_i),$$

and similarly for other combinations of x, y, z. The matrix elements of perturbation energy are thus given by

$$\langle\Phi_j \,|\, \mathcal{H}_{k\cdot p} \,|\, \Phi_{j'}\rangle = (\hbar/m)^2 \sum_i [\langle j \,|\, k\cdot p \,|\, i\rangle\langle i \,|\, k\cdot p \,|\, j'\rangle] / (\epsilon_0 - \epsilon_i), \quad (21)$$

where j, j' = 1, 2, 3, and i ranges over all other bands.

If we let $\epsilon_i \approx \epsilon_l$, a constant, then from completeness of the set Φ, we can write

$$\langle j \,|\, \mathcal{H}_{k\cdot p} \,|\, j'\rangle = (\hbar/m)^2 [\langle j \,|\, (k\cdot p)^2 \,|\, j'\rangle] / (\epsilon_0 - \epsilon_l). \quad (22)$$

Using $(k\cdot p)^2 = \hbar^2[k^2_x(\partial^2/\partial x^2) + k^2_y(\partial^2/\partial y^2) + k^2_z(\partial^2/\partial z^2) + k_x k_y(\partial^2/\partial x\partial y) + \ldots]$, and $r = (x^2 + y^2 + z^2)^{1/2}$, the elements of the matrix may be determined one by one:

$$\langle 1 \,|\, (k.p)^2 \,|\, 1\rangle \sim k^2_x \int x f(r)(\partial^2/\partial x^2)[x f(r)]dr$$

$$+ k^2_y \int x f(r)(\partial^2/\partial y^2)[x f(r)]dr + \ldots \quad (23)$$

Upon performing the operations indicated, we find that the coefficients of $k_i k_j$ ($i \neq j$) are odd functions and thus integrate to zero. We are left with

$$D_{11} = (\hbar^2 k^2{}_x/2m) + (\hbar/m)^2 k^2{}_x \sum_i [\langle 1|p_x|i\rangle\langle i|p_x|1\rangle]/(\epsilon_0 - \epsilon_1)$$

$$+(\hbar^2/2m)(k^2{}_y + k^2{}_z) + (\hbar/m)^2(k^2{}_y + k^2{}_z)\sum_i [\langle 1|p_y|i\rangle\langle i|p_y|1\rangle]/(\epsilon_0 - \epsilon_1) .$$

Expressions of similar form are obtained for D_{22} and D_{33}. As examples of off-diagonal elements we will look at D_{12} and D_{13}.

$$\langle 1|(k\cdot p)^2|2\rangle \sim k^2{}_x \int x f(r)(\partial^2/\partial x^2)[y f(r)]dr$$

$$+ k^2{}_y \int x f(r)(\partial^2/\partial y^2)[y f(r)]dr + \ldots].$$

In this case we find that the coefficients of $k^2{}_i$ integrate to zero, as well as the coefficients of $k_x k_z$ and $k_y k_z$, leaving

$$D_{12} = (\hbar/m)^2 k_x k_y \sum_i [\langle 1|p_x|i\rangle\langle i|p_y|2\rangle]/(\epsilon_0 - \epsilon_1)$$

$$+ (\hbar/m)^2 k_x k_y \sum_i [\langle 1|p_y|i\rangle\langle i|p_x|2\rangle]/(\epsilon_0 - \epsilon_1).$$

For D_{13} the result is

$$D_{13} = (\hbar/m)^2 k_x k_z \sum_i [\langle 1|p_x|i\rangle\langle i|p_z|3\rangle]/(\epsilon_0 - \epsilon_1)$$

$$+ (\hbar/m)^2 k_x k_z \sum_i [\langle 1|p_z|i\rangle\langle i|p_x|3\rangle]/(\epsilon_0 - \epsilon_1).$$

The corresponding summations in the above two expressions are equal due to symmetry. The remaining elements are easily found, resulting in the

interaction matrix D,

$$D = \begin{bmatrix} Lk_x^2 + M(k_y^2 + k_z^2) & Nk_xk_y & Nk_xk_z \\ Nk_xk_y & Lk_y^2 + M(k_x^2 + k_z^2) & Nk_yk_z \\ Nk_xk_z & Nk_yk_z & Lk_z^2 + M(k_x^2 + k_y^2) \end{bmatrix}. \quad (24)$$

with $L \equiv (\hbar^2/2m) + (\hbar/m)^2\sum_i[\langle 1|p_x|i\rangle\langle i|p_x|1\rangle]/(\epsilon_0 - \epsilon_i)$

$$M \equiv (\hbar^2/2m) + (\hbar/m)^2\sum_i[\langle 1|p_y|i\rangle\langle i|p_y|1\rangle]/(\epsilon_0 - \epsilon_i)$$

$$N \equiv (\hbar/m)^2\sum_i[\langle 1|p_x|i\rangle\langle i|p_y|2\rangle + \langle 1|p_y|i\rangle\langle i|p_x|2\rangle]/(\epsilon_0 - \epsilon_i).$$

If we now include, for the zincblende structure, in the set of strongly interacting bands, the s-like conduction band (Γ_1) and the p-like valence band (Γ_{15}), we have four bands coupled by the momentum matrix element

$$P_M \equiv -i(\hbar/m)\langle S|p_i|X_i\rangle, \quad (25)$$

where X_i = X, Y, Z.

The matrix can then be written as

$$
D = \begin{array}{c} S \\ X \\ \\ Y \\ \\ Z \\ \\ \end{array}
\begin{bmatrix}
A'k^2+\epsilon_c+(\hbar^2k^2/2m) & Bk_yk_z+iP_Mk_x & Bk_xk_z+iP_Mk_y & Bk_xk_y+iP_Mk_z \\
Bk_yk_z-iP_Mk_x & L'k^2_x+M(k^2_y+k^2_z) & N'k_xk_y & N'k_xk_z \\
 & +\epsilon_v+(\hbar^2k^2/2m) & & \\
Bk_xk_z-iP_Mk_y & N'k_xk_y & L'k^2_y+M(k^2_x+k^2_z) & N'k_yk_z \\
 & & +\epsilon_v+(\hbar^2k^2/2m) & \\
Bk_xk_y-iP_Mk_z & N'k_xk_z & N'k_yk_z & L'k^2_z+M(k^2_x+k^2_y) \\
 & & & \epsilon_v+(\hbar^2k^2/2m)
\end{bmatrix} \quad (26)
$$

The coefficients are defined as follows:

$$A' = (\hbar/m)^2\sum_i{}^{\Gamma_{15}}|\langle S|p_x|u_i\rangle|^2/(\epsilon_c-\epsilon_i)$$

$$B = 2(\hbar/m)^2\sum_i{}^{\Gamma_{15}}\langle S|p_x|u_i\rangle\langle u_i|p_y|z\rangle/[(1/2)(\epsilon_c-\epsilon_i)-\epsilon_i]$$

$$L' = (\hbar/m)^2\sum_i{}^{\Gamma_1}|\langle X|p_x|u_i\rangle|^2/(\epsilon_v-\epsilon_i)$$

$$+(\hbar/m)^2\sum_i{}^{\Gamma_{12}}|\langle X|p_x|ui\rangle|^2/(\epsilon_v-\epsilon_i) = F' + 2G$$

$$M = (\hbar/m)^2\sum_i{}^{\Gamma_{15}}|\langle X|p_y|u_i\rangle|^2/(\epsilon_v-\epsilon_i)$$

$$+(\hbar/m)^2\sum_i{}^{\Gamma_{25}}|\langle X|p_y|u_i\rangle|^2/(\epsilon_v-\epsilon_i)$$

$$N' = (\hbar/m)^2\sum_i^{\Gamma_1}|\langle X|p_x|u_i\rangle|^2/(\epsilon_v-\epsilon_i)$$

$$-(1/2)(\hbar/m)^2\sum_i^{\Gamma_{12}}|\langle X|p_x|u_i\rangle|^2/(\epsilon_v-\epsilon_i)$$

$$+(\hbar/m)\sum_i^{\Gamma_{15}}|\langle X|p_y|u_i\rangle|^2/(\epsilon_v-\epsilon_i)$$

$$-(\hbar/m)^2\sum_i^{\Gamma_{25}}|\langle X|p_y|u_i\rangle|^2/(\epsilon_v-\epsilon_i).$$

$$= F' - G + H_1 - H_2$$

In each case the summation over i goes over higher bands of symmetry type shown above the summation sign. The conduction band (Γ_1 symmetry) and the valence band (Γ_{15} symmetry) interact strongly. Weak interactions with other bands, according to Loewdin perturbation theory, affecting coefficients L', M, N', lead to renormalized interactions between the bands of the strongly interacting set.

The matrix of Eq. (26) can be simplified. If we limit ourselves to very small values of k and use Loewdin perturbation theory between the single conduction band and the three valence bands, we have, considering the interaction P_M as a perturbation,

$$D = \begin{array}{c} S \\ X \\ Y \\ Z \end{array} \begin{bmatrix} Ak^2 + \epsilon_C & 0 & 0 & 0 \\ 0 & Lk^2_x + M(k^2_y + k^2_z) + \epsilon_v & Nk_xk_y & Nk_xk_z \\ 0 & Nk_xk_y & Lk^2_y + M(k^2_x + k^2_z) + \epsilon_v & Nk_xk_z \\ 0 & Nk_xk_z & Nk_yk_z & Lk^2_z + M(k^2_x + k^2_y) + \epsilon_v \end{bmatrix}. \quad (27)$$

where the coefficients are now defined as

$$A \equiv (\hbar/m)^2 \sum_i{}^{\Gamma_{15}} |\langle S|p_x|u_i\rangle|^2/(\epsilon_{C0}-\epsilon_i) + P^2/(\epsilon_{C0}-\epsilon_{V0})$$

$$L \equiv (\hbar/m)^2 \sum_i{}^{\Gamma_1} |\langle X|p_x|u_i\rangle|^2/(\epsilon_{V0}-\epsilon_i) + P^2/(\epsilon_{V0}-\epsilon_i)$$

$$+(\hbar/m)^2 \sum_i{}^{\Gamma_{12}} |\langle X|p_x|u_i\rangle|^2/(\epsilon_{V0}-\epsilon_i)$$

$M \equiv$ as before

$$N \equiv (\hbar/m)^2 \sum_i{}^{\Gamma_1} |\langle X|p_x|u_i\rangle|^2/(\epsilon_{V0}-\epsilon_i) + P^2/(\epsilon_{V0}-\epsilon_i)$$

$$-(\hbar/m)^2 \sum_i{}^{\Gamma_{12}} |\langle X|p_x|u_i\rangle|^2/(\epsilon_{V0}-\epsilon_i) + (\hbar/m)^2 \sum_i{}^{\Gamma_{15}} |\langle X|p_y|u_i\rangle|^2/(\epsilon_{V0}-\epsilon_i)$$

$$-(\hbar/m)^2 \sum_i{}^{\Gamma_{25}} |\langle X|p_y|u_i\rangle|^2/(\epsilon_{V0}-\epsilon_i).$$

Until this point the effect of spin has not been considered. The spin-orbit Hamiltonian is,[6]

$$\mathcal{H}_{SO} = \hbar/4m^2c^2(\nabla U \times \mathbf{p}) \cdot \sigma, \quad (28)$$

where σ represents the Pauli spin operator. Thus the total Hamiltonian becomes

$$\mathcal{H}_{total} = \mathcal{H}_{k \cdot p} + \mathcal{H}_{so}.$$

Including $\mathcal{H}_{so}$, as given by Eq. (28), in Eq. (3),

$$[(\hbar^2/2m)\nabla^2 + U(r) + (\hbar/4m^2c^2)(\nabla U(r)\times p)\cdot \sigma]u_k(r)e^{ik\cdot r} = \epsilon_k u_k(r)e^{ik\cdot r}, \quad (29)$$

or, using $p \equiv -i\hbar(\partial/\partial r)$,

$$[p^2/2m + (\hbar/m)(k\cdot p) + \hbar^2k^2/2m + U(r)]u_k(r)$$

$$+(\hbar/4m^2c^2)(\nabla U(r)\times p)\cdot\sigma u_k(r) + (\hbar^2/4m^2c^2)(\nabla U(r)\times k)\cdot \sigma u_k(r) = \epsilon_k u_k(r) \quad (30)$$

Equation (30) can be rewritten in the k_0 representation by following the steps leading to Eq. (5). This yields

$$[p^2/2m+(\hbar/m)(k_0\cdot p)+\hbar^2k_0^2/2m+U(r)+(\hbar/m)(k-k_0)\cdot p+(\hbar^2/2m)(k^2-k_0^2)$$

$$+(\hbar/4m^2c^2)[\nabla U(r)\times p]\cdot \sigma + (\hbar^2/4m^2c^2)(\nabla U(r)\times k)\cdot \sigma] = \epsilon_n(k)u_{nk}(r) \quad (31)$$

or, $[\mathcal{H}_{k_0}+(\hbar/m)(k-k_0)\cdot p+(\hbar^2/2m)(k^2-k_0^2)+(\hbar/4m^2c^2)(\nabla U(r)\times p)\cdot \sigma$

$$+ (\hbar^2/4m^2c^2)(\nabla U(r)\times k)\cdot\sigma]u_{nk}(r) = \epsilon_n(k)u_{nk}(r), \quad (32)$$

where $\mathcal{H}_{k_0} \equiv p^2/2m + (\hbar/m)(k_0\cdot p) + \hbar^2k^2/2m + U(r)$. Defining

$u_{nk}(r) = \sum_{n'} C_{nn'}(k-k_0) u_{n'k_0}(r)$, and substituting this expression into Eq. (32), and, as before, multiplying both sides by $u^*_{nk_0}(r)$ and integrating over the unit cell, we obtain

$$\sum_{n'}\{[\epsilon_n(k_0) + (\hbar^2/2m)(k^2-k_0^2)]\delta_{nn'} + (\hbar/m)(k-k_0)\cdot p_{nn'}$$

$$+(\hbar/4m^2c^2)(\nabla U(r)\times p)\cdot \sigma + (\hbar^2/4m^2c^2)(\nabla U(r)\times k)\cdot \sigma\}C_{nn'} = \epsilon_n(k)C_{nn'}. \quad (33)$$

The addition of spin results in eight basis states. Hence we have an eighth order matrix and therefore an eighth order secular equation. Switching to a new set of basis states , the spin orbit Hamiltonian may be written in diagonal form. The states which diagonalize the spin-orbit Hamiltonian are those corresponding to $|j, m_j\rangle$ equal to $|3/2, 3/2\rangle$, $|3/2, 1/2\rangle$, and $|1/2, 1/2\rangle$[3].

Although two additional terms were introduced in the wave equation when spin was considered, only the k-independent term is kept since the crystal momentum is very much smaller than the electron momentum. The effect of spin-orbit splitting of the valence band (six-fold degenerate p-states) results in a four-fold degenerate set, Γ_8 for $j = 3/2$, and a two-fold degenerate set, Γ_7 for $j = 1/2$.

The eighth order secular equation may be solved numerically when the values of the unknown parameters are taken from experiment. In order to obtain analytic expressions, certain approximations must be made. For example, the $\mathbf{k}\cdot\mathbf{p}$ interaction matrix, Eq. (27), is accurate for small kinetic energies in the conduction and valence bands compared to ϵ_{gap}. Adding the spin-orbit interaction to this matrix, we obtain an 8×8 matrix composed of a 2×2 block corresponding to the conduction band, a 4×4 block which corresponds to the valence band (j=3/2), and a 2 × 2 block for the split-off band. Diagonalizing, one obtains[2]

$$E_C = \epsilon_{C0} + \hbar^2k^2/2m + A''k^2,$$

for the conduction band, and, with Δ_S representing the spin orbit splitting of the valence band and given by

$$\Delta_S = -(3i\hbar/4m^2c^2)\langle X|(\partial U(r)/\partial z)p_x - (\partial U(r)/\partial x)p_z|Z\rangle, \tag{34}$$

for the valence band

$$E_{V,3/2} = \epsilon_{V0} + \Delta_S/3 + \hbar^2k^2/2m + (L+2M)k^2/3$$

$$\pm\{(L-M)^2k^4 + (1/3)[N^2-(L-M)^2](k^2_xk^2_y + k^2_xk^2_z + k^2_yk^2_z)\}^{1/2} \tag{35}$$

$$E_{v,1/2} = \epsilon_{v0} - 2\Delta_s/3 + \hbar^2k^2/2m + (L''+2M)k^2/3,$$

where +(-) in $E_{v,3/2}$ refers to the light (heavy) hole band, and

$$A'' \equiv A' + P_M^2[2/3E_g + 1/3(E_g+\Delta_s)]$$

$$L'' \equiv F' + 2G - P_M^2/(E_g+\Delta_s),$$

with $E_g \equiv \epsilon_{c0}-(\epsilon_{v0} + \Delta_s)$, and the constants L, M, N, A', P_M, F', and G as defined earlier.

In the narrow-gap approximation, applicable to GaAs, the denominator of the constants G, H_1, and H_2 is much larger than the denominator of F, and the square root in the expression for $E_{v,3/2}$ can be expanded. Rewriting and neglecting terms of second order, we get,

$$E_{hh} \approx E_{v0}+\Delta_s/3+\hbar^2k^2/2m+Mk^2+(L-M-N)(k^2{}_xk^2{}_y+k^2{}_xk^2{}_z+k^2{}_yk^2{}_z)/k^2 \qquad (36)$$

$$E_{lh} \approx E_{v0}+\Delta_s/3+\hbar^2k^2/2m+(2L+M)k^2/3-(L-M-N)(k^2{}_xk^2{}_y+k^2{}_xk^2{}_z+k^2{}_yk^2{}_z)/k^2,$$

where the heavy hole band corresponds to the quantum number $m_j=\pm3/2$, and the light hole band to $m_j=\pm1/2$.

In this approximation where k was assumed to be small, the conduction and valence bands were treated according to Loewdin

perturbation theory for the $\mathbf{k}\cdot\mathbf{p}$ interaction, and with spin introduced, we obtain, for a small direct-gap material, the following expressions for the energies:

$$E_c \approx \epsilon_{c0} + \hbar^2k^2/2m + A'k^2 + P_M{}^2k^2[2/3E_g + 1/3(E_g+\Delta_s)]$$

$$E_{hh} \approx \epsilon_{v0} + \Delta_s/3 + \hbar^2k^2/2m + Mk^2 + (L-M-N)(k^2{}_x k^2{}_y + k^2{}_x k^2{}_z + k^2{}_y k^2{}_z)/k^2 \qquad (37)$$

$$E_{lh} \approx \epsilon_{v0} + \Delta_s/3 + \hbar^2k^2/2m + (2L+M)k^2/3 - (L-M-N)(k^2{}_x k^2{}_y + k^2{}_x k^2{}_z + k^2{}_y k^2{}_z)/k^2$$

$$E_{so} \approx \epsilon_{v0} - 2\Delta_s/3 + \hbar^2k^2/2m + (L+2M)k^2/3 + P_M{}^2k^2[1/3E_g - 1/3(E_g+\Delta_s)].$$

Since ϵ_{v0} represents the $k = 0$ valence band energy without spin-orbit energy, we replace $\epsilon_{v0} + \Delta_s/3$ by E_v, and $\epsilon_{v0} - 2\Delta_s/3$ by $E_v - \Delta_s$.

III. THE DIRECT ABSORPTION COEFFICIENT

A. <100> Direction

We considered the case of absorption in the <100> direction and also calculated the coefficient for the directionally averaged case. We used Eqs. (37) to calculate the joint density of states with E_c corresponding to E_f and E_{hh}, E_{lh}, E_{so} corresponding to E_i in Eq. (B-21). We first examined the heavy hole to conduction band transition. We have

$$J_{c,hh} = \int_{BZ} dk(2/8\pi^3)\delta\{E_g-\hbar\omega+A'k^2+[(2P_M{}^2/3E_g)+P_M{}^2/3(E_g+\Delta_s)]k^2-Mk^2$$
$$-(L-M-N)(k_x{}^2k_y{}^2+k_x{}^2k_z{}^2+k_y{}^2k_z{}^2)/k^2\},$$

or, in spherical coordinates,

$$J_{c,hh} = \int_{BZ}(2/8\pi^3)\delta\{E_g-\hbar\omega+[A'+(2P_M{}^2/3E_g)+P_M{}^2/3(E_g+\Delta_s)-M]k^2$$
$$-(L-M-N)k^2(\sin^4\theta\cos^2\theta\sin^2\Phi+\sin^2\theta\cos^2\theta)\}k^2\sin\theta dk d\theta d\Phi. \qquad (38)$$

In the <100> direction $\theta = (\pi/2)$, $\Phi = 0$, and Eq. (38) becomes

$$J_{c,hh} = (2/8\pi^3)\int_{BZ}\delta[A + Bk^2]k^2 dk d\theta d\Phi, \qquad (39)$$

where we defined $\qquad A \equiv E_g-\hbar\omega$

$$B = A' + (2P_M^2/3E_g) + P_M^2/3(E_g + \Delta_s) - M.$$

Letting $X = A + Bk^2$, then $dX = 2kBdk$, and integrating over θ and ϕ, we have

$$J_{c,hh} = (2/8\pi^3)(4\pi)\int \delta(X)k^2 dX/2kB,$$

or, substituting for k in terms of X,

$$J_{c,hh} = (2/8\pi^3)(4\pi)(1/2)\int \delta(X)(X-A)^{1/2}/B^{3/2}$$

$$= (2\pi^2)^{-1}B^{-3/2}(-A)^{1/2}. \qquad (40)$$

This result was substituted into Eq. (B-20), and yielded, for the <100> direction,

$$\alpha_{hh-c}(\omega) \approx (2e^2/ncm^2\omega)\,|\mathcal{H}'_{hh-c}|^2[A' + 2P_M^2/3E_g + P_M^2/3(E_g+\Delta_s) - M]^{-3/2}$$

$$\times (\hbar\omega - E_g)^{1/2} \qquad (41)$$

The same method, applied to the light hole-conduction band transition, resulted in

$$\alpha_{lh-c}(\omega) \approx (2e^2/ncm^2\omega)\,|\mathcal{H}'_{lh-c}|^2[A' + 2P_M^2/3E_g + P_M^2/3(E_g+\Delta_s)$$

$$-(2L+M)/3]^{-3/2} \times (\hbar\omega - E_g)^{1/2}, \qquad (42)$$

and, for the split-off to conduction band transition,

$$\alpha_{so-c}(\omega) \approx (2e^2/ncm^2\omega)\,|\mathcal{H}'_{so-c}|^2[A'+2P_M^2/3E_g-(L+2M)/3]^{-3/2}$$

$$\times(\hbar\omega-E_g-\Delta_s)^{1/2} \qquad (43)$$

Combining Eqs. (41)-(43) to account for the summation in Eq. (B-20), we have

$$<100>: \quad \alpha(\omega) = \alpha_{hh-c}(\omega) + \alpha_{lh-c}(\omega) + \alpha_{so-c}(\omega)$$

When the directional dependence, as appearing in Eq. (38), is isotropically averaged, the coefficient of the anisotropy term, (L-M-N), becomes 0.2, and the components of the averaged direct absorption coefficient are

$$\alpha_{hh-c}(\omega) \approx (2e^2/ncm^2\omega)\,|\mathcal{H}_{hh-c}|^2[A'+2P_M^2/3E_g+P_M^2/3(E_g+\Delta_s)$$

$$-M-0.2(L-M-N)]^{-3/2} \times (\hbar\omega-E_g)^{1/2} \qquad (44)$$

$$\alpha_{lh-c}(\omega) \approx (2e^2/ncm^2\omega)\,|\mathcal{H}_{lh-c}|^2\,[A'+2P_M^2/3E_g+P_M^2/3(E_g+\Delta_s)$$

$$-(2L+M)/3-0.2(L-M-N)]^{3/2} \times (\hbar\omega-E_g)^{1/2}. \qquad (45)$$

The contribution of the split-off band, being independent of direction, is still given by Eq. (43).

B. Matrix Elements and Constants

Examination of the expressions for $\alpha(\omega)$ shows that they contain the

following constants which were defined in Section II: A', L, M, N, P_M. They may be expressed in terms of the parameters ϵ_P, ϵ_Q, ϵ_R[7] for diamond structure materials, where $\epsilon_P \sim P^2$

$$\epsilon_Q \sim |\langle\Gamma_{15}|p|\Gamma'_{25}\rangle|^2$$

$$\epsilon_R \sim |\langle\Gamma'_{12}|p|\Gamma'_{25}\rangle|^2,$$

with Γ'_{25} representing the valence band. In terms of these parameters the numerical values of the matrix elements for Group IV materials are,

$$F = -\epsilon_P/E_g$$

$$M = -\epsilon_Q/[\epsilon(\Gamma_{15})-\epsilon(\Gamma'_{25})] \tag{46}$$

$$G = -\epsilon_R/[\epsilon(\Gamma'_{12})-\epsilon(\Gamma'_{25})].$$

For Group IV materials the values of ϵ_P, ϵ_Q, ϵ_R are:

$$\epsilon_P = 25.9 \text{ eV}, \quad \epsilon_Q = 17.2 \text{ eV}, \quad \epsilon_R = 14.2 \text{ eV}.$$

Equations (46) are transformed for the zincblende structure by including an anti-symmetric potential.[8] This results in Eqs. (47).

$$F = -\epsilon_P[\epsilon(\Gamma_{15_C})-\epsilon(\Gamma_{15_V})+\epsilon(\Gamma_{15})-\epsilon(\Gamma'_{25})]/2[\epsilon(\Gamma_{1_C})-\epsilon(\Gamma_{15_V})][\epsilon(\Gamma_{15_C})-\epsilon(\Gamma'_{25_V})]$$

$$M = -\epsilon_Q / [\epsilon(\Gamma_{15C}) - \epsilon(\Gamma_{15V})] \tag{47}$$

$$G = -\epsilon_R[\epsilon(\Gamma_{15C}) - \epsilon(\Gamma_{15V}) + \epsilon(\Gamma_{15}) - \epsilon(\Gamma'_{25})] / 2[\epsilon(\Gamma_{12\,C}) - \epsilon(\Gamma_{15V})][\epsilon(\Gamma_{15C}) - \epsilon(\Gamma_{15V})],$$

and, for the interaction between the Γ_{1C} conduction band and the higher Γ_{15C} state,

$$A' = -\epsilon P[\epsilon(\Gamma_{15C}) - \epsilon(\Gamma_{15V}) - \epsilon(\Gamma_{15}) + \epsilon(\Gamma'_{25})] / 2[\epsilon(\Gamma_{15\,C}) - \epsilon(\Gamma_{15V}) - Eg]$$

$$\times\ [\epsilon(\Gamma_{15C}) - \epsilon(\Gamma_{15V})] \tag{48}$$

In Eqs. (47) and (48), Γ with subscripts c, v refers to the Group III-V material, while Γ without the letter subscripts refers to the corresponding Group IV material. If the energy levels at Γ are known, e.g. from experiment, the constants can be calculated. Using the representative values[8] for Ge and GaAs (in eV),

Ge: $\epsilon(\Gamma'_{25}) = 0$, $\epsilon(\Gamma_{15}) = 2.8$, $\epsilon(\Gamma'_{12}) = 12$

GaAs: $\epsilon(\Gamma_{15V}) = 0$, $\epsilon(\Gamma_{1C}) = 1.5$, $\epsilon(\Gamma_{15C}) = 4.6$, $\epsilon(\Gamma_{12C}) = 12$,

then the values of the constants are

$F \approx -13.89$, $M \approx -3.74$, $G \approx -0.95$, $L \approx -15.79$, $N \approx -16.68$, $A' \approx -1.63$.

These results can can be checked quickly by using Eqs. (37) and calculating the effective masses. For the directionally averaged case ($T \to 0$) we have

$$m^*_c \approx 0.065m_0 \quad (0.067m_0)$$

$$m^*_{hh} \approx 0.551m_0 \quad (0.51m_0)$$

$$m^*_{lh} \approx 0.085m_0 \quad (0.082m_0)$$

$$m^*_{so} \approx 0.128m_0 \quad (0.154m_0).$$

Comparison values given in parenthesis are commonly accepted values derived from various experiments[9]. Reasonable agreement is evident. In evaluating the constants we intentionally limited ourselves to those interactions between bands as given in Eqs. (47) and (48), although contributions from higher bands exist. They are however much smaller due to larger separation, and thus are neglected.

C. Reduction of $\alpha(\omega)$ to Numerical Value

Using the calculated values of the constants, the expressions for $\alpha(\omega)$ in the various directions were simplified. Since the contribution of the split-off band has the same form regardless of direction, we began with it.

$$\alpha_{so-c}(\omega) \approx (2e^2/ncm^2\omega)\left|\mathcal{H}'_{so-c}\right|^2[A'+2P_M^2/3(E_g+\Delta_s)-(L+2M)/3]^{-3/2}$$

$$\times(\hbar\omega-E_g-\Delta_s)^{1/2}, \qquad (43)$$

where $\mathcal{H}' = \langle f|\varepsilon\cdot p|i\rangle = \varepsilon\cdot\langle f|p|i\rangle = \cos\Theta\langle f|p|i\rangle$. Θ represents the angle between the polarization vector and the dipole moment. Since we are concerned with transitions between the Γ_{15_V} (valence) band and the Γ_{1C} (conduction) band, we can relate the matrix element of $\mathcal{H}'$ to P_M, and hence to the parameter ϵ_P. $|\mathcal{H}'|^2 = \cos^2\Theta|\langle\Gamma_{1C}|p|\Gamma_{15_V}\rangle|^2$

$$= \cos^2\Theta\, m^2 P_M^2/\hbar^2 \qquad (49)$$

$$= \cos^2\Theta(m\epsilon_P/2).$$

Using the calculated values of the matrix elements appearing in Eq. (43) above, the mass term can be calculated,

$$[A'+2P_M^2/3(E_g+\Delta)-(L+2M)/3]^{-3/2} = (15.43)^{-3/2} = 0.0165. \qquad (50)$$

Substituting Eqs. (49) and (50) into Eq. (43), and remembering that the expression (50) is in terms of $\hbar^2/2m$, $\alpha_{so-c}(\omega)$ becomes

$$\alpha_{so-c}(\omega)\approx 0.0165(2^{3/2}e^2\epsilon_P\sqrt{m}/nc\hbar^3)\cos^2\Theta\,\omega^{-1}(\hbar\omega-E_g-\Delta_s)^{1/2}.$$

Checking dimensionality we get

$$\alpha_{so-c}(\omega) \sim [(E\times L)\times E\times\sqrt{E}/c]/[c\times(E^2\times t^2)\times\sqrt{E}] \rightarrow L^{-1}, \text{ as required.}$$

Then,

$$\alpha_{so-c}(\omega)\approx(0.0165)\{[2^{3/2}(4.8\times10^{-10})^2 25.9(1.6\times10^{-12})(9.1\times10^{-28})^{1/2}$$

$$(1.3\times10^{-6})/[3.4(3\times10^{10})(1.06\times10^{-27})^2 3(1.6\times10^{-12})]\}(\hbar\omega)^{-1}(\hbar\omega-E_g-\Delta_s)^{1/2},$$

where the average value of $\cos^2\Theta$ was taken as 1/3 and n, the refractive index, as 3.4. Performing the calculation yielded

$$\alpha_{so-c}(\omega)\approx(0.0165)(2.163\times10^6)(\hbar\omega)^{-1}(\hbar\omega-E_g-\Delta_s)^{1/2}. \quad (51)$$

Similarly we can write $\alpha_{hh-c}(\omega)$ and $\alpha_{lh-c}(\omega)$ for the direction considered:

$$\langle 100\rangle: \alpha_{hh-c}(\omega)\approx(0.0130)(2.163\times10^6)(\hbar\omega)^{-1}(\hbar\omega-E_g-\Delta_s)^{1/2}$$

$$\alpha_{lh-c}(\omega)\approx(0.0075)(2.163\times10^6)(\hbar\omega)^{-1}(\hbar\omega-E_g-\Delta_s)^{1/2} \quad (52)$$

$$\langle Avg\rangle: \alpha_{hh-c}(\omega)\approx(0.0140)(2.163\times10^6)(\hbar\omega)^{-1}(\hbar\omega-E_g-\Delta_s)^{1/2}$$

$$\alpha_{lh-c}(\omega)\approx(0.0071)(2.163\times10^6)(\hbar\omega)^{-1}(\hbar\omega-E_g-\Delta_s)^{1/2} \quad (53)$$

Appropriately combining Eqs (51) - (53) gives the expressions for the absorption coefficient for the selected directions in the crystal. This was done in Eq. (54).

$$\langle 100\rangle: \quad \alpha(\omega)\approx44342(\hbar\omega)^{-1}(\hbar\omega-E_g)^{1/2}+35960(\hbar\omega)^{-1}(\hbar\omega-E_g-\Delta_s)^{1/2}$$

$$\langle Avg\rangle: \quad \alpha(\omega)\approx45639(\hbar\omega)^{-1}(\hbar\omega-E_g)^{1/2}+35690(\hbar\omega)^{-1}(\hbar\omega-E_g-\Delta_s)^{1/2}. \quad (54)$$

Units of $\alpha(\omega)$ are cm^{-1}.

D. Exciton Contribution to $\alpha(\omega)$

Until this point the effect of excitons has not been considered in developing expressions for the absorption coefficient, hence designated $\alpha_0(\omega)$. $\alpha_0(\omega)$ was shown to equal zero for values of $\hbar\omega \leq E_g$, and increased as $(\hbar\omega)^{-1}(\hbar\omega - Eg)^{1/2}$ for $\hbar\omega > E_g$. Experimental evidence however suggests a more complicated relationship between the absorption coefficient and the incident light. Specifically, when, in the absorption process, an exciton is created,[10,11] the Coulomb interaction between the electron and hole can significantly affect the absorption coefficient, especially near the absorption edge. Applying Elliott's theory,[12] as developed for simple non-degenerate parabolic bands, to the more complicated case of GaAs, we find that the absorption coefficient for $\hbar\omega > E_g$ is modified by a factor $2\pi\gamma_x/[1-\exp(-2\pi\gamma_x)]$.[13,14] Thus, in the region of continuous absorption,

$$\alpha(\omega) \approx \alpha_0(\omega) \times 2\pi\gamma_x/[1-\exp(-2\pi\gamma_x)], \qquad (55)$$

where $\gamma_x = [R_{x1}/(\hbar\omega - Eg)]^{1/2}$, and the value of the exciton binding energy in GaAs is reported to be in the range $R_{x1} \approx 4.2 - 4.4$ meV.[15]

Equation (55) clearly shows that the exciton effect near $\hbar\omega \approx E_g$ is significant, diminishing as $\hbar\omega$ increases. When $\gamma_x << 1$, or $\hbar\omega - Eg >> R_{x1}$, then $\alpha(\omega) \rightarrow \alpha_0(\omega)$, as can be seen by expanding the denominator in Eq. (55) and neglecting terms of order higher than $2\pi\gamma_x$. Conversely, for $\gamma_x >> 1$, or $\hbar\omega - E_g << R_{x1}$, then $\alpha(\omega) \rightarrow \alpha_0(\omega)2\pi\gamma_x$, where the exponential factor is considered to be approximately zero.

The quantity R_{x1} is related to the gap energy, E_g, and the exciton energy, E_x, by the relation

$$E_x = E_g - R_{x1}/n^2 \ , n = 1, 2, 3, \ldots ,$$

and Elliott[12] predicted a series of lines at energies $\hbar\omega = Eg - R_{x1}/n^2$, with intensities decreasing as n^{-3}. While for GaAs the first of these lines, corresponding to the lowest exciton state, occurs at an energy ~4.3 meV below E_g, subsequent lines are much closer and can be considered to consist of a quasi-continuum with $\alpha(\omega) \approx 2\pi\gamma_x\alpha_0(\omega)$, thus transitioning smoothly to $\alpha(\omega)$ for $\hbar\omega > E_g$.

Since the lines for $n \geq 2$ are not usually discernable, the absorption spectrum at low temperatures generally shows a sharp peak at $E_x = E_g - R_{x1}$, for GaAs $\alpha(E_x) \approx 2.5 \times 10^4$ cm^{-1}, and decreases to the approximately constant value near E_g before approaching $\alpha_0(\omega)$ for $\hbar\omega >> E_g$. Thus, in III-V compounds, the primary effect of the exciton on the absorption coefficient is to modify its value near the band edge.

IV. HYDROSTATIC PRESSURE EFFECTS

The application of hydrostatic pressure to a crystal causes a change in volume, i.e. it brings the atoms closer together. The decreased separation between atoms results in a changed energy gap and thus the separation between two bands, $E_n - E_{n'}$, changes with pressure. Hydrostatic pressure does not, however, change the crystal symmetry, [8] and hence the selection rules for the transitions remain unchanged. In addition to the constant matrix elements, Δ_s due to spin-splitting may also be considered constant with pressure.[16] A small change in the lattice constant causes a linear variation in E_n, and hence we can write

$$E_n = E_n(0) + (dE_n/dP)_T \Delta P \tag{56}$$

where $(dE_n/dP)_T$ denotes the pressure coefficient at constant temperature. The coefficient is different for the various bands and may be positive or negative. (In zincblende structures $dE_g/dP > 0$, i.e. Γ_6 moves up with respect to Γ_8). Values of the pressure coefficients for Group IV and Group III-V materials change only slightly from one substance to another, and accepted values for the direct gap (zone center) for GaAs are:[17-22]

$$(dE_0/dP)_T \approx 11\times10^{-6} \text{ eV/bar}$$

$$(dE_1/dP)T \approx 5\times10^{-6} \text{ eV/bar} \tag{57}$$

$$(dE_2/dP)T \approx 3.6\times10^{-6} \text{ eV/bar},$$

where E_i (i = 0, 1, 2) refers to bands Γ_{1C}, Γ_{15C}, and Γ_{12C} respectively.

Having earlier obtained numerical values for the constants F, M, G, etc., we now modify them to include the effect of hydrostatic pressure. Since the matrix elements themselves are considered invariant with pressure, we have, for example,

$$|\langle\ |\ \rangle| \sim F\epsilon_0 = F_P(E_0+\Delta E_{0,P}),$$

where the subscript P denotes the pressure dependence, and from Eq. (57) we have

$$\Delta E_{0,P} = (\partial E_0/\partial P)_T \Delta P.$$

Similarly we obtain for the other "constants",

$$M_P = ME_1/(E_1+\Delta E_{1,P}),$$

$$G_P = GE_2/(E_2+\Delta E_{2,P}),$$

$$A'_P = A'(E_1-E_0)/[(E_1+\Delta E_{1,P})-(E_0+\Delta E_{0,P})].$$

Upon substituting the new constants into the expressions for $\alpha(\omega)$, we

obtain $\alpha(\omega,P)$. For example, we can write the split-off band contribution to the pressure dependent absorption coefficient as

$$\alpha_{SO-C}(\omega,P)\approx 2.163\times 10^{6}[A'_{P}+2P^{2}_{M}/3(E_0+\Delta E_{0,P}+\Delta_S)-(L_P+2M_P)/3]^{-3/2}$$

$$\times(\hbar\omega)^{-1}(\hbar\omega-\Delta_S-E_0-\Delta E_{0,P})^{1/2}, \qquad (58)$$

where P_M continues to denote the matrix element and P the pressure. Equation (58) can be evaluated readily if pressure-modified constants are calculated and used, or it may be recast into a form including the pressure coefficients directly. Thus,

$$\alpha_{SO-C}(\omega,P)\approx 2.163\times 10^{6}\ \{A'(E_1-E_0)/[(E_1+\Delta E_{1,P})-(E_0+\Delta E_{0,P})]$$

$$+2P^{2}_{M}/3(E_0+\Delta E_{0,P}+\Delta_S)-FE_0/3(E_0+\Delta E_{0,P})-2GE_2/3(E_2+\Delta E_{2,P})$$

$$-2ME_1/3(E_1+\Delta E_{1,P})\}^{-3/2}(\hbar\omega)^{-1}(\hbar\omega-\Delta_S-E_0-\Delta E_{0,P})^{1/2}, \qquad (59)$$

where the constants A', F, G, and M have the values listed after Eq. (48). Although relevant information is contained in Eq. (59), it may be presented in a more appealing form after some algebraic manipulation. Expanding applicable terms of Eq. (59) and limiting ourselves to first order, the terms are modified as follows:

$$A'(E_1-E_0)/(E_1-E_0+E_{1,P}-E_{0,P}) \rightarrow A'[1-(\Delta E_{1,P}-\Delta E_{0,P})/(E_1-E_0)]$$

$$2P^2{}_M/3(E_0+\Delta E_{0,P}+\Delta_S) \rightarrow [2P^2{}_M/3(E_0+\Delta_S)][1-\Delta E_{0,P}/(E_0+\Delta_S)]$$

$$F\epsilon_0/(E_0+\Delta E_{0,P}) \rightarrow F[1-\Delta E_{0,P}/E_0]$$

$$2GE_2/3(E_2+\Delta E_{2,P}) \rightarrow (2G/3)[1-\Delta E_{2,P}/E_2]$$

$$2ME_1/3(E_1+\Delta E_{1,P}) \rightarrow (2M/3)[1-\Delta E_{1,P}/E_1].$$

Substituting these approximations into Eq. (59) yields,

$$\alpha_{SO-C}(\omega,P)\approx 2.163\times 10^6 \ \{A'[1-(\Delta E_{1,P}-\Delta E_{0,P})/(E_1-E_0)]$$

$$+[2P^2{}_M/3(E_0+\Delta_S)][1-\Delta E_{0,P}/(E_0+\Delta_S)] - (F/3)[1-\Delta E_{0,P}/E_0]$$

$$-(2G/3)[1-E_{1,P}/E_1]-(2M/3)[1-E_{1,P}/E_1]\}^{-3/2}$$

$$\times(\hbar\omega)^{-1}(\hbar\omega-\Delta_S-E_0-\Delta E_{0,P})^{1/2}.$$

Separating the terms in brackets { } into pressure-dependent and pressure-independent groups and defining

$$Q \equiv A'+2P^2{}_M/3(E_0+\Delta_S)-F/3-2G/3-2M/3$$

$$R(P) \equiv -A'[(\Delta E_{1,P}-\Delta E_{0,P})/(E_1-E_0)]-2P^2{}_M\Delta E_{0,P}/3(E_0+\Delta_S)^2$$

$$+F\Delta E_{0,P}/3E_0+2G\Delta E_{2,P}/3E_2+2M\Delta E_{1,P}/3E_1, \qquad (60)$$

we can write

$$\alpha_{so-c}(\omega,P) \approx 2.163\times10^{6}[Q+R(P)]^{-3/2}(\hbar\omega)^{-1}(\hbar\omega-\Delta_s-E_0-\Delta E_{0,P})^{1/2}. \quad (61)$$

Again expanding to first order we have,

$$\alpha_{so-c}(\omega,P) \approx 2.163\times10^{6}Q^{-3/2}[1-3R(P)/2Q](\hbar\omega)^{-1}(\hbar\omega-\Delta_s-E_0-\Delta E_{0,P})^{1/2}. \quad (62)$$

It is possible to write Eq. (62) in terms of $\alpha_0(\omega)$ by simply expanding the square-root term and then combining the two truncated series, keeping only terms up to first order in $\Delta E_{i,P}$. The result is

$$\alpha_{so-c}(\omega,P) \approx 2.163\times10^{6}Q^{-3/2}(\hbar\omega)^{-1}(\hbar\omega-\Delta_s-E)^{1/2}[1-3R(P)/2Q$$

$$-\Delta E_{0,P}/2(\hbar\omega-\Delta_s-E)+ \text{h.o.t.}] \quad (63)$$

which has the form

$$\alpha_{so-c}(\omega,P) \approx \alpha_0(\omega)\times f(P).$$

The quantity E in Eq. (63) in this case must be taken as $E_0 + \Delta E_{0,P}$ in order to account for the pressure-induced shift in the energy gap. It is apparent that Eq. (63) reduces to the expression obtained earlier for $\alpha_{so-c}(\omega)$, e. g. Eq. (51), when $\Delta P = 0$. The contribution of the split-off band to the pressure - dependent absorption coefficient can thus be calculated from

Eqs. (58) or (59), or using the Definitions (60), by Eqs. (61) - (63). We prefer the form of Eq. (62) and will use this form for the remaining contributions.

The contribution of the heavy hole band in the <u><100> direction</u> can be written as

$$\alpha_{hh-c}(\omega,P) \approx 2.163\times10^{6}\{A'[1-(\Delta E_{1,P}-\Delta E_{0,P})/(E_1-E_0)]$$

$$+(2P^2_M/3E_0)[1-\Delta E_{0,P}/E_0]+[P^2_M/3(E_0+\Delta_S)][1-\Delta E_{0,P}/(E_0+\Delta_S)$$

$$-M[1-\Delta E_{1,P}/E_1]\}^{-3/2}(\hbar\omega)^{-1}(\hbar\omega-E_0-\Delta E_{0,P})^{1/2}, \qquad (64)$$

where the expansions are again to first order.

By the same procedure as used in the case of the split-off band, Eq. (64) can be put into a more convenient form. The result is

$$\alpha_{hh-c}(\omega,P)\approx2.163\times10^{6}Q^{-3/2}[1-3R(P)/2Q](\hbar\omega)^{-1}(\hbar\omega-E_0-\Delta E_{0,P})^{1/2}, \qquad (65)$$

where now

$$Q \equiv A'+2P^2_M/3E_0+P^2_M/3(E_0+\Delta_S)-M$$

$$R(P) \equiv -A'(\Delta E_{1,P}-\Delta E_{0,P})/(E_1-E_0)-2P^2_M\Delta E_{0,P}/3E_0^2-P^2M\Delta E_{0,P}/3(E_0+\Delta_S)^2$$

$$+M\Delta E_{1,P}/E_1. \qquad (66)$$

For the light hole band we obtain

$$\alpha_{lh-c}(\omega,P) \approx 2.163\times10^{6} Q^{-3/2}[1-3R(P)/2Q](\hbar\omega)^{-1}(\hbar\omega-E_0-\Delta E_0)^{1/2},$$

which is identical to Eq. (65), but where the definitions of Q and R(P) are, for the <u><100> direction</u>

$$Q \equiv A'+2P^2{}_M/3E_0+P^2{}_M/3(E_0+\Delta_s)-2F/3-4G/3-M/3$$

$$R(P) \equiv -A'(\Delta E_{1,P}-\Delta E_{0,P})/(E_1-E_0)-2P^2{}_M\Delta E_{0,P}/3E_0{}^2-P^2{}_M\Delta E_{0,P}/3(E_0+\Delta_s)^2$$

$$+2F\Delta E_{0,P}/3E_0+4G\Delta E_{2,P}/3E_2+M\Delta E_{1,P}/3E_1 \qquad (67)$$

Within our approximations, the general expression for the absorption coefficient will be of the form of Eq. (65), with Q and R(P) varying as we consider different directions. For the <u><Avg> direction</u>, <u>heavy hole contribution</u>, we use

$$Q \equiv A'+2P^2{}_M/3E_0+P^2{}_M/3(E_0+\Delta_s)-0.60G-0.60M$$

$$R(P) \equiv -A'(\Delta E_{1,P}-\Delta E_{0,P})/E_1-E_0)-2P^2{}_M\Delta E_{0,P}/3E_0{}^2-P^2{}_M\Delta E_{0,P}/3(E_0+\Delta_s)$$

$$+0.60G\Delta E_{2,P}/E_2+0.60M\Delta E_{1,P}/E_1, \qquad (68)$$

while for the <u><Avg> direction</u>, <u>light hole contribution</u>, we use

$$Q \equiv A'+2P^2{}_M/3E_0+P^2{}_M/3(E_0+\Delta_s)-2F/3-0.73G-0.73M$$

$$R(P) = -A'(\Delta E_{1,P}-\Delta E_{0,P})/(E_1-E_0)-2P^2{}_M\Delta E_{0,P}/3E_0{}^2-P^2{}_M\Delta E_{0,P}/3(E_0+\Delta_S)^2$$

$$+2F\Delta E_{0,P}/3E_0+0.73G\Delta E_{2,P}/E_2+0.73M\Delta E_{1,P}/E_1 \qquad (69)$$

In order to obtain $\alpha(\omega,P)$, the directionally independent split-off band must be added to the appropriate $\alpha_{hh-c}(\omega,P)$ and $\alpha_{lh-c}(\omega,P)$.

Since hydrostatic compression decreases the lattice constant and increases the width of the (direct) energy gap, experiments have been done to determine the pressure dependence of E_g. Welber and coworkers[20] applied pressure to GaAs at room temperature and monitored the absorption edge. Their result was the relation

$$E_g \approx 1.45 + 0.0126P - 3.77\times10^{-5}P^2 \quad (eV), \qquad (70)$$

where P is in kbar.

Another external variable affecting E_g is temperature. Varshni[23] proposed a temperature dependence given by

$$E_\Gamma(T) \approx E_\Gamma(0) - \alpha T^2/(T+\beta) \quad (eV), \qquad (71)$$

with $\alpha = 8.871\times10^{-4}$ eV/K, and $\beta = 572$ K.

Additional results were then considered and the values of the constants were suggested to be $\alpha = 5.405\times10^{-4}$ eV/K and $\beta = 204$ K.

V. MAGNETIC FIELD EFFECT

A. Simple Bands

As an introduction to the effect of a magnetic field on the absorption coefficient we first consider a simple case: A free particle of mass m and charge $-e$ and spherical non-degenerate bands, with the magnetic field uniform and in the $+z$ direction.[6] Using the Landau gauge, the vector potential is $A = H(0,x,0)$, and the Hamiltonian is

$$\mathcal{H} = (2m)^{-1}[p-(e/c)A]^2$$

$$= (2m)^{-1}[p^2{}_x+p^2{}_z+(p_y-eHx/c)^2].$$

Using the definition of the cyclotron frequency, $\omega_c \equiv -eB/mc$, the Hamiltonian becomes

$$\mathcal{H} = (2m)^{-1}[p^2{}_x+p^2{}_z+(p_y+m\omega_c x)^2],$$

and the Schroedinger Equation, $\mathcal{H}\Psi = E\Psi$, can be written as

$$(2m)^{-1}[p^2{}_x+p^2{}_z+(p_y+m\omega_c x)^2]\Psi(x) = E\Psi(x),$$

or,

$$(\hbar^2/2m)(\partial^2\Psi(x)/\partial x^2)+(\hbar^2k^2{}_z/2m)\Psi(x)+(2m)^{-1}(\hbar k_y+m\omega_c x)^2\Psi(x) = E\Psi(x)$$

where $p_{y,z} \equiv \hbar k_{y,z}$.

Rearranging this expression,

$$-(\hbar^2/2m)(\partial^2\Psi(x)/\partial x^2)+[(m\omega_C/2)(x+\hbar k_y/m\omega_C)^2$$

$$+\hbar^2 k^2_z/2m]\Psi(x) = E\Psi(x). \qquad (72)$$

Equation (72) has the form of a simple harmonic oscillator equation in one dimension, with equilibrium position at $x' = \hbar k_y/m\omega c = -c\hbar k_y/eB$, and natural frequency ω_C The eigenvalues are

$$E_n = (n+1/2)\hbar\omega_C + \hbar k^2_z/2m.$$

Since the equilibrium position of the oscillator must be within the material (consider a parallelepiped of dimensions L_x, L_y, L_z), a limitation is imposed on the range of k_y, i.e. $-L_x/2 < x' < L_x/2$, or upon writing x' in terms of k_y,

$$-(L_x/2)(eH/c\hbar) < k_y < (L_x/2)(eB/c\hbar).$$

There are $L_y/2\pi$ allowed values of k_y and we have a degeneracy of levels, for fixed k_z, of $(L_xL_y/2\pi)(eB/c\hbar)$. If spin is neglected, this expression must be multiplied by a factor 2. Further, the number of

allowed values of k_z, such that $|k_z| < k_{z0}$, is $L_z k_{z0}/\pi$ which also gives the allowed values of $E_k < E_{k0} = \hbar^2 k_{z0}^2/2m$. Solving for k_{z0} and substituting, we obtain for the number of allowed values

$$(L_z/\pi)(2mE_{k0}/\hbar^2)^{1/2} = (L_z/\hbar\pi)(2mE_{k0})^{1/2}.$$

Writing E_k for E_{k0} and differentiating with respect to E_k results in the number of allowed energy levels in dE_k. Thus,

$$N(E_k)dE_k = (L_z/2\pi\hbar)(2m)^{1/2}(E_k)^{-1/2}. \tag{73}$$

In order to find the distribution of all the levels, we sum over the distribution functions and use the degeneracy factor. The density of states then becomes, for simple bands, using $\Delta n = 0$,

$$J_{cv}=(L_xL_y/2\pi)(eH/c\hbar)[L_z(2m_r)^{1/2}/2\pi\hbar]\sum_n[\hbar\omega-E_g-(n+1/2)\,\hbar\omega_{cr}]^{-1/2}, \tag{74}$$

where m_r is the reduced mass, and $\omega_{cr} \equiv \omega_c + \omega_v = eB/cm_r$.

Equation (74) is generally written as

$$J_{cv} = (V/4\pi^2)(eH/c\hbar)[(2m_r)^{1/2}/\hbar]\sum_n[\hbar\omega-E_g-(n+1/2)\,\hbar\omega_{cr}]^{-1/2}, \tag{75}$$

since $L_xL_yL_z = V$, the volume.

Using Eq. (75), the absorption coefficient becomes

$$\alpha(\omega,H)=(4\pi^2e^2/ncm^2\omega V)\,|\mathcal{H}'|^2\times(V/4\pi^2)(eB/c\hbar)[(2m_r)^{1/2}/\hbar]$$

$$\times\sum_n[\hbar\omega-E_g-(n+1/2)\,\hbar\omega_{cr}]^{-1/2},$$

or, upon simplifying,

$$\alpha(\omega,H)=[e^2E_p/6ncm(\hbar\omega)](eH/c\hbar)(2m_r)^{1/2}\sum_n[\hbar\omega-E_g-(n+1/2)\,\hbar\omega_{cr}]^{-1/2}. \quad (76)$$

Using the definition of $\omega_{cr} \equiv eH/cm_r$, we write

$$\alpha(\omega,H) = [e^2E_p(2m_r)^{3/2}/6ncm(\hbar\omega)\hbar^2](\hbar\omega_{cr}/2)\sum_n[\hbar\omega-E_g$$

$$-(n+1/2)\,\hbar\omega_{cr}]^{-1/2}. \quad (77)$$

Equation (77) compares with the zero-field, no spin case given by

$$\alpha_0(\omega)=[e^2E_p(2m_r)^{3/2}/6ncm(\hbar\omega)\hbar^2](\hbar\omega-E_g)^{1/2},$$

or, upon writing $\alpha(\omega,0) = C(\hbar\omega-Eg)^{1/2}$, we see that

$$\alpha(\omega,H) = (C/2)\hbar\omega_{cr}(\hbar\omega-E_n)^{-1/2},$$

where $E_n \equiv E_g + (n+1/2)\hbar\omega_{cr}$.

A dimensional check shows that

$$\alpha(\omega,B) \sim [e^2E_pm_r{}^{3/2}/cm(\hbar\omega)\hbar^2](\hbar\omega_{cr}/E^{1/2})$$

$$\sim [E\times L\times E\times E^{3/2}\times(t^3/L^3)\times E \;/\; (L/t)\times(E/L^2)\times t^2\times E\times E^2\times t^2\times E^{1/2}] \sim L^{-1},$$

as required.

Examination of Eq. (77) shows that the application of a magnetic field changes the energy bands from the simple situation shown in Fig. 1a, to the more complicated case shown in Fig. 1b. Further, using Eq. (77), we can find $\alpha(\omega,B)$. Using the values for m_c and m_v determined earlier ($m_c \approx 0.067m$, $m_v \approx 0.505m$, $m_r \approx 0.059m$) and, for purposes of illustration choosing a field of 1 Weber/m^2 = 10^4 G, we have, using $\hbar\omega_c = \hbar(eB/cm)$,

$$\hbar\omega_{cr} \approx \quad 1.158\times10^{-4}[B/(m_r/m)] \quad (\text{eV}) = 1.963\times10^{-3}\ (\text{eV}).$$

Then, for example, using the value of $\hbar\omega_{cr}$ just calculated, we have

$$\alpha(\omega,1) \approx (2^{3/2}e^2E_p m^{1/2} 0.059^{3/2}/6nc\hbar^2)(\hbar\omega_{cr}/2)(\hbar\omega)^{-1}$$

$$\times\textstyle\sum_n[\hbar\omega-E_g-(n+1/2)\,\hbar\omega_{cr}]^{-1/2}$$

$$\approx(2.163\times10^6)(0.014)(9.82\times10^{-4})(\hbar\omega)^{-1}\textstyle\sum[\hbar\omega-E_g-(n+1/2)\,\hbar\omega_{cr}]^{-1/2},$$

or, $$\alpha(\omega,1)\approx 29.635(\hbar\omega)^{-1}\textstyle\sum_n[\hbar\omega-E_g-(n+1/2)\,\hbar\omega_{cr}]^{-1/2}. \qquad (78)$$

The energy levels of degenerate bands in the absence of external perturbation were calculated using Kane's **k** . **p** method. Luttinger and Kohn[24] investigated the problem of cyclotron resonance for degenerate

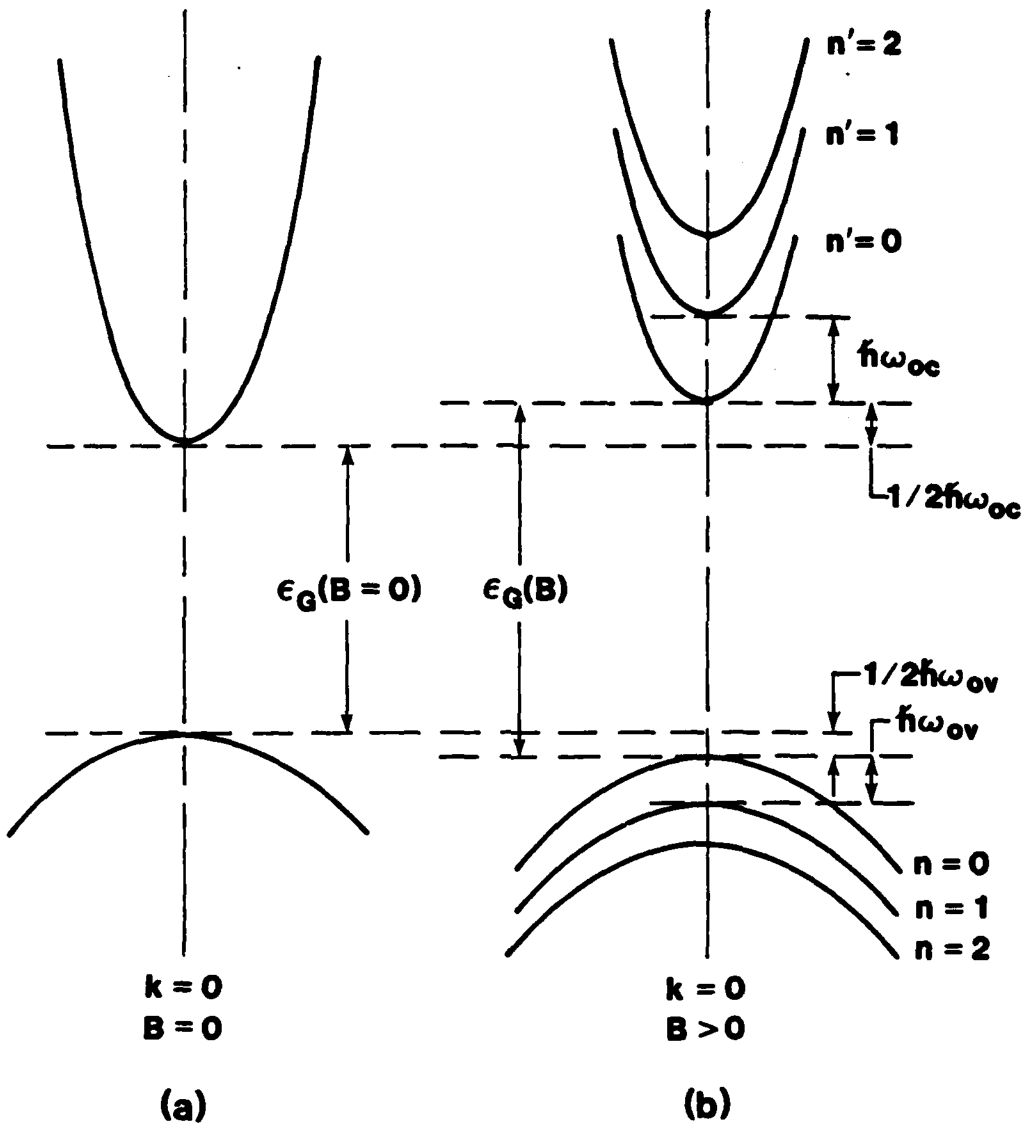

Fig. 1. Energy vs. wavenumber diagram for simple conduction and valence bands in the absence of magnetic field (a), and in the presence of a magnetic field (b).

bands, and Luttinger [25] described a general method for determining the energy levels of holes in a degenerate band. Since in our samples the degeneracy was lifted by strain (see Sect. VI-F), we were essentially dealing with the simple band situation described above.

B. Excitons in Magnetic Fields

Group III-V compounds generally have large dielectric constants and comparatively small effective masses at the conduction and and valence band extrema. Therefore excitons in these materials have a large spatial extent, with the exciton radius given by

$$a_{ex} = \epsilon_0 \hbar^2 / e^2 \mu,$$

where μ is the reduced effective mass, ϵ_0 is the dielectric constant. The ground state energy is below the gap energy by the amount,

$$R_{x_1} = e^4 \mu / 2\epsilon_0^2 \hbar^2.$$

As noted earlier, the exciton effect is mainly apparent in a modification of the absorption edge, and spectra do not generally show much structure. Thus, although the valence band maximum in GaAs is complex, the absence of detail in the spectra means that a simple hydrogenic model is sufficient to obtain the exciton states and

energies.[26] Usually spectra show only transitions associated with the lowest exciton state, and interband magneto-optical phenomena are basically explained in terms of the Landau levels, possibly perturbed by the electron-hole interaction.[26]

In quantum well structures the exciton can be considered to be two-dimensional with a binding energy approximately four times larger than in the three-dimensional case.[27] The Hamiltonian can be written as[28]

$$\mathcal{H} = \mathcal{H}_e + \mathcal{H}_h + \mathcal{H}_x,$$

where $\mathcal{H}_e$ and $\mathcal{H}_h$ represent electron and hole motion in the z-direction, and

$$\mathcal{H}_x = P^2/2M + p^2/2\mu - e^2/\epsilon(r^2+z^2)^{1/2}. \qquad (79)$$

In Eq. (79), $P = p_e + p_h$, $M = m_e + m_h$, μ is the reduced mass, and $r = r_e - r_h$, $z = z_e - z_h$. Naturally M and μ have different values depending on whether heavy or light holes are being considered. **p** is the momentum conjugate to r, and generally the total momentum, P, is taken to equal zero. In order to include the external magnetic field, we can rewrite Eq. (79) as

$$\mathcal{H} = (2m_e)^{-1}[p_e - (e/2c)\mathbf{B} \times r_e]^2 + (2m_h)^{-1}[p_h + (e/2c)\mathbf{B} \times r_h]$$

$$-e^2/\epsilon|r_e - r_h|. \qquad (80)$$

When the magnetic field is strong enough to allow omitting the Coulomb term in Eq. (80), we are left with an expression leading to the Landau levels. This was considered in the previous section. The two-dimensional situation (well width negligible), for unrestricted values of the magnetic field (B_z), was investigated by Akimoto and Hasegawa.[29] They determined approximate expressions for the energy as a function of B_z in the "low" and "high" field regimes. Low field has been loosely defined as the region where

$$\hbar(eB/2\mu c) << \mu e^4/2\hbar^2\epsilon_0^2,$$

and high field where the converse holds.[26] We have, for the "low" field

$$E_n/R_y^* = -(n+1/2)^{-2} + (5/8)(n+1/2)^4(\hbar\omega_0)^2/(R_y^*)^2 + \ldots, \quad n=0,1,2,\ldots, \qquad (81)$$

and, for the "high" field,

$$E_n/R_y^* = (2n+1)\hbar\omega_0/R_y^* - 3[\hbar\omega_0/(2n-1)R_y^*]^{1/2} + \ldots, \quad n=0,1,2,\ldots. \qquad (82)$$

In these two expressions the following definitions apply:

$$\hbar\omega_0 = \hbar(eB/2\mu c), \text{ and } R_y^* = \mu e^4/2\hbar^2\epsilon_0^2.$$

For GaAs we remain in the low field regime for H<60kG, and since we are concerned with the lowest level exciton, we can rewrite Eq. (81) as

$$E_0 \approx -4R_y^* + (5/8)(1/2)^4(\hbar\omega_0)^2/R_y^*. \qquad (83)$$

In Fig. 2 we illustrate the magnetic field dependence of energy in the case of Landau levels (simple bands) using the relation $E_n = (n+1/2)\hbar eB/\mu c$, and in the case of excitons using Eq. (83).

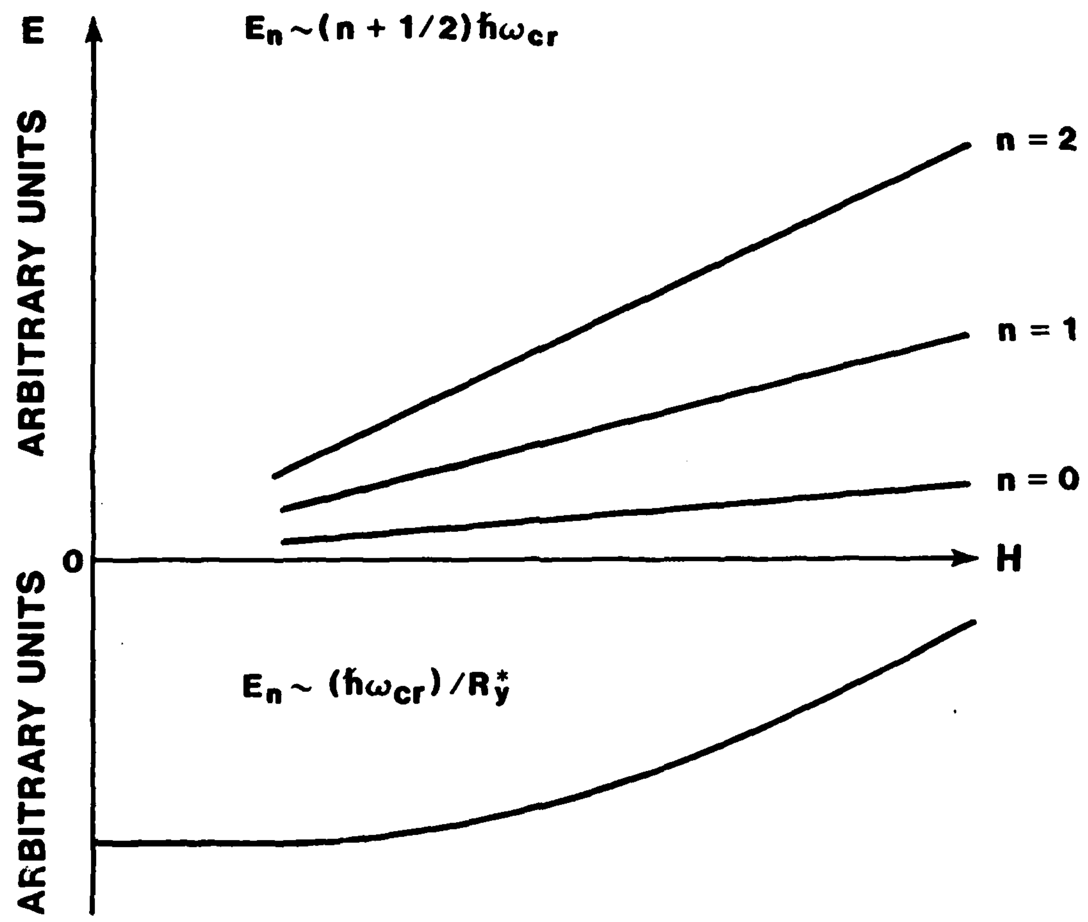

Fig. 2. Magnetic field dependence for Landau energies (top) and excitons (bottom). Note that energy scales are different to show effect.

VI. EXPERIMENT

A. Experimental Objective

The purpose of this experiment was to develop a method to allow the optical investigation, at low temperatures, of semiconductor structures subjected simultaneously to high pressure and high magnetic field. This objective was met by the experiment described in the following paragraphs. Although we demonstrated the feasibility of the experimental method by performing laser induced luminescence measurements, the experiment is readily adaptable to investigations involving absorption, transmission, and excitation spectroscopy.

B. General Experiment Description

The novel feature of this experiment is that optical access to the sample to be investigated is by means of an optical fiber. This alleviates many of the problems often associated with measurements involving high pressures, e.g. limitations imposed by pressure chamber and/or Dewar windows, transmissivity of the pressure medium, and also, in the configuration we used, it allows simultaneous determination of magnetic and pressure effects.

In our experiment the sample was attached directly to one end of the

optical fiber and suspended in the pressure chamber. Fiber access to the pressure domain was through a pressure plug. The chamber, at the end of a probe, was inserted into the magnetic field on the axis of a superconducting magnet (solenoid). The sample was illuminated by an Argon$^+$ Ion laser beam which was coupled into the other end of the fiber through a microscope objective. The luminescence signal from the sample returned through the same fiber, and the collimated signal was split off and directed to a monochromator and detector.[30]

The magnet is capable of providing fields to 65 kG, and the pressure system was used to 4 kbar (~60000 psi). Hydrostatic pressure is exerted on the sample by growing a uniform crystal of helium around it under controlled conditions.

C. Preliminary Investigations

Certain preliminary work was required to test the feasibility of the proposed method. This included determination of fiber suitability at temperatures ≤ 4 K, and preparation of fiber ends (polishing). Additionally a means of attaching the sample to the fiber had to be found, as well as providing a seal around the fiber where it entered the pressure region. That optical losses had to be kept to a minimum was understood.

Fiber ends were polished to 0.3 μm smoothness using progressively finer grit abrasives, with the acceptance test being visual smoothness under 100× magnification. A Gaussian beam propagation calculation was used to select the objective to match the beam waist to the fiber core diameter. Positional adjustments to the input end of the fiber were made by means of a 3-degree freedom micrometer stage holding the fiber, and transmission was maximized initially by using a power meter at the sample end of the fiber. A beam splitter was used along with folding mirrors (FM) to direct the return signal from the sample (initially a mirror) to a spectrometer. This inital arrangement is shown in Fig. 3.

In this arrangement, FMs 1-3 were used to position the beam on the microscope objective which, in turn, placed the beam waist on the the end of the fiber. The return signal placement was adjusted by means of mirrors FM4 and FM5. The lens, L, focused the signal on the spectrometer input slit. After initial positioning of the optical elements resulted in a visible spot on the screen, assuming the spectrometer was properly adjusted, the signal was maximized (visually) by adjustment of fiber position and the beam splitter, BS. Greater alignment accuracy was then obtained by replacing the screen with a photomultiplier tube (PMT). Displaying the PMT output

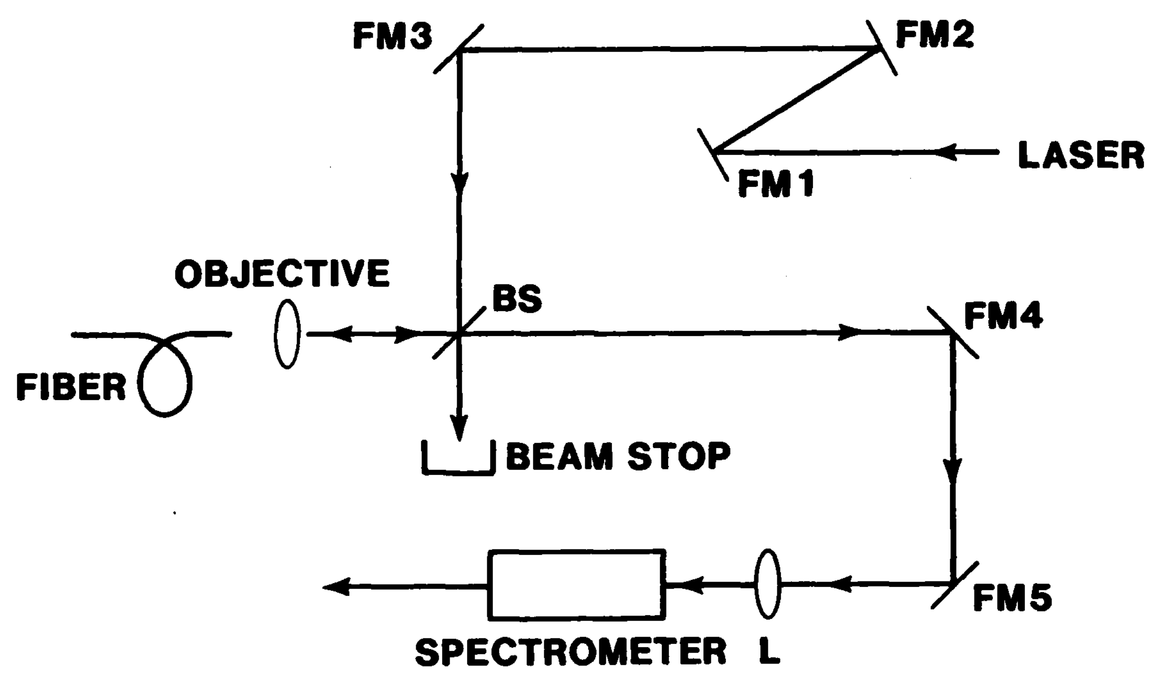

Fig. 3. Initial experimental configuration as used in preliminary investigations.

on an oscilloscope, fine adjustments were completed. For this step a chopper wheel was placed between FM2 and FM3, and the beam stop was replaced by a photodiode to provide the external trigger signal to the scope. This set-up performed satisfactorily with a CdS sample

The laser in this preliminary test was a Spectra Physics Model 164 Argon$^+$Ion laser with Model 265 Exciter, used to pump a Spectra Physics Model 375 dye laser with Rhodamine 6G dye. The spectrometer was a Jobin-Yvon Model H-20V, and the PMT was an RCA 7767 with S-1 response.

Although the set-up shown in Fig. 3 worked well, two significant problems soon became apparent. Sample adhesion to the fiber was not good, and signal losses when the end of the fiber and sample were immersed in liquid nitrogen were noticeable. The sample adhesion problem was solved, after experimentation, by thinning GE Adhesive and Insulating Varnish No. 7031 with a 50/50 mixture of toluene and methanol. A general guide required 1 part varnish and 5-10 parts thinner by volume. Optimum results were obtained when the mixture reached a consistency to form a bead at the end of a pin without dropping off. The adhesive then had to be used to be used promptly since it dried rather quickly. The magnitude of the signal loss problem did not become apparent until, in the final

experimental configuration, approximately four feet of the fiber (inside the probe) were cooled to liquid nitrogen temperature and below.

This particular fiber (SS-600, General Fiber Optics, Inc.) supposedly consisted of a fused silica core with doped silica cladding, and the indices were supposed to track each other with temperature. We therefore felt initially that the poor or nonexistent fluorescence signals were attributable to other causes, e.g. sample quality and/or adhesion and placement of the sample on the fiber. A test, which should have been performed earlier, showed that transmitted power became negligible when approximately four feet of coiled fiber where immersed in liquid nitrogen. Our conclusion is that, in place of the doped silica cladding advertised, our fiber had a polymer cladding whose index had changed sufficiently at 76 K to allow most of the light to escape through the sides. An Al-coated quartz fiber manufactured by Hughes Aircraft Company, designated P-27, with a core diameter of 100 μm solved the problem. This fiber showed negligible loss at 76 K and was used henceforth. A further advantage of P-27 was that, upon cleaving, it presented a smooth surface without polishing. The Al coating was cleared from the end surface using a laboratory-grade NaOH solution.

D. Experimental Configuration and Equipment

Since the optical system used in the preliminary tests performed well, it was used with only minor adaptations for the experiment. The changes were required because the positions of the laser and monochromator used for the data runs were dictated by available bench space. Figure 4 shows a diagram of the optics configuration. In this experimental configuration, all optical elements beyond FM3 were mounted on a platform adjusted to the height of the monochromator input slit. Thus FMs 1 - 3 are used to raise the laser beam to the appropriate level, and only lateral adjustments to the other optical elements are required. During all data runs the Argon$^+$ Ion laser was tuned to 5145 angstrom (2409.9 meV) and an output power of 1.2 - 1.4 W (cw). The beam splitter reflects 4% of the incident light. The red filter with a cut off near 6000 angstrom prevented reflected laser light from entering the SPEX 0.75 m double monochromator. A RCA 7102 photodetector was used at the output slit with a Fluke 415B HV Power Supply, and its output was recorded on a HP 7044B x-y Recorder.

The fiber was then sealed in the pressure plug and inserted into the probe. Both components were made of heat-treated BeCu. A sketch of the plug is

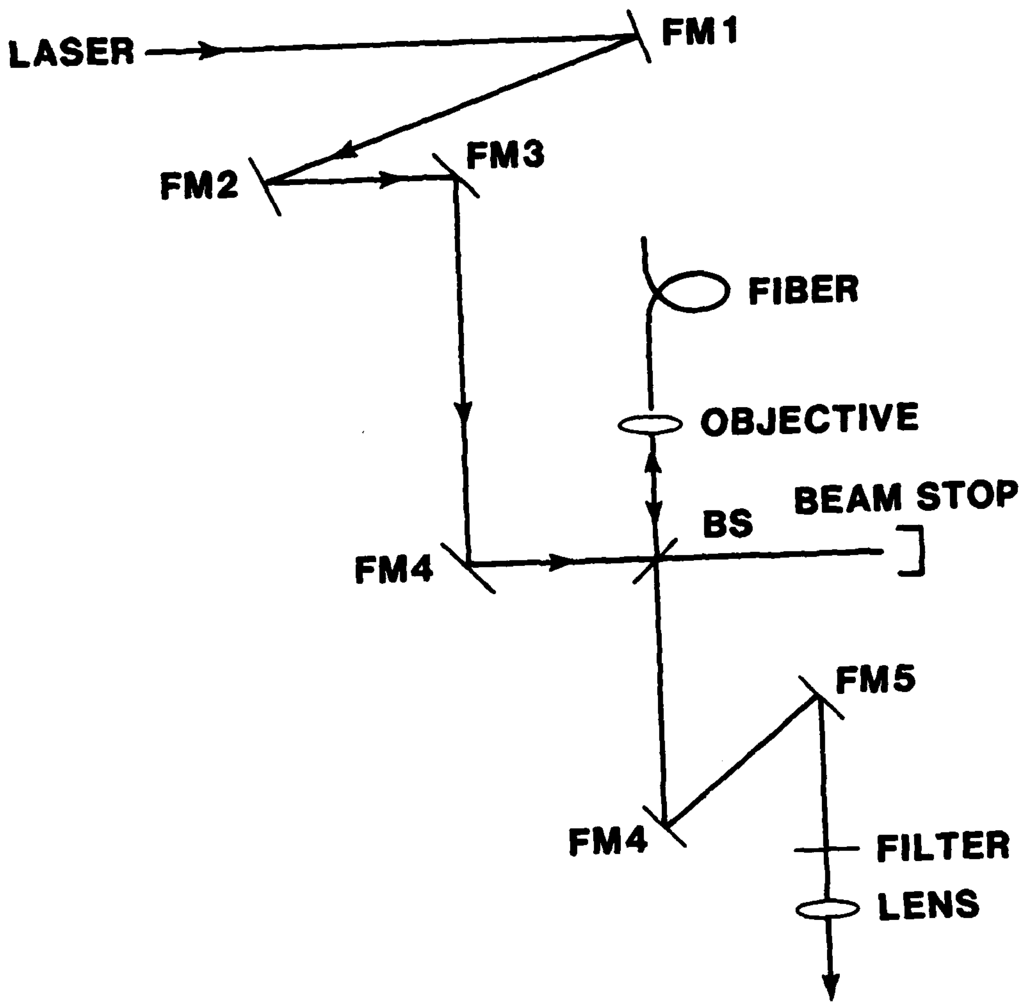

Fig. 4. Placement of optical elements. Laser beam is coupled into the optical fiber to illuminate the sample, and the return signal is directed to the monochromator.

shown in Fig. 5, with relevant dimensions given. The probe has an outside diameter of 0.250 inch, and and inside diameter of 0.0625 inch. The diameter of the chamber opening is 0.125 inch.

The seal between the probe shaft and the bomb is ensured by exact machining of angles and compression provided by threaded fittings. The fiber was sealed in the pressure plug with epoxy. The magnet is contained in a triple Dewar, as shown in Fig. 6, and driven by a Varian V4102 Superconducting Magnet Power Supply. Level sensors in the outer and middle Dewars and a pressure sensor in the inner Dewar provided necessary information.

Hydrostatic pressure on the sample was provided by a method dubbed "Solid Helium Pressure Generation Technique".[31] Basically this technique involves maintaining pressure on liquid helium as it solidifies slowly from the bottom of the pressure chamber and surrounds the sample. After the solid-liquid interface has passed the sample, the probe can be lowered to the appropriate position since additional cooling can be considered to occur at constant volume due to blockage of the probe capillary. The pressure system is shown in Fig. 7. The system was charged initially to ~2500 psi with helium gas. Pump 1 was then used to a pressure

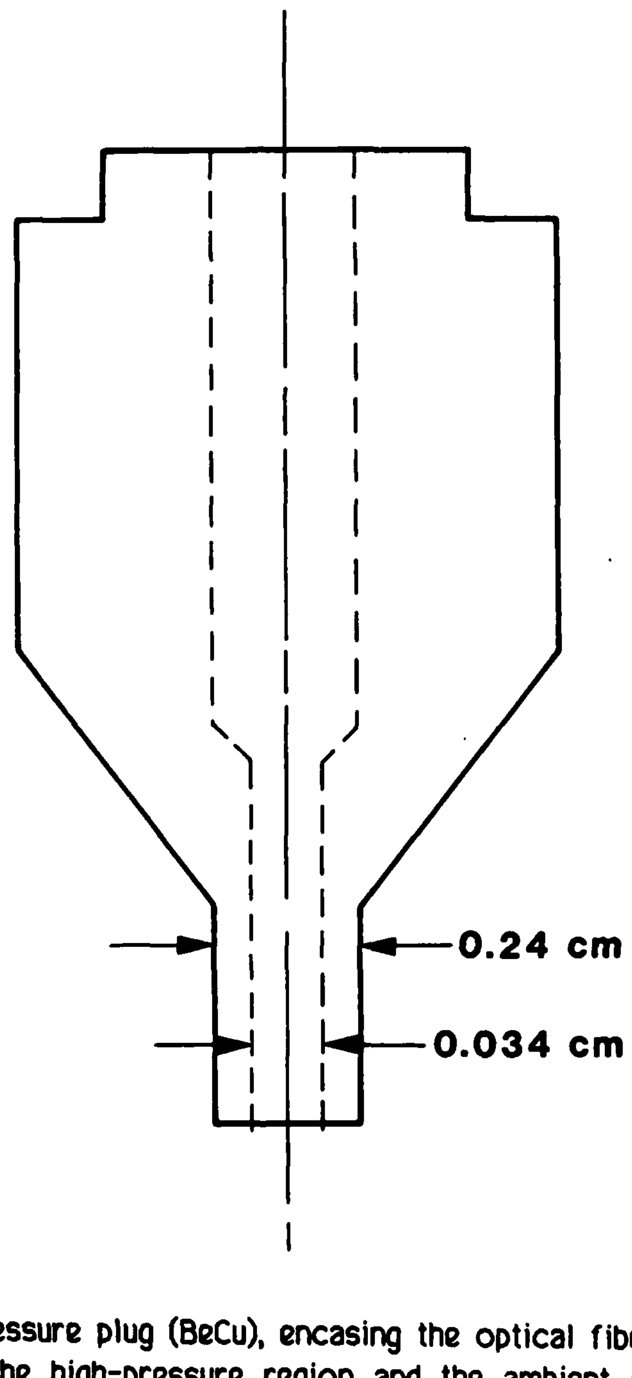

Fig. 5. The pressure plug (BeCu), encasing the optical fiber, provides the seal between the high-pressure region and the ambient atmosphere and allows optical access to the pressure region.

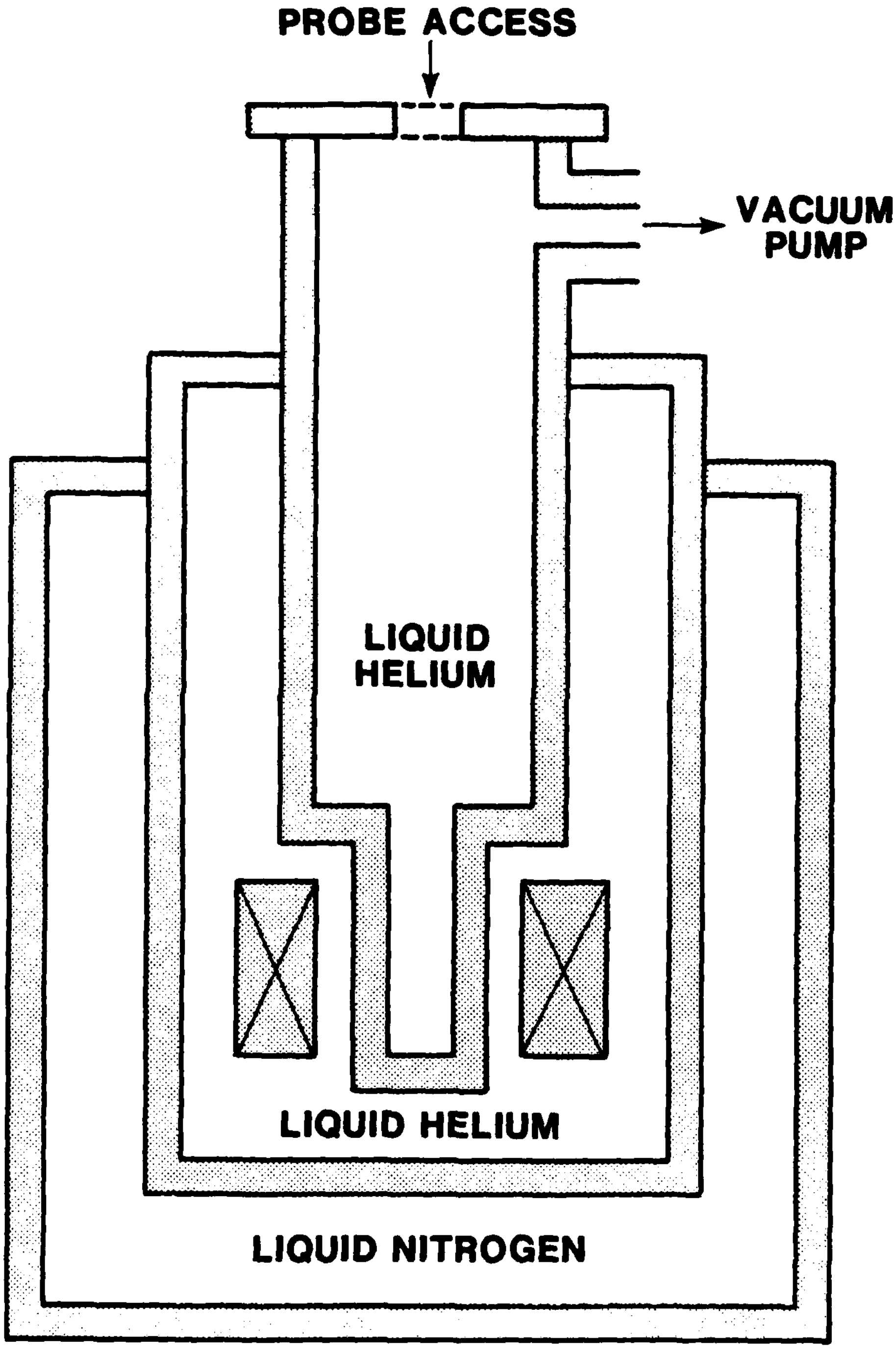

Fig. 6. Triple Dewar system showing magnet position and access ports.

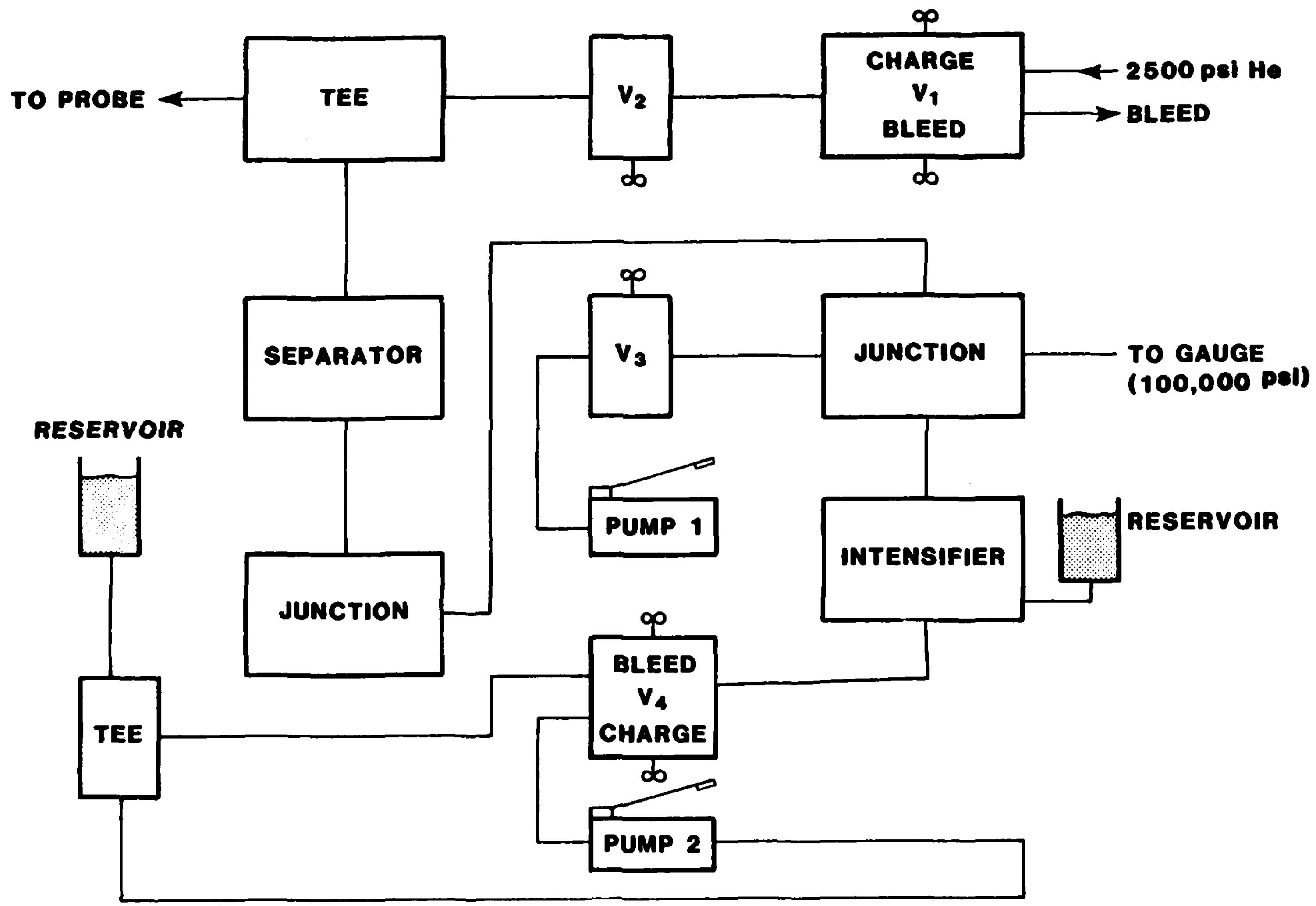

Fig. 7. Diagram of the pressure generating system.

of ~20,000 psi, and thereafter maximum pressure was attained using Pump 2. Detailed operating instructions are included under Experimental Procedures. After the system had been prepared for a data run, the actual measurement and data recording was controlled by a Computer Automated Measurement and Control (CAMAC) system developed by Dr. E. D. Jones of Sandia National Laboratory.[32]

E. Experimental Procedures

1. Fiber Preparation

A length of fiber was cut from the roll. The length had to be sufficient to allow raising the probe vertically above the Dewar assembly while the other end of the fiber was mounted in the adjustable fiber holder. Both ends of the fiber were cut using a fiber scribe, and examined under a 100× microscope for flatness. If carefully done, fiber P-27 did not need to be polished. The jagged aluminum coating was then removed from the ends with a NaOH solution. The fiber was inserted through the pressure plug and sealed. The seal was provided by Eccobond 285 Black with Catalyst 24LV, mixed in a ratio, by weight, of 100 parts Eccobond to 7-8 parts of Catalyst 24LV. Curing time at room temperature is ~24 hours. In order to locate the sealant in the critical region in the narrow part of the pressure

plug, a configuration as shown in Fig. 8 was used. The epoxy was inserted into the sleeve attached to the nipple of the pressure plug by using a pipette and was pulled down into the plug by a vacuum. The back seal during this process was provided by a rubber cap through which the fiber had been fed with a syringe which was then withdrawn. The vacuum was left on the system for approximately ten minutes after which the epoxy-filled upper sleeve was carefully cut off and the fiber cleaned. This had to be done since the plug does not fit into the pressure joint with the sleeve attached. The assembly was then left to cure.

2. Sample Attachment

After curing, the sleeve was removed and the fiber with pressure plug was inserted into the probe and secured in the pressure joint with the proper fitting. The compression exerted when the fitting was tightened served to improve the seal around the fiber. If the positon of the plug on the fiber was carefully measured, slightly over one inch of fiber protruded from the probe. The probe was then mounted vertically above an elevator stage. The end of the fiber and the sample were cleaned with methanol (and lens paper) and the sample, positioned on the stage, was brought up into

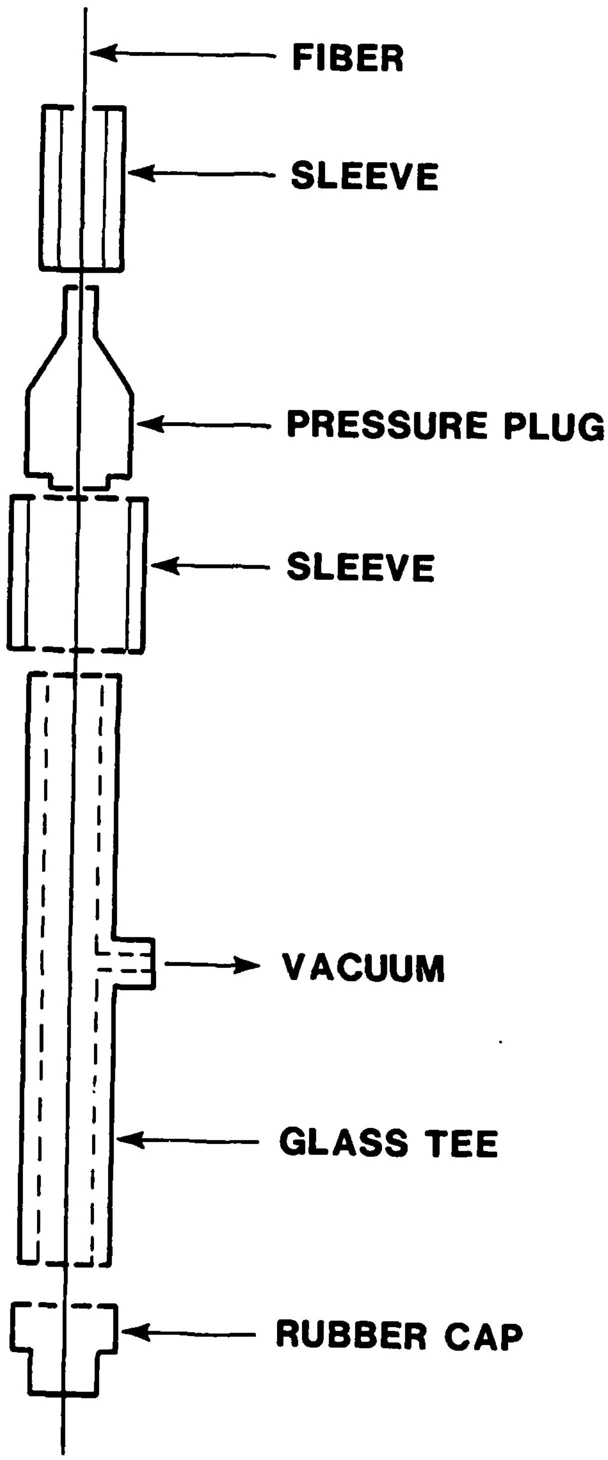

Fig. 8. Pressure plug holder used during sealing around the optical fiber.

contact with the fiber. Since the sample size was usually about 1/16 inch square, we generally tried to center the fiber on the sample. When the two were in contact the adhesive was prepared (GE 7031 plus 50% toluene/50% methanol). Upon reaching the desired consistency, it was applied to two sides of the fiber at the juncture with the sample. Care had to be taken to ensure that the sample did not become attached to the platform, or that the fiber shifted on the sample. If this occurs, the adhesive must be removed (acetone) and fiber and sample must be recleaned before starting anew. The adhesive, when properly prepared, dries quickly and allows attachment of the pressure chamber within one hour.

3. Alignment

The probe was then ready for insertion into the Dewar. After this had been accomplished, the other end of the fiber was positioned in the fiber holder. The Dewars could be filled at this point if only magnetic field measurements were planned, but a different procedure applies for pressure measurements. With the laser operating, the monochromator was scanned to locate the luminescence peak, and adjustments of the fiber position and optical elements were used to maximize the signal. If necessary, attenuators could be placed in the beam path.

4. Measurements of Magnetic Field Effects

With the system prepared as outlined above, the magnet was adjusted to the desired field strength and the energy interval to be recorded was selected. The monochromator was set to the starting point of the scan interval and data recording was controlled by the CAMAC system.

5. Measurements of Pressure Effects

When pressure measurements were intended, the procedure differed in that probe insertion had to include specific steps. To start with, the Dewars had to be filled to the appropriate levels before insertion was begun. Additionally, the system must be pressurized and a Cu-constantan thermocouple had to be attached to the chamber to give an indication of temperature. Step-by-step instructions for achieving the desired pressure with the system shown in Fig. 7 are given below. A full bottle of helium gas (~2500 psi) was connected to the system. Referring to Fig 7,

a. Open V2 and V1 Bleed (1/2 turn)

b. Open V1 Charge until hissing sound

c. Adjust hiss for slow rate with V1 Charge

d. Close V1 Bleed

e. Wait for system to charge to bottle pressure

f. Close V2 and V1 Charge

g. Open V1 Bleed

h. Close valve on Pump 1

i. Open V3

j. Use Pump 1 to ~20,000psi (or operating pressure, if less)

k. Close V3 and open valve on Pump 1

l. Open V4 Charge

m. Use Pump 2 to desire maximum pressure.

The system was depressurized by following the steps listed below, after closing the valve on the helium bottle.

a. Open V4 Bleed SLOWLY (to ~20,000 psi)

b. Close V4 Bleed

c. CAREFULLY open V3 for slow decrease to ~2500 psi

d. Close V3

e. Close V1 Bleed

f. Open V2

g. Open V1 Bleed until slow hiss.

With the system pressurized according to the outlined procedure, the probe was lowered slowly into the Dewar, while monitoring the

temperature with the thermocouple. It is important to lower the probe slowly enough that the thermocouple and pressure chamber can be considered to be in thermal equilibrium. When the freezing temperature of helium at the selected pressure was approached, the rate of descent was slowed to approximately 1 inch/hour to allow a uniform helium crystal to grow around the sample. Once the solid-liquid interface passed the sample, the rate of descent was increased. During this entire process the probe was suspended from a pulley arrangement, and a plastic bag was used around the probe at the top of the Dewar to prevent the access of air. The thermocouple was referenced to liquid nitrogen and the freezing temperature of helium was taken from P vs T charts.

Once the probe was in position, alignment and recording procedures were as before. In order to perform a measurement at another pressure, the probe was raised until the temperature of the chamber was above the helium melting point, the pressure was adjusted, and the process was repeated. This method is described in detail in Reference (31).

F. Samples

A large number of samples were examined in literally hundreds of experimental runs during the course of this experiment. Naturally many of

these runs were required to establish experimental procedures during the initial stages of the experiment and can not be counted as actual data runs. The samples ranged from bulk materials (GaAs, InGaAs) to single and multiple quantum well structures, as well as strained-layer superlattices. The quantum well and superlattice structures were constructed of alternating layers of different semiconductor materials with various layer widths and numbers of layers. Samples were predominantly of the type GaAs/AlAsorGaAs/$AL_xGa_{1-x}As$, and $In_xGa_{1-x}As$/GaAs, where the subscript x refers to the percentage of the particular component present in the layer. The number of layers ranged from the case of a single layer of GaAs sandwiched between two layers of AlAs in the single quantum well to multiple wells of six to twelve periods, and to superlattices with fifty or more periods. The typical sample included a substratum, a buffer layer, the alternating well and barrier layers, and a cap layer.

L. R. Dawson (SNL) grew the structures by molecular beam epitaxy on a <100> GaAs substratum.(33,34) The substratum was placed in a pressure- and temperature-controlled growth chamber, and effusion cell shutters were opened for specific time intervals to control the molecular beam depositions for the different layers. The advantage of this computer

controlled process lies in the accurate control it affords over layer thickness and composition.[35,36]

The potential energy profile of such a heterostructure is shown in Fig. 9. In the case of $GaAs/Al_xGa_{1-x}As$, the GaAs wells are bounded by AlGaAs barriers whose height is determined by the fraction of Al present. For values of $x \leq 0.4$, $Al_xGa_{1-x}As$ maintains a direct gap at Γ.[37] Electron and hole energies are quantized, with levels for "heavy" and "light" holes in the valence band wells, and transitions between electron and hole states conform to the selection rule $\Delta n = 0$. In this particular structure strain effects are negligible since a good lattice match exists. The wells can be quite rectangular with nominal depth of ~85% of ΔE_g for the conduction band, and ~15% of ΔE_g for the valence band,[38] and the gap at T = 0 K given by [39]

$$E_g \approx 1.52 + 1.52X \quad (\text{eV}). \tag{84}$$

The band gap difference, ΔE_g, has been determined empirically to be[37]

$$\Delta E_g = 1.155x + 0.37x^2 \quad (\text{eV}). \tag{85}$$

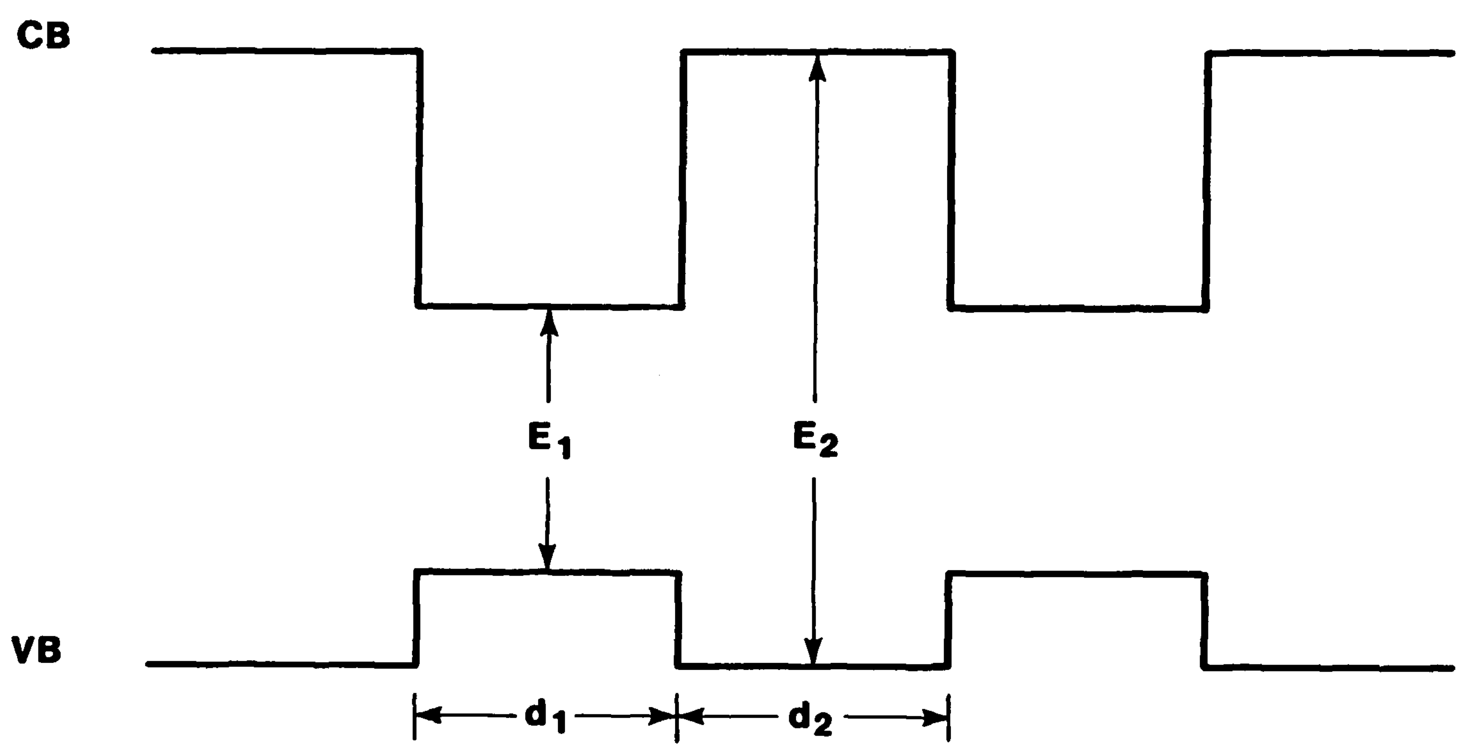

Fig. 9. Potential energy profile of heterostructure with alternating layers of thicknesses d_1 and d_2 and gap energies E_1 and E_2.

In the case of $In_xGa_{1-x}As/GaAs$ structures, the GaAs layers form the barriers for the InGaAs wells, where the amount of In present determines the minimum gap energy. In this situation GaAs remains transparent near the InGaAs gap, and this gap is given by

$$E_g \approx 1.52 - 1.601x + 0.536x^2 \quad (eV). \qquad (86)$$

These structures, unlike GaAs/AlGaAs, are not lattice matched. Although this can result in dislocations in thick layers, the mismatch is fully accomodated by strain if the layers are thin enough. If the orientation of the superlattice is in the <100> direction, the strain can be decomposed into hydrostatic and uniaxial <100> components.[40] The hydrostatic strain results in an increase in E_g, while the uniaxial component lifts the degeneracy of the valence band maxima.[41] The expression for E_g, Eq. (86), does not include this effect. A value of $x = 0.25$ corresponds to a lattice mismatch of 1.8%,[40] and the value of E_g as a function of lattice constant is shown in Fig. 10.

In simple photoluminescence measurements, these samples are expected to show a single peak from the InGaAs well due to diffusion of

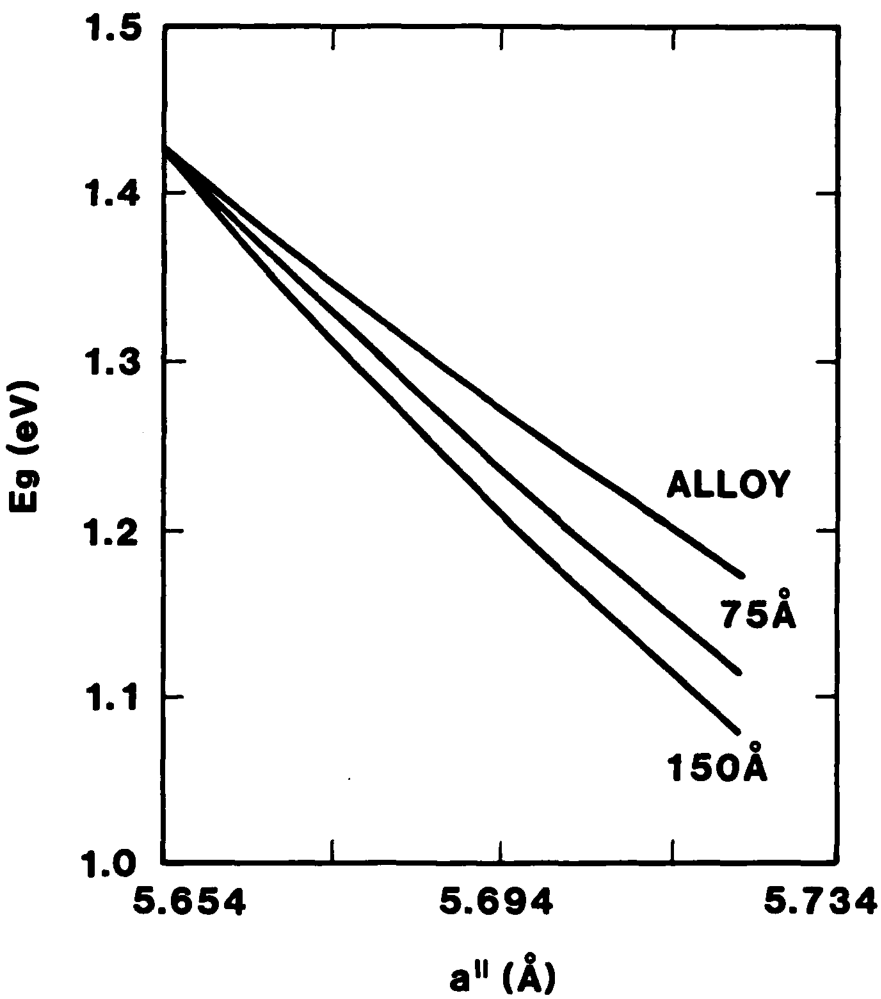

Fig. 10. Band gap of GaAs-In_xGa_{1-x} As as a function of lattice constant parallel to the interface. The curve labeled Alloy refers to bulk InGaAs, and the dimensions listed apply to the layers of both materials (in different samples).(40)

the carriers to the well before recombination. The transition involves the first quantum well levels and may also involve exciton effects.(33,42) The position of the peak energy is a function of the amount of In and the well width. The application of hydrostatic pressure, as in our experiment, is then expected to shift this peak to higher energy without altering its shape. For GaAs/AlGaAs structures, experiments have shown that in undoped samples exciton recombination is the dominant radiative process, while intrinsic band-to-band recombination dominates in modulation doped samples.(43)

A major difference between the multilayer heterostructures and bulk alloy materials is the effect on optical properties resulting from the periodicity of the layers, especially when the layer thickness approaches the DeBroglie wavelength of the electronic particle. This limitation on carrier motion in the direction normal to the layers is then analogous to the confinement of carriers to a one-dimensional potential well. If the well depth is considered to be infinite, then the energy can be written, for $L_z \ll L_x, L_y$, as

$$E = E_n + (\hbar^2/2m)(k_x^2+k_y^2), \tag{87}$$

where $E_n = (\hbar^2/2m)(n\pi/L_z)^2$, $n = 1, 2, 3, \ldots$.

For each value of E_n a two-dimensional energy band forms in the $k_x k_y$ plane and, as L_z decreases, the energy of the discrete band states will increase. This is the quantum size effect. The confinement effect on excitons has been discussed earlier.

When the barrier thickness is large, optical effects, e.g. absorption, are basically described by the single well. However, when wells are brought close together by reducing the thickness of the finite barriers, the coupled-well regime is reached. The interaction between the bound states then splits these levels. For a small number of coupled wells the splitting can be detected. For example, transitions involving symmetric and anti-symmetric combinations of the n = 1 bound states yield a fine structure within this level. As the number of coupled wells increases, this discrete structure tends to disappear and a broad band (several meV) appears in the superlattice regime.

We now calculate the band edge effective masses for $In_xGa_{1-x}As$. In order to do this we used the expressions for energies developed by the $\mathbf{k}\cdot\mathbf{p}$ method, as given in Eqs. (37), and first obtain the values of the constants

for this materials. Interpolating between the $E(\Gamma_i)$ values of InAs and GaAs,[44] we have, for $x = 0.2$:

$E(\Gamma_{15V}) = 0$, $E(\Gamma_{1C}) = 1.28$, $E(\Gamma_{15C}) = 4.56$, $E(\Gamma_{12C}) = 12$, $\epsilon_p = 25.2$, $\Delta = 0.35$, all in eV. Using these values, we obtain

$$F = -16.33,\ M = -3.77,\ G = -0.95,\ A' = -1.52,\ L = -18.23,\ N = -19.15.$$

From Eqs. (37), we then have for the effective masses in the <100> direction,

$$m_e = 0.056m_0 \quad (0.058m_0)^{(40)}$$

$$m_{hh} = 0.36m_0 \quad (0.35m_0)^{(41)}$$

$$m_{lh} = 0.08m_0 \quad (0.09m_0)^{(41)}$$

$$m_{so} = 0.16m_0 .$$

The values in parentheses were taken from the references indicated and were obtained by other methods. The close agreement adds validity to our model.

The primary sample (M316) selected for presentation in Section VII was a strained layer superlattice composed of 60 periods of $In_xGa_{1-x}As/GaAs$, grown on an $In_{0.1}Ga_{0.9}As$ buffer layer atop a <100>

p-type GaAs wafer. Well and barrier thicknesses were 120 angstrom each, the buffer layer was 1μm thick, and the GaAs barrier layers were doped with Si over 20 angstrom at their centers. Strain in this sample was 0.7%. Carrier concentration was 9.6×10^{11} cm^{-2}, and mobility was 23,000 cm^2/V sec at 4 K.[45]

AD-A166 419 MAGNETO-OPTIC STUDIES OF SEMICONDUCTOR STRUCTURES AT HYDROSTATIC PRESSURE..(U) AIR FORCE INST OF TECH WRIGHT-PATTERSON AFB OH H ACKERMANN DEC 85 2/2

UNCLASSIFIED AFIT/CI/NR-86-25D F/G 20/12 NL

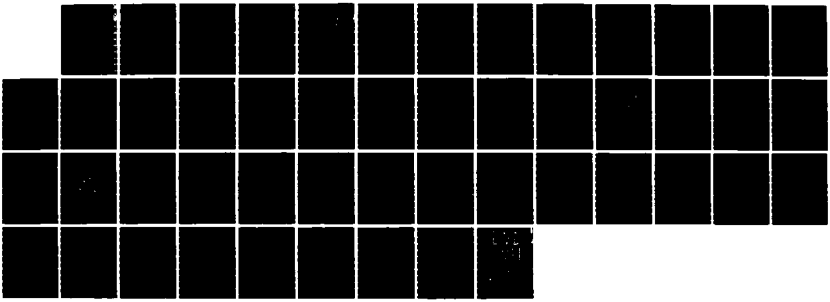

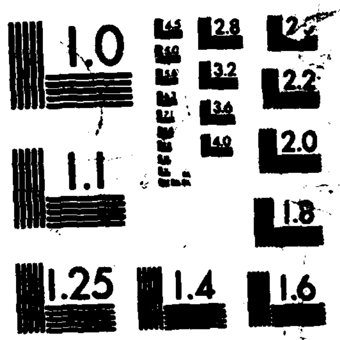

MICROCOP CHART

VII. DATA AND RESULTS

A. Hydrostatic Pressure and Magnetic Field Effects

As mentioned in the discussion of samples in Section VI, we selected Sample M316, an $In_{0.2}Ga_{0.8}As/GaAs$ strained layer superlattice, to show the effects of hydrostatic pressure and also the appearance of the Landau levels with increasing magnetic field. The strain in this particular sample (0.7%), due to the lattice mismatch, lifts the valence band degeneracy and presents us with the simple-band situation covered by the calculations at the beginning of Section V. We can therefore anticipate the energy values of the Landau levels from the relation (cgs)

$$E_n \approx E_0 + (n+1/2)\hbar\omega_c = E_0 + (n+1/2)\hbar eB/\mu c,$$

where μ is the reduced effective mass.

Since the pressure coefficients for GaAs and other Group III-V materials at Γ are all approximately 0.012 ± 0.002 eV/kbar,[14] we can expect the shift of E_g with pressure to be described by

$$E_g(P) \approx E_g(0) + 0.012P,$$

where E is in eV and P in kbar.

From the combination of pressure and magnetic field data, we can then

determine the value of the energy gap of the material and its dependence on the external parameters, as well as the reduced effective mass, μ, and $\Delta\mu(P)$. Figures 11 and 12 show the luminescence spectra at a pressure of 1 bar, B=1 and 60 kG respectively. Although data were taken at many other values of the magnetic field, these examples are representative of the spectral structure observed and clearly show the Landau levels at the higher field value. These experimental runs were then repeated with different amounts of pressure applied to the sample. Figures 13 and 14 show the spectra at $P \approx 4$ kbar and $B \approx 1$ and 60 kG, repectively. In these figures the logarithmic intensity has been added (broader curve, right-hand scale) since the Landau levels are easier to discern in this manner.

Comparing the linear spectra at P = 1 bar and $P \approx 4$ kbar, and noticing the identical shapes, we have good evidence that the sample was, in fact, subjected to almost pure hydrostatic pressure. Spectra obtained at $B \approx 1$ kG for various pressures are, except for the peak shift, indistinguishable. This is an excellent validation of the pressure generating technique.(31)

An indication of the shift of the luminescence peak energy with pressure is shown in Fig. 15, with spectra taken at P = 1 bar, ~2 kbar, ~4 kbar (left to right), and $B \approx 60$ kG. The small variation in these spectral

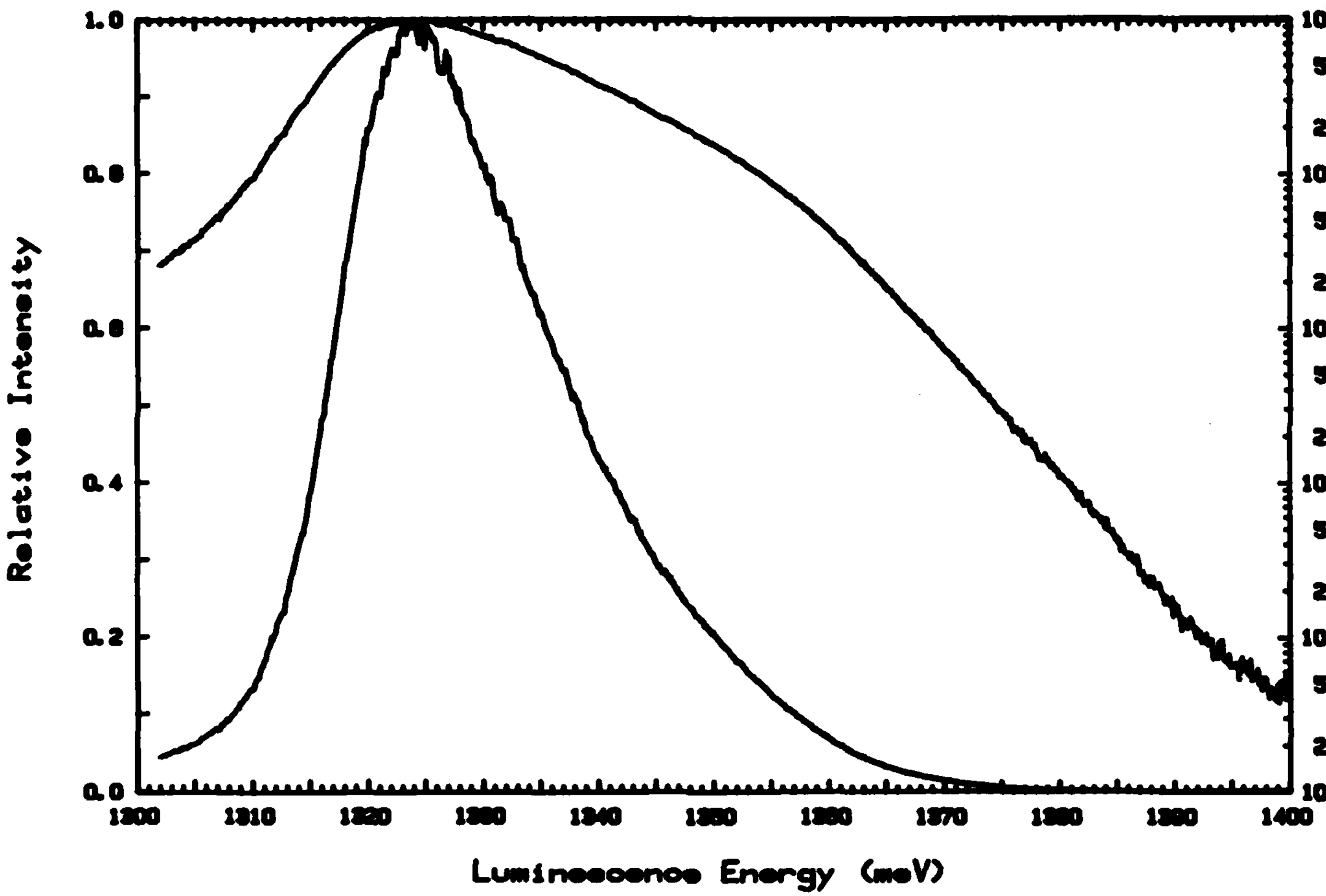

Fig. 11. Luminescence spectrum of Sample M316 with P = 1 bar, B ≈ 1kG. Broader curve represents the logarithmic intensity.

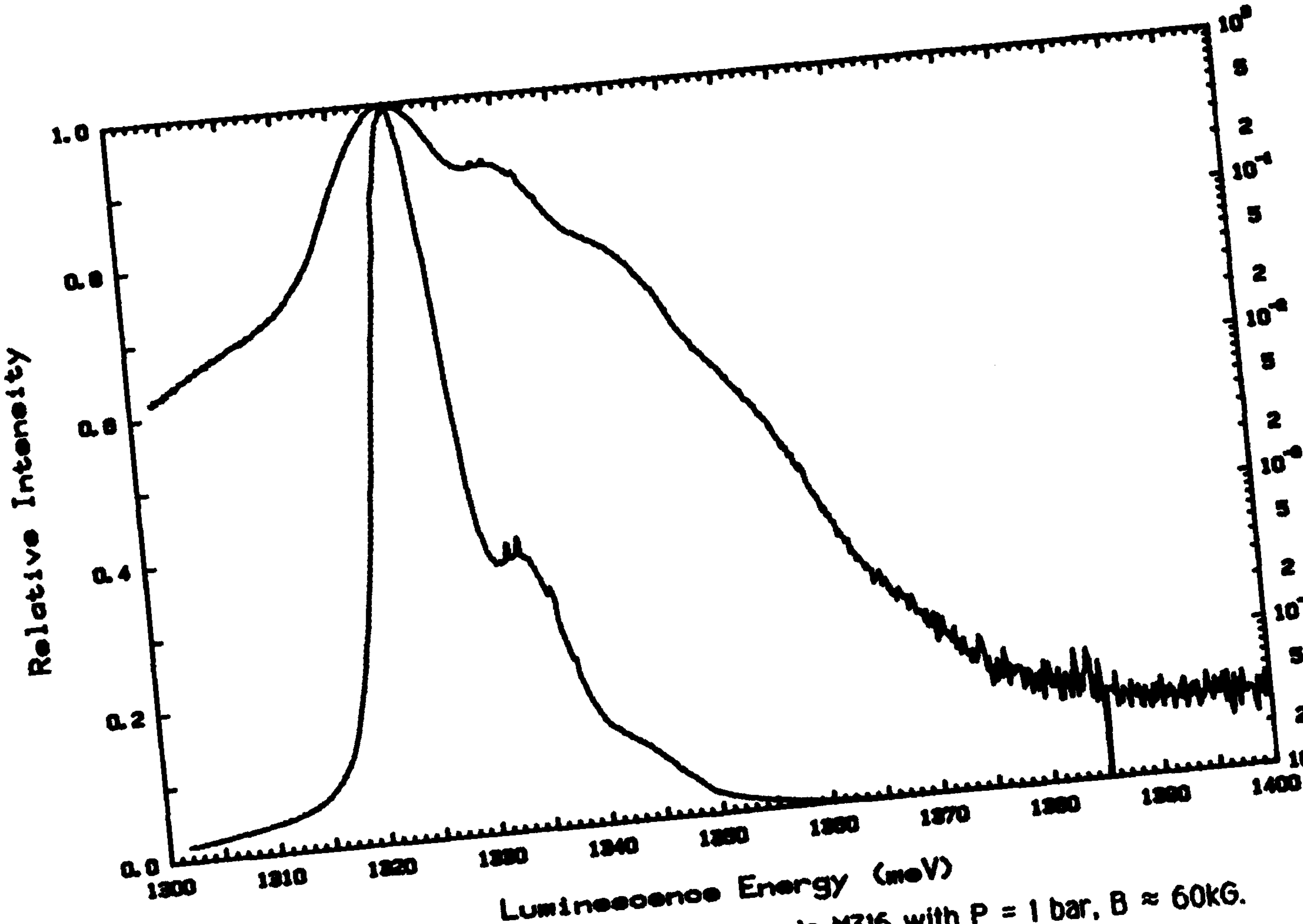

Fig. 12. Luminescence spectrum of Sample M316 with P = 1 bar, B ≈ 60kG. Broader curve represents the logarithmic intensity.

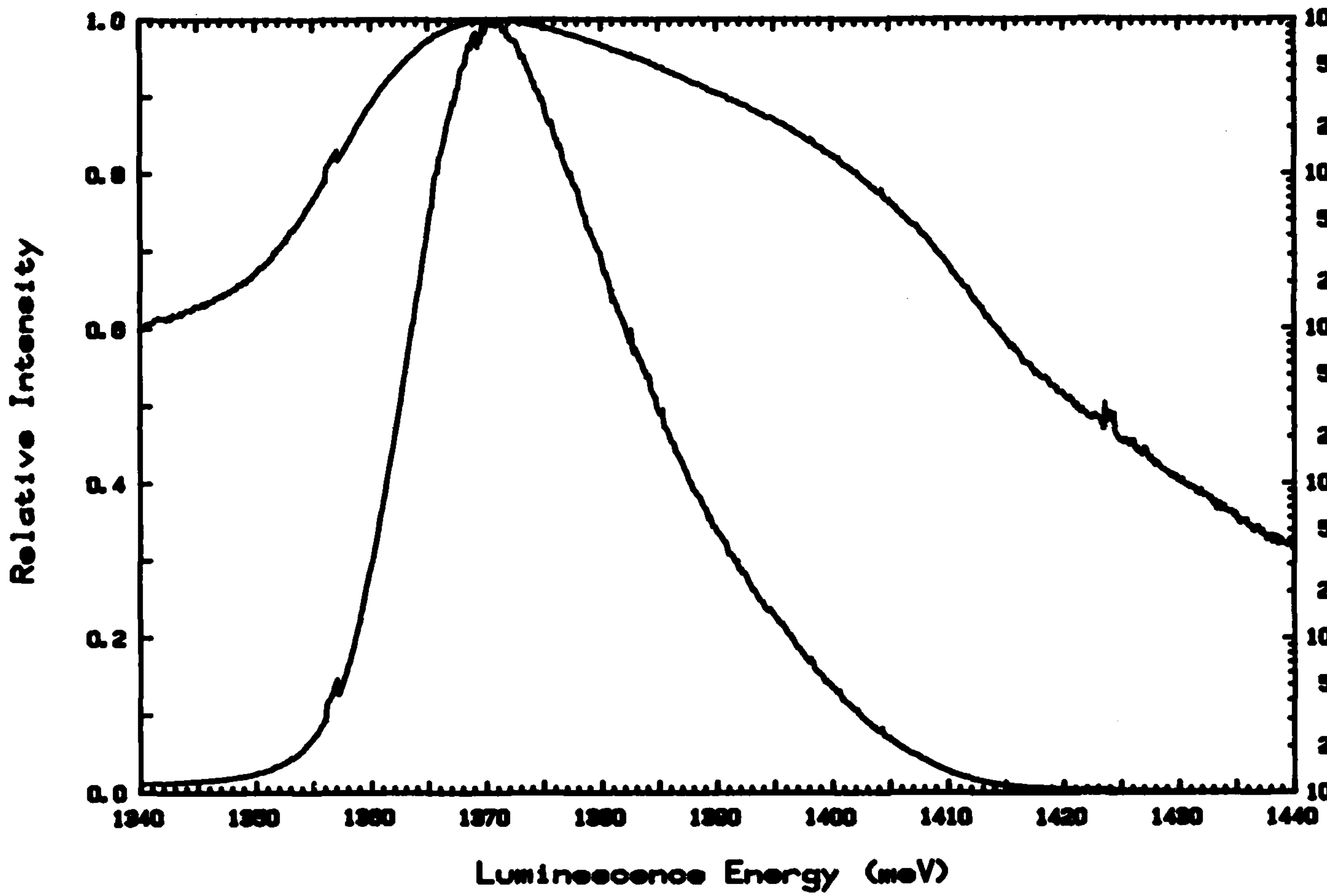

Fig. 13. Luminescence spectrum of Sample M316 with P ≈ 4 kbar, B ≈ 1kG.
Broader curve represents the logarithmic intensity.

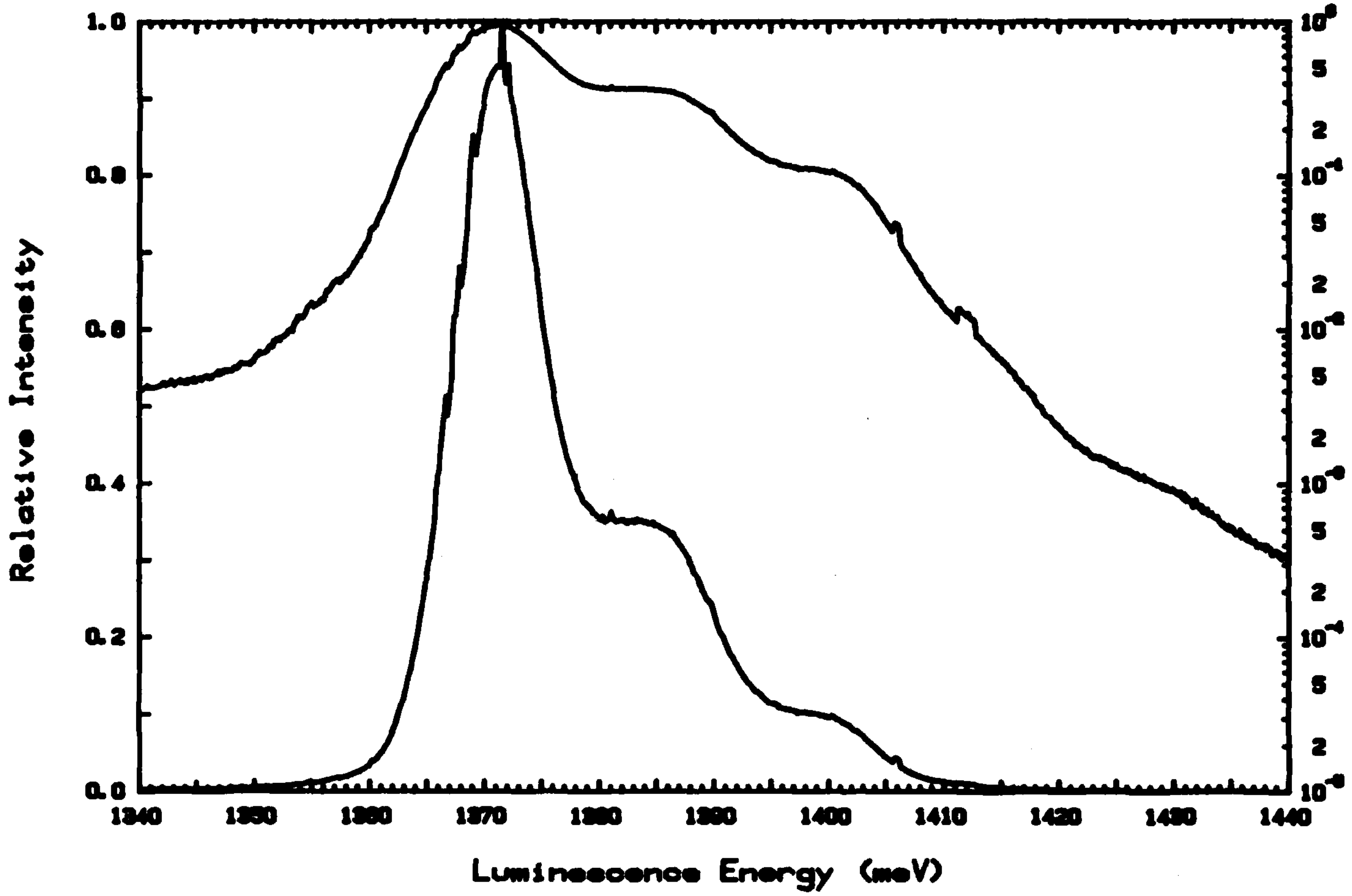

Fig. 14. Luminescence spectrum of Sample M316 with P ≈ 4 kbar, B ≈ 60kG. Broader curve represents the logarithmic intensity.

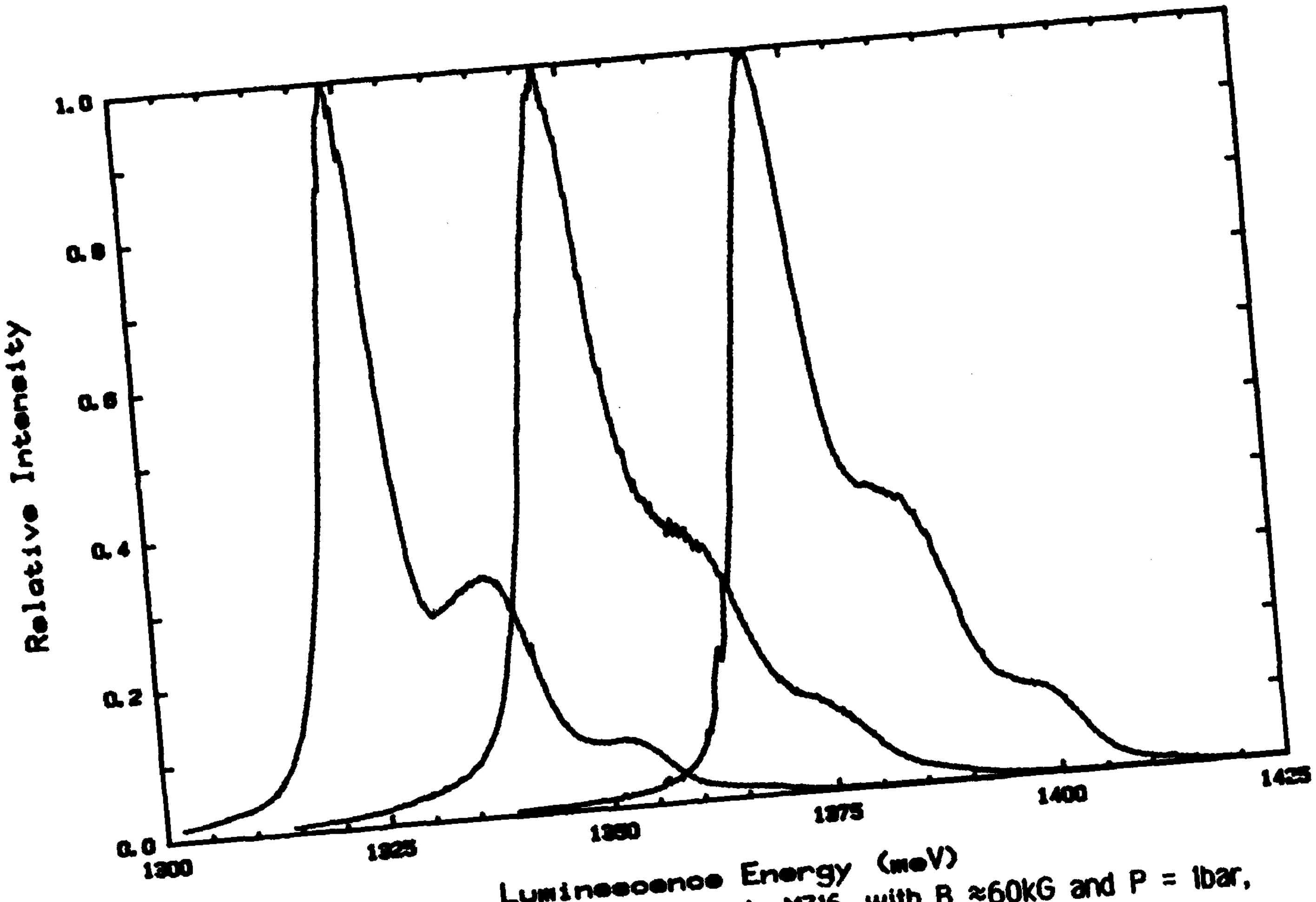

Fig. 15. Luminescence spectra, Sample M316, with B ≈60kG and P = 1bar, ≈2 kbar, ≈4kbar (left to right), showing peak-energy dependence on pressure.

curves resulted from the fact that these curves are from different run-series with varying power levels and monochromator slit settings, and do not indicate non-hydrostatic pressure effects. A least squares fit to the peaks as a function of pressure gives an indication of the pressure dependence of the band gap, $\Delta Eg \approx 0.0122$ eV/kbar. This is shown in Fig. 16. We can thus write

$$E_g(P) \approx E_g(0) + 0.0122P,$$

where $E_g(0)$ is the value of the energy gap in eV and P is in kbar. The measured pressure dependence thus falls almost into the middle of the expected range.

The positions of the Landau level energies as a function of magnetic field result in the classic "fan-diagram" shown in Fig. 17, for T = 4 K and pressure of 1 bar. The numbers associated with the different rays of the fan indicate the particular level (n=o,1,2,...). Similar results were obtained for other values of pressure with the appropriate shift of the y - axis intercept. Information obtainable from these plots includes E_g and the reduced effective mass. A good approximation of the energy gap of the material is obtained from the intersection of the rays ($n \geq 2$) with the

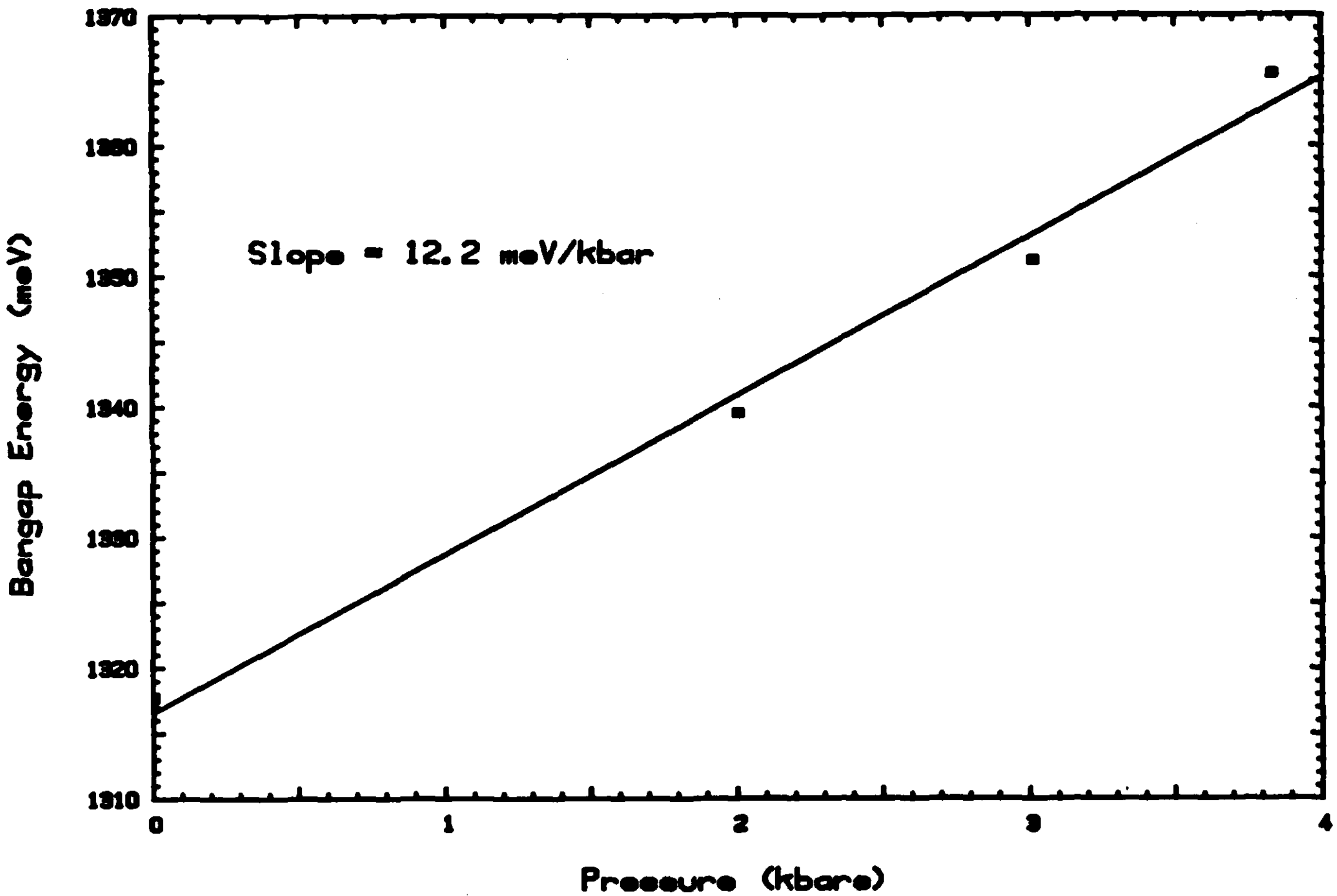

Fig. 16. Dependence of the band-gap energy on pressure, Sample M316.

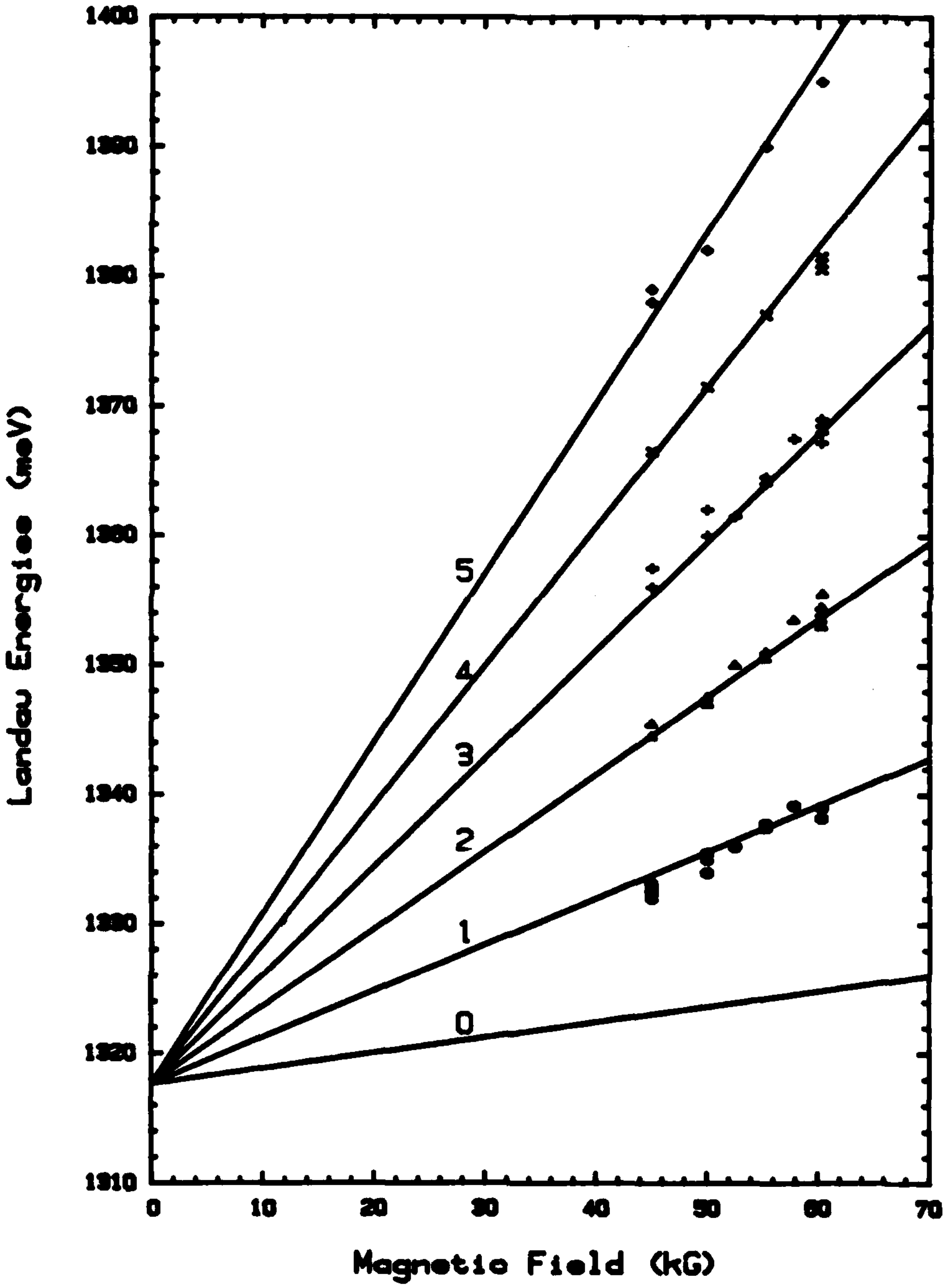

Fig. 17. Landau level energies as function of magnetic field, Sample M316, at T = 4 ^{0}K, P = 1bar.

y-axis at zero magnetic field. The reduced effective mass was obtained from the slopes of the lines, where we considered

$$E_n \approx E_0 + (n+1/2)\hbar\omega_c = (n+1/2)\hbar eB/c\mu.$$

Another way to look at the data shown in Fig.17 is to plot the Landau level energies as a function of the normalized magnetic field, (n+1/2)B. This places all the experimental points along one line and thus provides a simpler tool for analysis. This was done in Fig. 18 for P = 1bar.

The intercepts in Figs. 17 and 18 show $E_g \approx 1.318$ eV. As a first order approximation we have, for the direct gap in $In_{0.2}Ga_{0.8}As$,

$$E_g \approx 1.52 - 1.601x + 0.536x^2, \tag{88}$$

or $$E_g \approx 1.2212 \text{ eV}.$$

To this value we must add the changes in levels due to the wells in the conduction and valence bands. Using the effective masses from the $k \cdot p$ method and, for this approximation, assuming infinite wells,

$$E_1 = (\hbar^2\pi^2/2m^*L_z^2),$$

where m^* is the effective mass and L_z the width of the well,

we have,

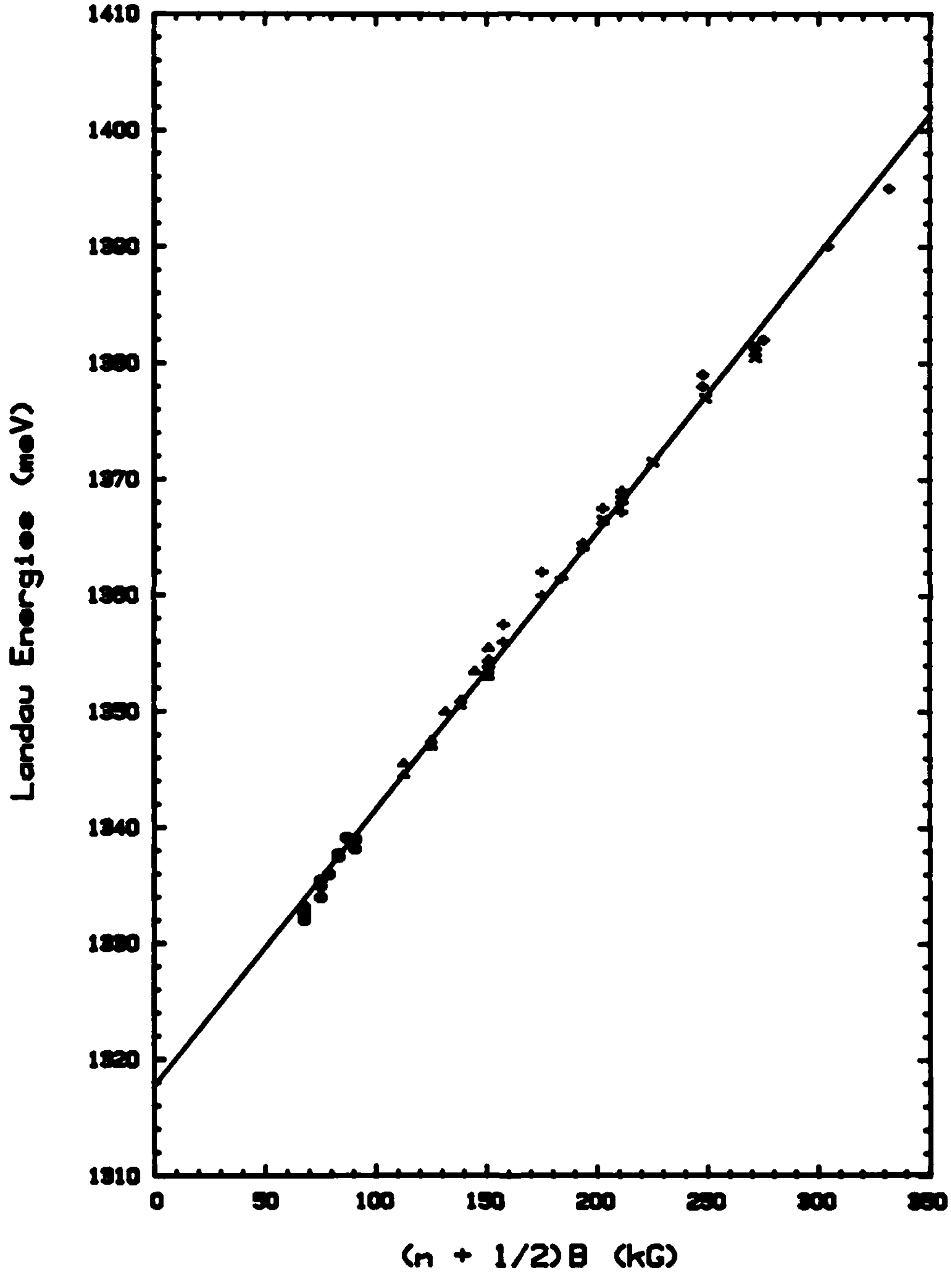

Fig. 18. Landau level energies as function of normalized magnetic field, Sample M316, at T = 4 ^{0}K, P = 1 bar.

$$E_{1,c} \approx 0.0441\ \text{eV},\ E_{1,hh} \approx 0.0069\ \text{eV},\ E_{1,lh} \approx 0.0309\ \text{eV}.$$

Since we are dealing with a conduction band to light-hole band transition,[45] we obtain as an estimate of the energy gap, $E_g \approx 1.296$ eV. This calculated value differs somewhat from the experimental result (by ~20meV), but is within the range of variation observed across samples. Thus, if at the point of investigation L_z is 100 instead of the reported 120 angstrom, the calculated energy gap would be $E_g \approx 1.324$ eV, much closer to the experimental value.

The least-squares value for the slope in Fig. 18 is $\mu^{-1} = 20.7 \pm 0.2$ (in terms of m_0). The electron effective mass, from a conduction band to acceptor level transition, was found to be $m_e = 0.069m_0$.[45] Using this value along with the experimental reduced effective mass, we can determine the effective hole mass involved in this transition. From

$$1/\mu = 1/m_e + 1/m_h$$

we have $m_h = 0.16m_0$.

Although this mass is larger than the light hole mass calculated from the k·p method, it is in excellent agreement with the value obtained from

oscillatory magnetoresistance measurements, $m_h = 0.16m_0$. Similar magneto-resistance measurements on many p-type samples gave results for m_h ranging from 0.13 to $0.17m_0$.[45] A possible explanation for this difference between the calculated and measured value may be the change in the band structure of the superlattice versus the bulk material.[45]

In Fig. 19 we show the pressure dependence of the Landau level energies plotted against the normalized magnetic field. The pressures are, from top to bottom: 3.83 kbar, 3.013 kbar, 2.005 kbar, and 1 bar. The reduced effective masses may be obtained from the slopes of the fitted lines. If we consider

$$(n+1/2)\hbar e/\mu = \Delta E/\Delta B,$$

and write $\mu = xm_0$, then we have

$$(n+1/2)1.16\times10^{-2}/x = \Delta E/\Delta B \ \ (\mathrm{meV/kG}),$$

and

$$x = 1.16\times10^{-2}(n+1/2)/\Delta E/\Delta B.$$

For the pressures listed, we obtain, in the same order,

$$\mu^{-1} \sim 19.3\pm0.3,\ 19.7\pm0.2,\ 20.4\pm0.3,\ \text{and}\ 20.7\pm0.2.$$

Taking the two extremes, P = 1 bar and P = 3.83 kbar, and plotting them as in Fig. 20, we see the pressure dependence of the reduced effective mass.

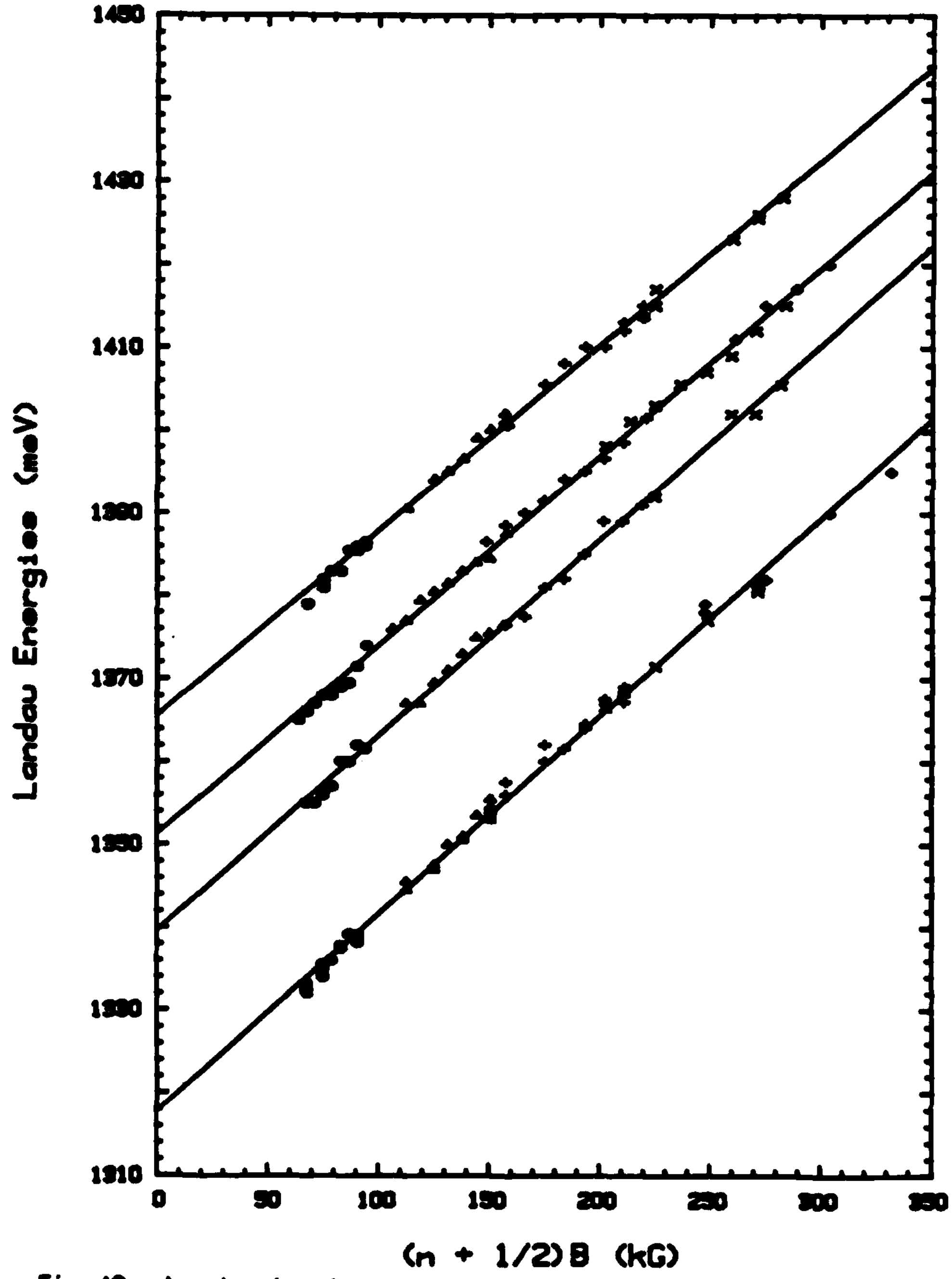

Fig. 19. Landau level energies as function of normalized magnetic field, Sample M316, at T = 4 ^{0}K, P = 3.830 kbar, 3.013 kbar, 2.005 kbar, and 1 bar (top to bottom).

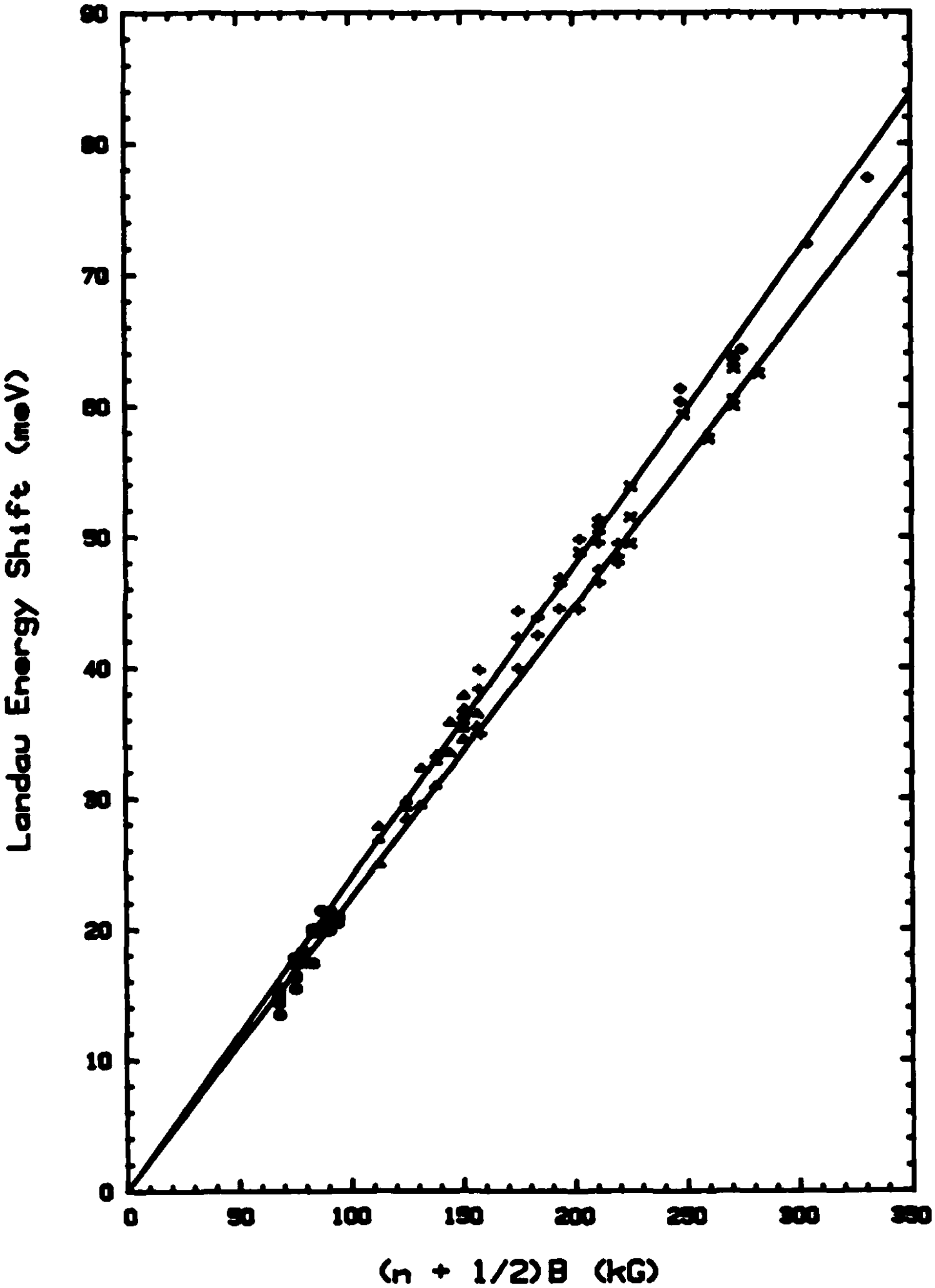

Fig. 20. Landau level energies as function of normalized magnetic field, Sample M316, at T = 4 ^{0}K, P = 1 bar (upper) and P = 3.83 kbar (lower).

Plotting the percentage change of the data points of effective mass versus pressure, as in Fig. 21, yields a rough estimate for the pressure effect on the reduced effective mass. The experimental value of 1.2 %/kbar is comparable to the calculated change of 0.8%/kbar[46]. For this calculation we used the mass terms as in Eqs. (37) and the pressure dependent constants as developed in Section IV, along with the interpolated values for the energy levels. We obtained the conduction band effective mass from the the expression

$$1 + A'(E_1-E_0)/(E_1-E_0+\Delta E_1-\Delta E_0) + 2P_M{}^2/3(E_0+\Delta E_0) + P_M{}^2/3(E_0+\Delta_S+\Delta E_0),$$

and the light hole effective mass from

$$1 + 2FE_0/3(E_0+\Delta E_0) + 4GE_2/3(E_2+\Delta E_2) + ME_1/3(E_1+\Delta E_1),$$

where the constants, including P_M, were given in Section III and

$\Delta E_i \equiv (\partial E_i/\partial P)_T \Delta P$, as before. Carrying out the calculations for pressures of 1 bar and 4 kbar, we found a percentage change for the reduced effective mass of ~ 0.83%/kbar.

We discussed earlier that in undoped GaAs/Al(Ga)As structures transitions are exciton dominated. An example of a luminescence spectrum showing this is given in Fig. 22. The three curves shown are for values of

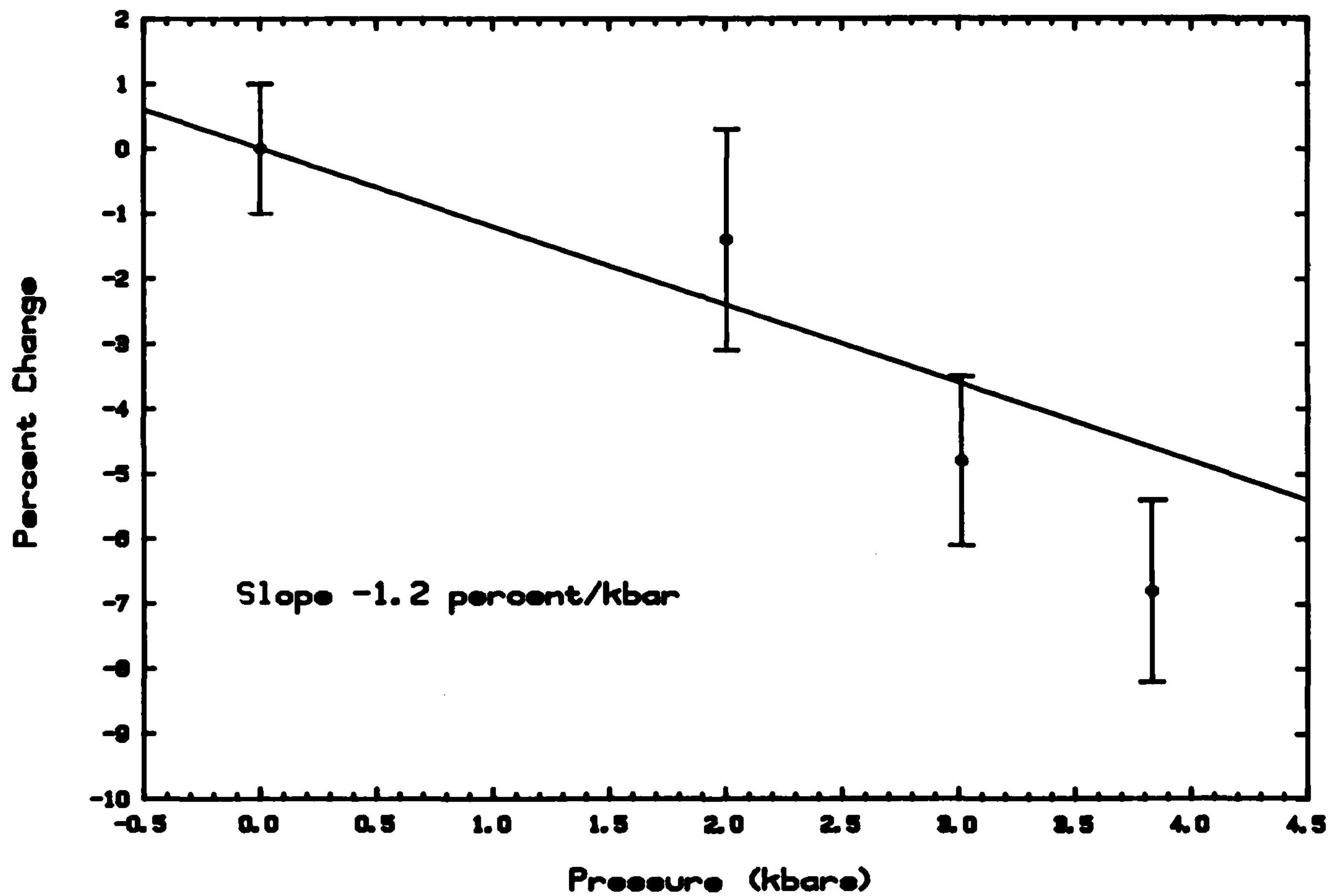

Fig. 21. Percentage change of effective mass with pressure for the selected data points yields an estimate of the pressure dependence of the reduced effective mass.

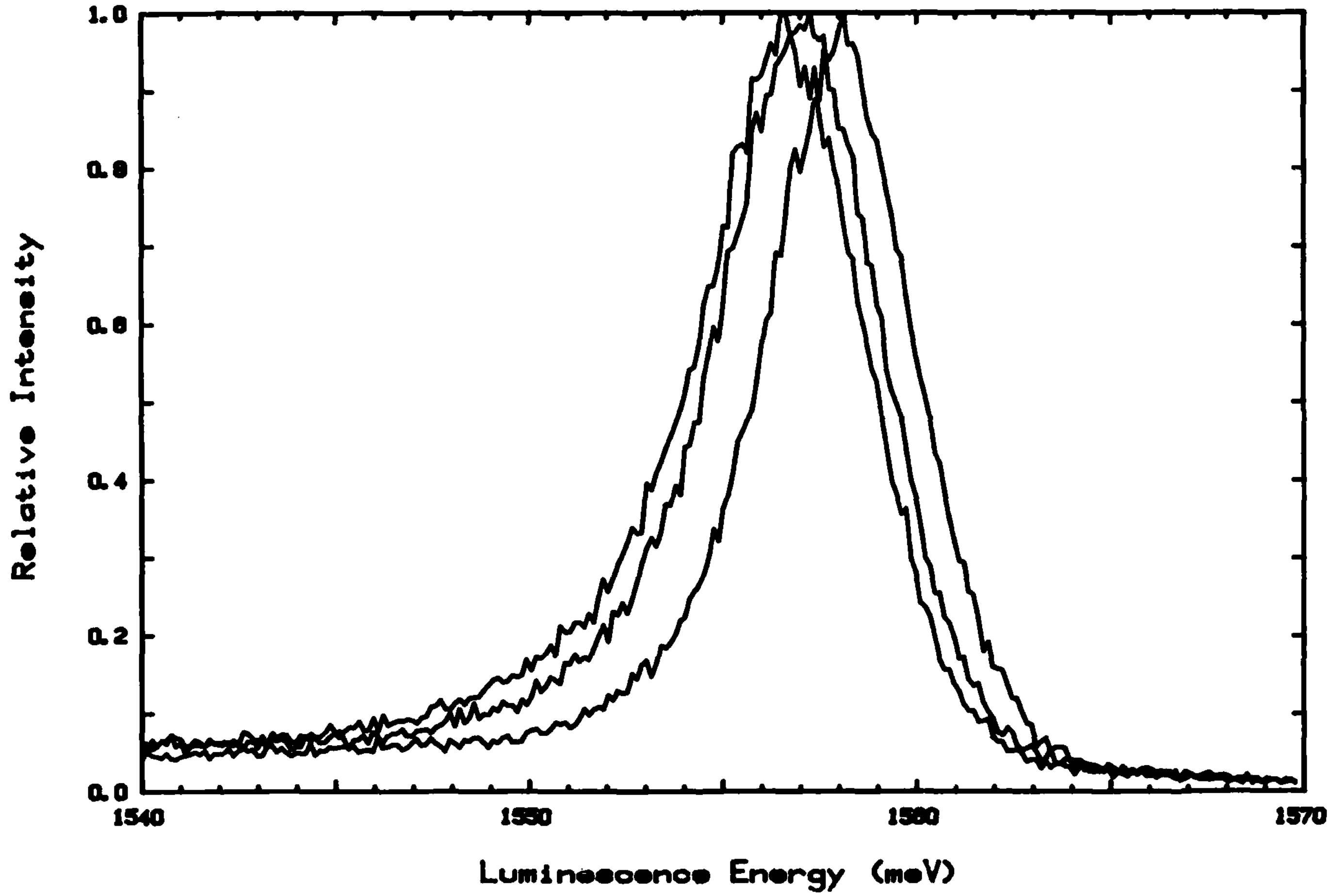

Fig. 22. Exciton-dominated luminescence spectra, Sample T0082 (GaAs/AlGaAs), at T = 4 ^{0}K, P = 1 bar, and B = 0 kG, 27.530 kG, 55.547 kG (left to right).

$B = 0$, 27.530, 55.547 kG, from left to right. This sample, T0082, is a GaAs/AlAs quantum well structure with 60 Angstrom wells and 25 Angstrom barriers. Data were taken at T = 4 K, P = 1 bar. In addition to the quantum well transitions shown, this sample also exhibited luminescence peaks near 1490 meV (impurity) and near 1515 meV (GaAs layer). Peak positions for all three transitions are plotted against magnetic field in Fig. 23, with a curve fitted to the GaAs transitions. The quadratic nature of the shift over the range of magnetic field investigated is clearly evident. The amount of the shift is, however, significantly larger than indicated by Eq. (83). Using GaAs effective masses as calculated we obtain $R_y^* \approx 4.2$ meV and $\hbar\omega_0 \approx 9.2$ meV, giving,

$$\Delta E \sim (5/8)(1/2)^4(\hbar\omega_0)^2/R_y^* \approx 0.8 \text{ meV},$$

for B = 60 kG. This compares to an observed shift of ~ 2 meV. The discrepancy is due to the fact that Eq. (83) has been developed for a fully confined 2-dimensional exciton. Exciton energy shift due to a magnetic field however depends on the exciton diameter which increases with L_z.[28] Our experimental results agree closely with those obtained by others.[47]

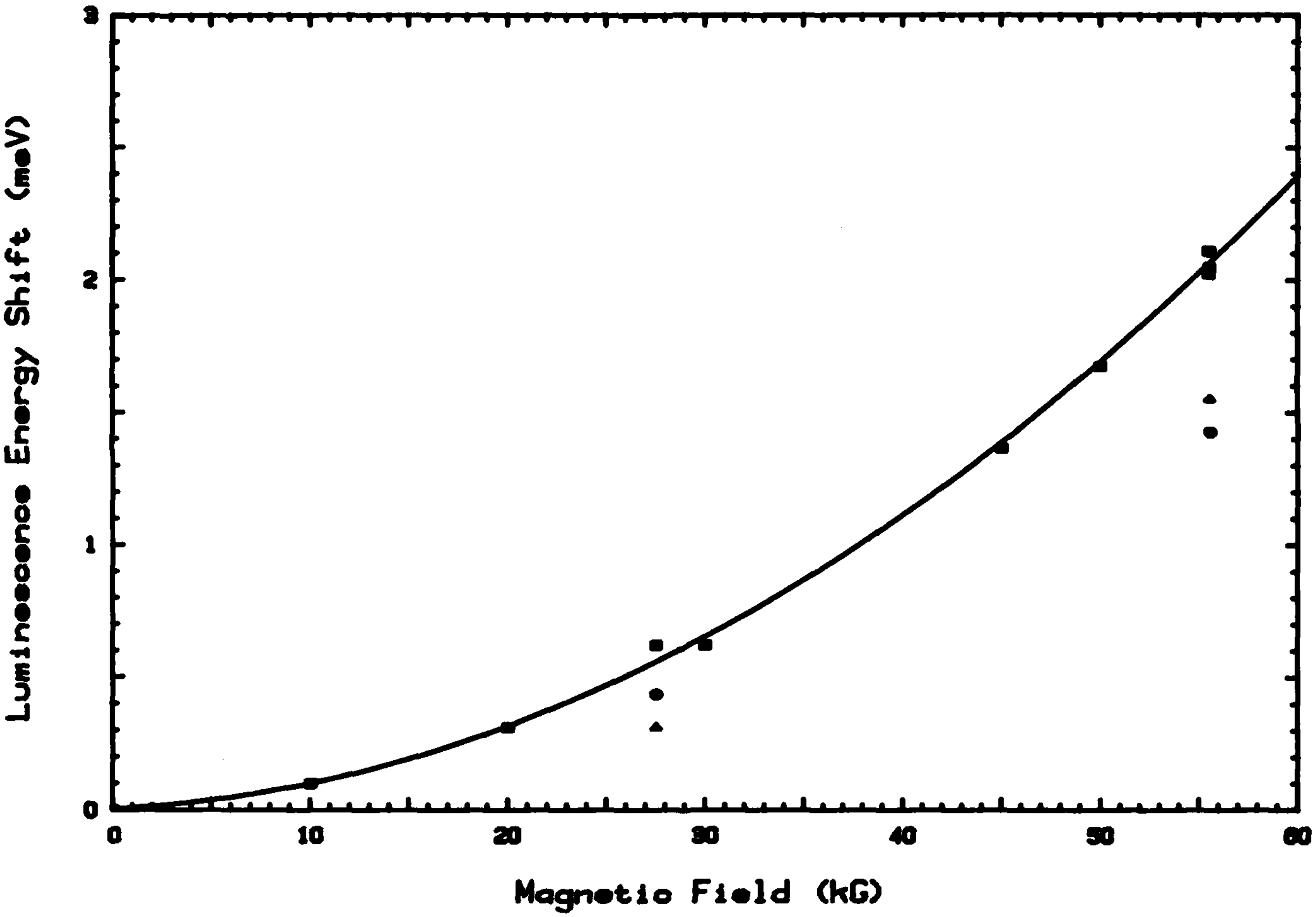

Fig. 23. Sample T0082 peak-energy shifts with magnetic field. Squares denote GaAs layer peaks; triangles denote impurity peaks; solid circles denote quantum wells.

B. Temperature Effects

Since the primary purpose of our experiment concerned low temperature ($\leq$4K) pressure and magnetic field effects, temperature effects, per se, were not investigated in detail. However, for completeness, we conducted several experimental runs, with temperature as the variable, to determine the temperature induced shift of the luminescence peaks. This was accomplished with a slightly different experimental configuration than described in Section VI. For these measurements, the sample was mounted in a vacuum on the cold head of a CTI-Cryogenics closed cycle helium refrigerator and illuminated by the laser beam through a window in the Dewar. The refrigerator was capable of providing sample temperatures in the range of 10 - 300K. As in the main experiment, the fluorescence signal was directed to the monochromator and recorded. The results for a selected sample (T00066), a GaAs/AlAs multiple quantum well structure with layer thicknesses of 40 and 25 angstrom, are shown in Fig. 24 for T = 0, 120, 180, 240 K, from right to left. The sharp peaks near 1515 and 1530 meV are grating ghosts. Figure 24 clearly shows the shift to lower energies with increasing temperature, as well as the growth of the high energy tail as higher levels

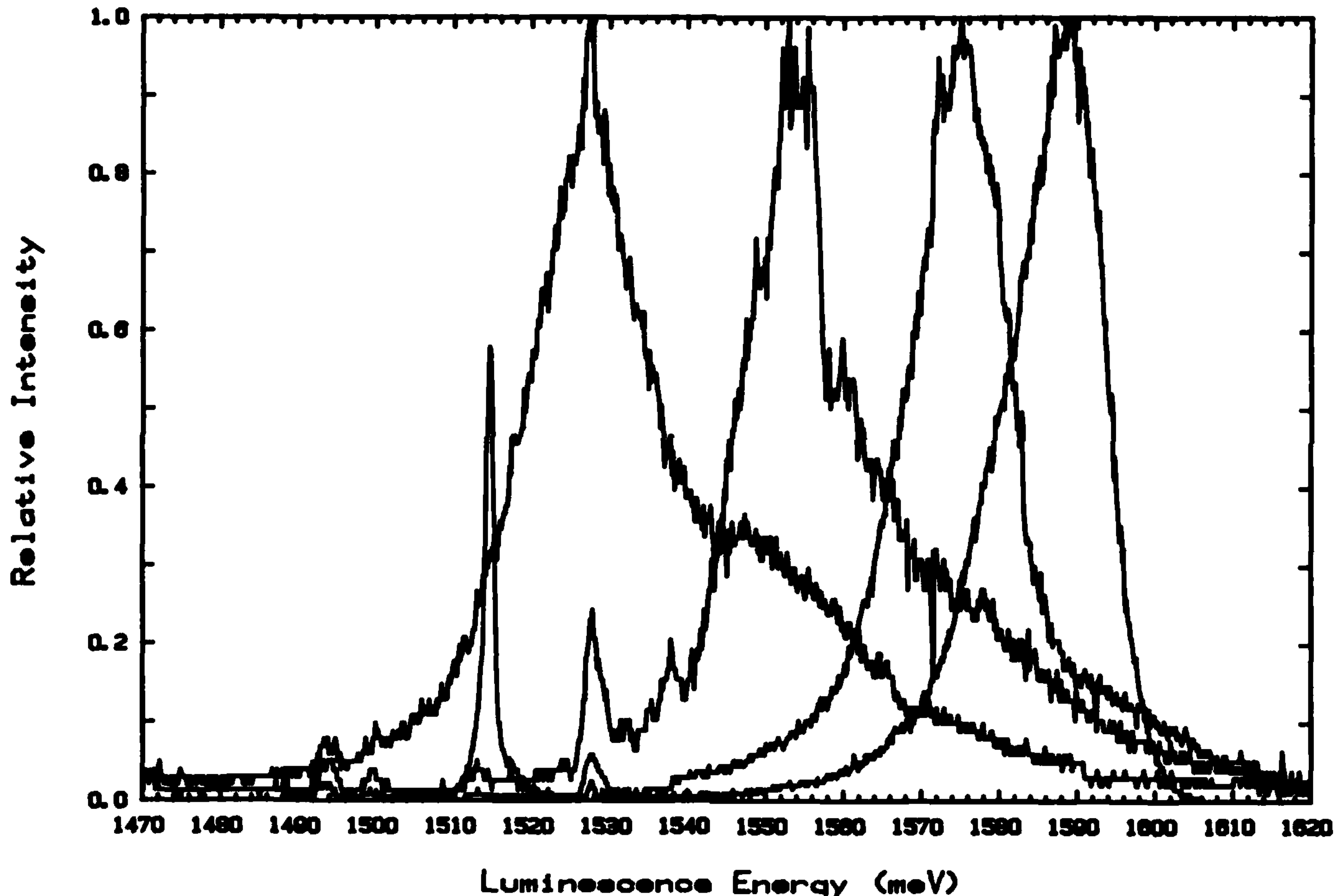

Fig. 24. Luminescence spectra, Sample T00066, as function of temperature, with T = 10 ^{0}K, 120 ^{0}K, 180 ^{0}K, 240 ^{0}K (right to left). Sharp peaks near 1515 and 1530 meV are grating ghosts.

are thermally populated.

Applying the formula for the gap energy as a function of temperature,

$$E(T) \approx E_g(0) - \alpha T^2/(T+\beta), \tag{71}$$

with the GaAs values for α and β, (α = 8.871 × 10^{-4} eV/K, β = 572 K), and estimating the value of $E_g(0)$ from Fig. 24 by extending the straight portion of the low energy slope of the right-hand curve to the x-axis intercept (~1.572 eV), we obtain, for example, for 240 K,

$$E(240) \approx 1.572 - 0.063 \approx 1.509 \text{ eV}.$$

This is the same value obtained when the low energy straight-line portion of the left-hand curve is extended to the x-axis.

VIII. CONCLUSION

The experimental investigation of different semiconductor structures, primarily strained-layer superlattices, yielded interesting results which warrant further investigation. Thus, although the measured pressure coefficients for E_g fall within the range of experimentally determined values for the appropriate Group III-V materials, we measured consistently different values for our n- and p-type samples. Since the strain in these samples has different values, the possible effect of strain on the pressure coefficient should be investigated.

A similar difference was determined to exist in the pressure coefficients for the reduced effective masses of the n- and p-type samples. Additionally, our measurements indicate significant variance of the hole-mass pressure dependence from the value based on $\mathbf{k} \cdot \mathbf{p}$ calculation for bulk material. The measured dependence is considerably higher than anticipated. A possible explanation may be pressure-induced valence band mixing in the superlattice. This aspect should be investigated theoretically and through further experiments with specifically tailored samples to determine a trend.

The developed experimental method is readily adaptable to measurements involving transmission, absorption, or excitation spectroscopy, and experiments should be conducted to investigate these topics for specific samples under the influence of pressure and/or magnetic field.

Appendix A

The Empty Lattice

The empty lattice, also known as the free electron model, considers the crystal potential to be equal to zero but maintains symmetry properties. III-V compounds, e.g. GaAs, form in the zincblende structure which consists of two interpenetrating face-centered cubic lattices.[48,6] An example of this structure is shown in Fig. A-1.[49] The First Brillouin zone of a face-centered cubic lattice consists of a truncated octahedron and is illustrated in Fig. A-2, along with the symmetry points and axes.[6] We determine the eigenvalues at the symmetry points Γ, X, L of the reduced zone for the face-centered cubic structure,

$$E_k = (\hbar^2/2m)(k + G)^2, \qquad \text{(A-1)}$$

where $G \equiv$ reciprocal lattice vector. [48,6] The primitive translation vectors joining the corner of the cube to the midpoints of the adjacent faces are

$$\tau_1 = (a/2)\,(011), \quad \tau_2 = (a/2)\,(101), \quad \tau_3 = (a/2)\,(110),$$

with $a \equiv$ lattice constant. The primitive reciprocal lattice vectors are obtained from the equations $h_i = 2\pi\,(\tau_j \times \tau_k) \,/\, (\tau_1 \cdot \tau_2 \times \tau_3)$. (A-2)

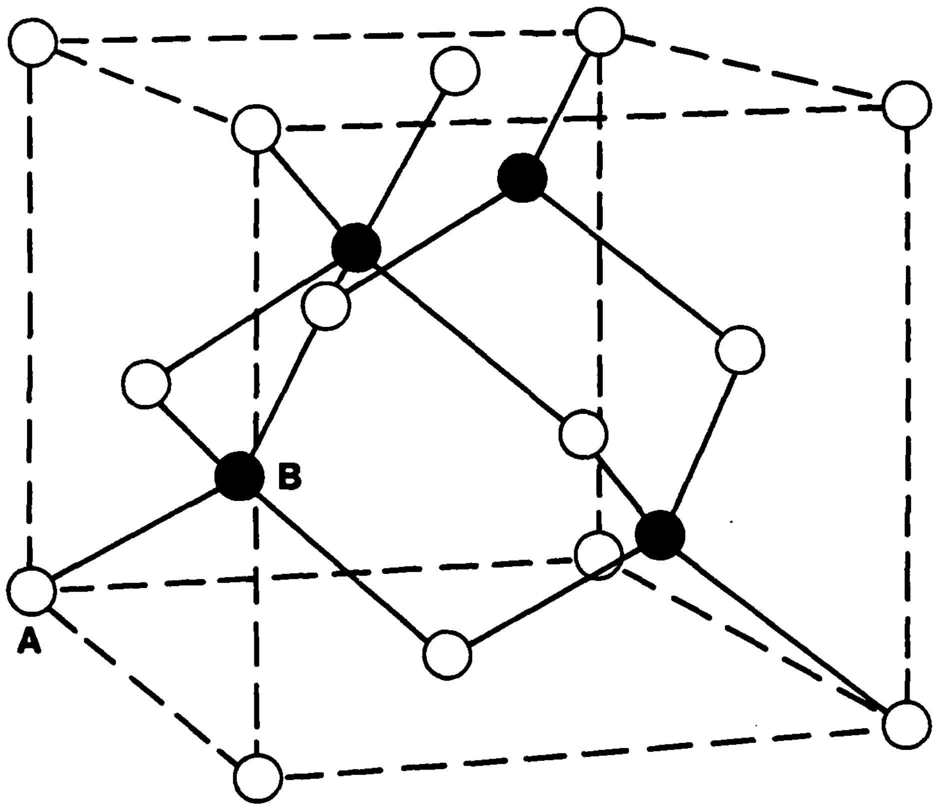

Fig. A-1. The face-centered cubic lattice.

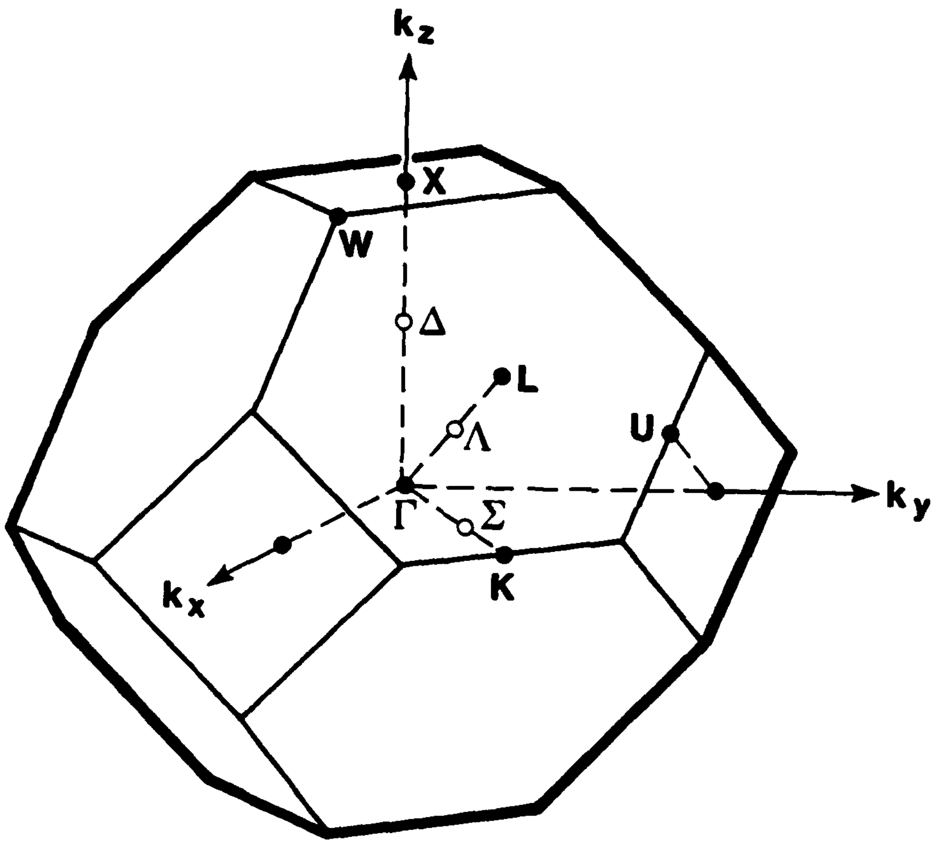

Fig. A-2. The first Brillouin zone of the face-centered cubic lattice showing selected symmetry points and axes.

where i, j, k are cyclic permutations of 1, 2, 3. We obtain

$$h_1 = (2\pi/a)(\bar{1}11),\ h_2 = (2\pi/a)(1\bar{1}1),\ h_3 = (2\pi/a)(11\bar{1}).$$

We limit ourselves to the first four reciprocal lattice vectors and their variations using h_i. We have,

$$G_0 = (2\pi/a)(000)$$

$$G_1 = (2\pi/a)(111)$$

$$G_2 = (2\pi/a)(200)$$

$$G_3 = (2\pi/a)(220).$$

The variations of G_i, i =0, 1, 2, 3, are the following:

G_0 : (000)

G_1 : (111), $(\bar{1}\bar{1}\bar{1})$, $(1\bar{1}\bar{1})$, $(\bar{1}1\bar{1})$, $(\bar{1}\bar{1}1)$, $(\bar{1}11)$, $(1\bar{1}1)$, $(11\bar{1})$

G_2 : (200), (020), (002), $(\bar{2}00)$, $(0\bar{2}0)$, $(00\bar{2})$

G_3 : (220), (202), (022), $(\bar{2}\bar{2}0)$, $(\bar{2}0\bar{2})$, $(0\bar{2}\bar{2})$, $(2\bar{2}0)$, $(\bar{2}20)$, $(\bar{2}02)$,

$(20\bar{2})$, $(02\bar{2})$, $(0\bar{2}2)$.

Using these values of G_i in Equation (A-1), we obtain, at the point Γ [k =(2π/a)(000)],

$$E_k(\Gamma) = (\hbar^2/2m)\,G_i^{\,2} = (\hbar^2/2m)(2\pi/a)^2\,(000)^2, \qquad i = 0$$

$$= (\hbar^2/2m)(2\pi/a)^2\,(111)^2, \qquad i = 1$$

$$= (\hbar^2/2m)(2\pi/a)^2\,(200)^2, \qquad i = 2$$

$$= (\hbar^2/2m)(2\pi/a)^2\,(220)^2, \qquad i = 3.$$

At the point X, where $k = (2\pi/a)(100)$,

$$E_k\,(X) = (\hbar^2/2m)\,(2\pi/a)^2[(100) + G_i)]^2.$$

Substituting for G_i,

$$E_k(X,G_0) = (\hbar^2/2m)(2\pi/a)^2(100)^2$$

$$E_k(X,G_1) = (\hbar^2/2m)(2\pi/a)^2(211)^2,\ (0\bar{1}\bar{1})^2,\ (2\bar{1}\bar{1})^2,\ (01\bar{1})^2,\ (0\bar{1}1)^2,$$

$$(011)^2,\ (2\bar{1}1)^2,\ (21\bar{1})$$

$$E_k(X,G_2) = (\hbar^2/2m)(2\pi/a)^2(300)^2,\ (120)^2,\ (102)^2,\ (\bar{1}00)^2,\ (1\bar{2}0)^2,$$

$$(10\bar{2})^2$$

$$E_k(X,G_3) = (\hbar^2/2m)(2\pi/a)^2(320)^2,\ (302)^2,\ (122)^2,\ (\bar{1}\bar{2}0)^2,\ (\bar{1}0\bar{2})^2,$$

$$(1\bar{2}\bar{2})^2,\ (3\bar{2}0)^2,\ (\bar{1}20)^2,\ (30\bar{2})^2,\ (\bar{1}02)^2,\ (12\bar{2})^2,\ (1\bar{2}2)^2.$$

At the point L, where $k_i = (2\pi/a)(\tfrac{1}{2}\,\tfrac{1}{2}\,\tfrac{1}{2})$, we have,

$E_k(L,G_0) = (\hbar^2/2m)(2\pi/a)^2\,[(\tfrac{1}{2}\tfrac{1}{2}\tfrac{1}{2}) + G_i]$, or,

$E_k(L,G_0) \sim (\tfrac{1}{2}\tfrac{1}{2}\tfrac{1}{2})^2$

$E_k(L,G_1) \sim (3/2\ 3/2\ 3/2)^2, (\bar{1}/2\ \bar{1}/2\ \bar{1}/2)^2, (3/2\ \bar{1}/2\ \bar{1}/2)^2, (\bar{1}/2\ 3/2\ \bar{1}/2)^2,$

$(\bar{1}/2\ \bar{1}/2\,3/2)^2, (\bar{1}/2\ 3/2\ 3/2)^2, (3/2\ \bar{1}/2\ \bar{1}/2)^2, (3/2\ 3/2\ 1/2)^2$

$E_k(L,G_2) \sim (5/2\ 1/2\ 1/2)^2, (1/2\ 5/2\ 1/2)^2, (1/2\ 1/2\ 5/2)^2,$

$(\bar{3}/2\ 1/2\ 1/2)^2, (1/2\ \bar{3}/2\ 1/2)^2, (1/2\ 1/2\ \bar{3}/2)^2$

$E_k(L,G_3) \sim (5/2\ 5/2\ 1/2)^2, (5/2\ 1/2\ 5/2)^2, (1/2\ 5/2\ 5/2)^2,$

$(\bar{3}/2\ \bar{3}/2\ 1/2)^2, (\bar{3}/2\ 1/2\ \bar{3}/2)^2, (1/2\ \bar{3}/2\ \bar{3}/2)^2,$

$(5/2\ \bar{3}/2\ 1/2)^2, (\bar{3}/2\ 5/2\ 1/2)^2, (5/2\ 1/2\ \bar{3}/2)^2,$

$(\bar{3}/2\ 1/2\ 5/2)^2, (1/2\ 5/2\ \bar{3}/2)^2, (1/2\ \bar{3}/2\ 5/2)^2.$

We now have the following eigenvalues with degeneracies, g, as indicated:

Γ, g	X, g	L, g
$(000)^2$, 1	$(100)^2$, 2	$(1/2\ 1/2\ 1/2)^2$, 2
$(111)^2$, 8	$(011)^2$, 4	$(3/2\ 1/2\ 1/2)^2$, 6
$(200)^2$, 6	$(120)^2$, 8	$(1/2\ 3/2\ 3/2)^2$, 6
$(220)^2$, 12	$(211)^2$, 4	$(5/2\ 1/2\ 1/2)^2$ & $(3/2\ 3/2\ 3/2)^2$, 4
	$(300)^2$ & $(122)^2$, 5	$(5/2\ 3/2\ 1/2)^2$, 6

and $(320)^2$, 4 $(5/2\ 5/2\ 1/2)^2$, 3

Using this information the empty lattice can be portrayed as shown in Fig. A-3.

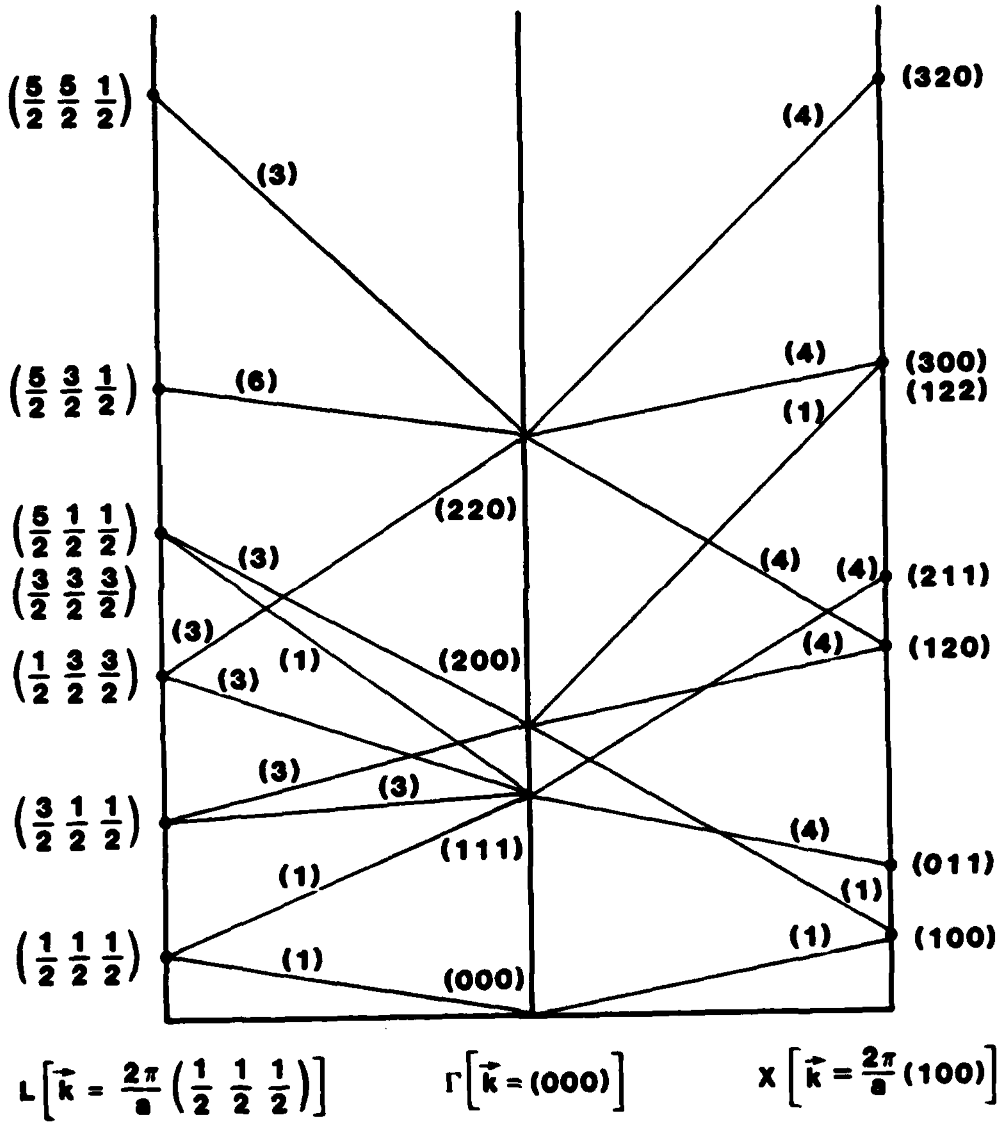

Fig. A-3. Energy diagram of the face-centered cubic "empty" lattice.

Appendix B

Fermi's Golden Rule (50-52)

We consider a system described by a Hamiltonian

$$H = H_0 + H',$$

which satisfies

$$i\hbar(d/dt)|t\rangle = H|t\rangle, \tag{B-1}$$

where H_0 is time independent, but H' may be time dependent. Then, using the interaction picture, we define

$$|t\rangle_I \equiv e^{iH_0t/\hbar}|t\rangle,$$

$$H'_I(t) \equiv e^{iH_0t/\hbar}H'(t)e^{-iH_0t/\hbar}. \tag{B-2}$$

Substituting Eqs. (B-2) into Eq. (B-1), we obtain

$$i\hbar(d/dt)|t\rangle_I = H'_I|t\rangle_I. \tag{B-3}$$

Writing

$$|t\rangle_I = |t_0\rangle_I + (i\hbar)^{-1}\int_{t_0}^{t} H'(t')|t'\rangle_I dt',$$

and substituting in the integrand for $|t'\rangle_I$, then

$$|t\rangle_I = |t_0\rangle_I + (i\hbar)^{-1}\int_{t_0}^{t} dt' H'_I(t')|t_0\rangle_I + (i\hbar)^{-2}\int_{t_0}^{t'} dt'' H'_I(t')H'(t'')|t''\rangle_I.$$

These substitutions are continued until we arrive at the expression

$$|t\rangle_I = U_I(t,t_0)|t_0\rangle_I, \tag{B-4}$$

where the following definitions hold:

$$U_I(t,t_0) \equiv \sum_n^{\infty} U_I^{(n)}(t,t_0)$$

$$U_I^{(0)}(t,t_0) \equiv 1 \tag{B-5}$$

$$U_I^{(n)}(t,t_0)=(i\hbar)^{-n}\int_{t_0}^{t}\int_{t_0}^{t'}\cdots\int_{t_0}^{t(n-1)} H'_I(t')H'_I(t'')\ldots H'_I(t^{(n)})dt'dt''\ldots dt^{(n)}.$$

$U_I(t,t_0)$, upon using Eq. (B-2), becomes

$$U_I(t,t_0)=(i\hbar)^{-n}\int_{t_0}^{t}\int_{t_0}^{t'}\cdots\int_{t_0}^{t(n-1)} e^{iH_0t'/\hbar}H'(t')e^{-iH_0(t'-t'')/\hbar}H'(t'') \times$$

$$e^{-iH_0(t''-t''')/\hbar}\ldots\exp[-i\,H_0(t^{(n-1)}-t^{(n)})]/\hbar)H'(t^{(n)})$$

$$\times \exp[-iH_0(t^{(n)})]/\hbar)dt'dt''\ldots dt^{(n)} \tag{B-6}$$

Using Eqs. (B-4) and (B-6), along with the Definitions (B-5), we can then write the transition probability for going from a stationary state $|t_0\rangle \equiv |i\rangle$ to a final state $|f\rangle$ after a time t as

$$P_{if} = |\langle f|t\rangle|^2 = |\sum_n \langle f|U_I^{(n)}(t,t_0)|i\rangle|^2 \tag{B-7}$$

Since $U_I^{(0)}(t, t_0) \equiv 1$ results in $\langle f | i \rangle = 0$ for different states, the

summation starts with n = 1, and for first order yields

$$P_{if} = |<f|U_I^{(1)}(t,t_0)|i>|^2,$$

or, $$P_{if} = |(i\hbar)^{-1}\int_{t_0}^{t} \exp[i(E_f - E_i)t'/\hbar]<f|H'(t')|i>dt'| \quad \text{(B-8)}$$

Higher order contributions to the transition probability may easily be developed. Since H' is usually considered to be a small perturbation, only the first non-vanishing term of Eq. (B-7) is kept.

If we define the operator S_I as

$$S_I \equiv \lim_{t=\infty,\ t=-\infty} U_I(t,t_0) \equiv \sum_n S_I^{(n)},$$

we can rewrite Eq. (B-7) as

$$P_{if} = |<f|S_I|i>|^2 = |\sum_n <f|S^{(n)}|i>|^2. \quad \text{(B-9)}$$

This allows us to write, for the first order contribution,

$$P_{if} = |(i\hbar)^{-1}\int_{-\infty}^{\infty}<f|H'|i>\exp[i(E_f - E_i)t/\hbar]dt|^2. \quad \text{(B-10)}$$

Now considering the Hamiltonian to be of the form

$$H' = \mathcal{H}'e^{-i\omega t} + \mathcal{H}'^{+}e^{i\omega t},$$

where $\mathcal{H}'$ and its hermitian adjoint are specified to be independent of time, the first order matrix element becomes

$$<f|S^1|i> = (i\hbar)^{-1}<f|\mathcal{H}'|i>\int_{-\infty}^{\infty}\exp[i(E_f-E_i-\hbar\omega)t/\hbar]dt$$

$$+(i\hbar)^{-1}<f|\mathcal{H}'|i>\int_{-\infty\infty\infty}\exp[i(E_f-E_i-\hbar\omega)t/\hbar]dt,$$

or, by using a definition of the δ-function,

$$<f|S^1|i> = -2\pi i\delta(E_f-E_i-\hbar\omega)<f|\mathcal{H}'|i>$$

$$-2\pi i\delta(E_f-E_i+\hbar\omega)<f|\mathcal{H}'|i>, \qquad \text{(B-11)}$$

where the first term on the right-hand side corresponds to absorption, i.e. $E_f-E_i = \hbar\omega$, and the second term to emission. Substituting the result for absorption into Eq. (B-10), we get

$$P_{if} = 4\pi^2\delta^2(E_f-E_i-\hbar\omega)\,|<f|\mathcal{H}'|i>|^2, \qquad \text{(B-12)}$$

where $\delta^2(E_f-E_i-\hbar\omega) = \delta(E_f-E_i-\hbar\omega)(2\pi\hbar)^{-1}\int_{-\infty}^{\infty}\exp[i(E_f-E_i-\hbar\omega)t/\hbar]dt$

$$=\delta(E_f-E_i-\hbar\omega)(t/2\pi\hbar)\big|_{-\infty}^{\infty}.$$

Substituting back into Eq. (B-12) and defining the transition probability per unit time as $\qquad W_{if} \equiv (P_{if}/t)\big|_{-\infty}^{\infty}$,

we arrive at a form of the "golden rule", first order,

$$W_{if} = (2\pi/\hbar)\delta(E_f - E_i - \hbar\omega)\,|\langle f|\mathcal{H}'|i\rangle|^2. \qquad \text{(B-13)}$$

In order to determine the direct absorption coefficient, we write the Hamiltonian for a charged particle in an electromagnetic field as

$$H_{total} = H_{particle} + H_{radiation} + H' \qquad \text{(B-14)}$$

where $H' = (e/2mc)(\mathbf{p}\cdot\mathbf{A} + \mathbf{A}\cdot\mathbf{p}) + (e^2/2mc^2)A^2 \approx (e/mc)(\mathbf{A}\cdot\mathbf{p})$.

The interaction Hamiltonian was simplified as shown by neglecting the squared vector potential term for first order, and using the fact that $(\mathbf{A}\cdot\mathbf{p} - \mathbf{p}\cdot\mathbf{A})$ can be shown to equal zero. Substituting into Eq. (B-13), we then have

$$W_{if} = (2\pi/\hbar)(e^2/m^2c^2)\delta(E_f - E_i - \hbar\omega)\,|\langle f|\mathbf{A}\cdot\mathbf{p}|i\rangle|^2. \qquad \text{(B-15)}$$

If the vector potential for a wave of frequency ω is written as

$$\mathbf{A}(\mathbf{r},t) = \mathbf{A}_0\boldsymbol{\varepsilon}e^{i(\mathbf{k}\cdot\mathbf{r} - \omega t)} + \text{c.c.},$$

where ε represents the polarization direction, and we recall that $H' = \mathcal{H}'e^{-i\omega t} + \mathcal{H}'^{+}e^{i\omega t}$, then we have, for the case of absorption,

$$W_{if} = (2\pi/\hbar)(eA_0/mc)^2\delta(E_f - E_i - \hbar\omega)\,|\langle f|e^{i\mathbf{k}\cdot\mathbf{r}}\boldsymbol{\varepsilon}\cdot\mathbf{p}|i\rangle|^2 \qquad \text{(B-16)}$$

Using the dipole approximation on the matrix element, i.e. expanding the exponential term and keeping only the first term of the expansion, we have

$$W_{if} \approx (2\pi/\hbar)(eA_0/mc)^2\delta(E_f-E_i-\hbar\omega)\left|\langle f|\epsilon\cdot p|i\rangle\right|^2, \qquad \text{(B-17)}$$

for vertical transitions ($k_i=k_f$).

Equation (B-17) can be used to determine the number of transitions per unit time per unit volume by summing over the possible states,

$$(d/dt)N_{if}(\omega)\approx(2\pi/\hbar)(eA_0/mc)^2$$

$$\times \sum_{V,C}\int_{BZ}dk(2/8\pi^3)\left|\langle f|\epsilon\cdot p|i\rangle\right|^2\delta(E_f-E_i-\hbar\omega), \qquad \text{(B-18)}$$

where the summation is over the valence and conduction bands, and the integral is over the Brillouin zone.

Defining the absorption coefficient, $\alpha_D(\omega)$, as the quotient of energy absorbed per unit time per unit volume and energy flux (energy density×velocity), then

$$\alpha(\omega) = [(d/dt)N_{if}(\omega)\times\hbar\omega]/U\times(c/n), \qquad \text{(B-19)}$$

where, since we are only concerned with direct absorption, the subscript D will henceforth be omitted, and the energy density of radiation, U, is given by

$$U = (n^2/2\pi c^2)\omega^2A_0^2,$$

n=(real)index of refraction. Combining Eqs. (B-18) and (B-19),

$$\alpha(\omega)\approx(4\pi^2e^2/ncm^2\omega)\sum_{V,C}\int_{BZ}dk(2/8\pi^3)|\mathcal{H}'_{V,C}|^2\delta(E_f-E_i-\hbar\omega), \tag{B-20}$$

where, for convenience, we let $\mathcal{H}'_{V,C}$ represent the matrix element $\langle f|\varepsilon\cdot p|i\rangle$.

Equation (B-20) shows that $A(\omega)$ depends on ω^{-1} and an integral. Removing the matrix element from the integral, we are left with an expression for the joint density of states for a pair of bands,

$$J_{C,V}=\int_{BZ}dk(2/8\pi^3)\delta(E_f-E_i-\hbar\omega). \tag{B-21}$$

Using Eq. (B-21) in (B-20), along with Eqs. (37), the absorption coefficient can be calculated.

REFERENCES

1. Seitz, F., Modern Theory of Solids, (McGraw-Hill, NY, 1940).
2. Shockley, W., "Energy Band Structures in Semiconductors", Phys. Rev. 78, 173(1950).
3. Kane, E. O., "Energy Band Structure in p-Type Germanium and Silicon", J. Phys. Chem. Solids, 1, 82(1956).
4. Kane, E. O., "The k.p Method", in Semiconductors and Semimetals, 1, R. K. Willardson and A. C. Beer, Eds., (Academic Press, NY, 1966).
5. Dresselhaus, G., A. F. Kip and C. Kittel, "Cyclotron Resonance of Electrons and Holes in Silicon and Germanium Crystals", Phys. Rev. 98, 368(1955).
6. Kittel, C., Quantum Theory of Solids, (John Wiley & Sons, NY, 1963).
7. Fawcett, W., "Valence Band Structure of Germanium", Proc. Phys. Soc. 85, 931(1965)
8. Tsidilkovski, I. M., Band Structure of Semiconductors, (Pergamon Press, Oxford, 1982).
9. Blakemore, J. S., "Semiconducting and other major properties of GaAs", J. Appl. Phys. 53, 10(1982)

10. Frenkel, J. "On the Transformation of Light into Heat in Solids", Phys. Rev. 37, 17(1931).

11. Wannier, G. H., "The Structure of Electronic Excitation Levels in Insulating Crystals", Phys. Rev. 52, 191(1937).

12. Elliott, R. J., "Intensity of Optical Absorption by Excitons", Phys. Rev. 108, 1384(1957).

13. Anselm, A., Introduction to Semiconductor Theory, (Mir Publ., Moscow, 1978).

14. Hodgson, J. N., Optical Absorption and Dispersion in Solids, (Chapman & Hall, Ltd., London, 1970).

15. Sell, D. D., "Resolved Free-Exciton Transitions in the Optical-Absorption Spectrum of GaAs", Phys. Rev. B6, 3750(1972).

16. Bendorius, R. and A. Shileika, "Electroreflectance Spectra of GaAs at Hydrostatic Pressure", Solid State Commun. 8, 1111(1970).

17. Paul, W., "Band Structure of Intermetallic Semiconductors from Pressure Experiments", J. Appl. Phys. Supp. 32, 2082(1961).

18. Edwards, A. L., et al., "The Effect of Pressure on Zinc Blende and Wurtzite Structures", J. Phys. Chem. Solids 11, 140(1959).

19. Feinleib, J., et al., "Effect of Pressure on the Spontaneous and Stimulated Emission from GaAs", Phys. Rev. 131, 2070(1963).

20. Welber, B., et al., "Dependence of the direct energy gap of GaAs on hydrostatic pressure", Phys. Rev. B-12, 5729(1975).

21. Abeles, F., Optical Properties of Solids (North Holland Publ. Co., Amsterdam, 1972).

22. Balkanski, M., (Ed), Handbook on Semiconductors, Vol 2 (North Holland Publ. Co., Amsterdam, 1980).

23. Varshni, Y. P., "Temperature Dependence of the Energy Gap in Semiconductors", Physica 34, 149(1967).

24. Luttinger, J. M. and W. Kohn, "Motion of Electrons and Holes in Perturbed Periodic Fields", Phys. Rev. 97, 869(1955).

25. Luttinger, J. M., "Quantum Theory of Cyclotron Resonance in Semiconductors: General Theory", Phys. Rev. 102, 1030(1956).

26. Dimmock, J. O., "Introduction to the Theory of Exciton States in Semiconductors", in Semiconductors and Semimetals, Vol. 4, (Eds) R. K. Willardson and A. C. Beer, (Academic Press, NY, 1967).

27. Shinada, M. and S. Sugano, "Interband Optical Transitions in Extremely

Anisotropic Semiconductors, I. Bound and Unbound Exciton Absorption", J. Phys. Soc. Japan 21, 1936(1966).

28. Miller, R. C., et al., "Observation of the excited level of excitons in GaAs quantum wells", Phys. Rev. B24, Nr. 2, 1134(1981).

29. Akimoto, A. and H. Hasegawa, "Interband Optical Transitions in Extremely Anisotropic Semiconductors, II. Coexistence of Excited and Landau Levels", J. Phys. Soc. Japan 22, Nr. 1, 181(1967).

30. Ackermann, H., E. D. Jones, J. E. Schirber, D. L. Overmyer, "Apparatus for Optical Studies of Materials at Hydrostatic Pressures and Low Temperatures in Magnetic Fields", Cryogenics 25, 496(1985)

31. Schirber, J. E., "The solid He pressure generation technique", Cryogenics, 1(1970).

32. Jones, E. D. and G. L. Wickstrom, "Laser Measurement Techniques - Laser Spectroscopy in Semiconductors", Proc. Southwest Conf. Optics, Albuquerque, NM, (March 1985).

33. Quillec, M., et al., "Growth Conditions and Characterization of InGaAs/GaAs Strained Layer Superlattices", J. Appl. Phys. 55(8), 2904(1984).

34. Laidig, N. D., et al., "Effects of Strain and Layer Thickness on the Growth of InxGa1-xAs/GaAs Strained Layer Superlattices", J. Vac. Sci. Techn. B(2), 181(1984).

35. Petroff, P. M., et al., "Crystal Growth Kinetics in (GaAs)n - (AlAs)m Superlattices Deposited by Molecular Beam Epitaxy", J. Crystal Growth 44, 5(1978).

36. Fleming, R. M., et al., "X-Ray Diffraction STudy of Interdiffusion and Growth in (GaAs)n(AlAs)m Multilayers", J. Appl. Phys. 51(1), 357(1979).

37. Greene, R. L. and K. K. Bajaj, "Effects of Magnetic Field on the Energy Levels of a Hydrogenic Impurity in GaAs/Ga1-xAlxAs Quantumwell Structures", Phys. Rev. B (31) Nr. 2, 913(1985).

38. Dingle, R., et al., "Quantum States of Confined Carriers in Very Thin AlxGa1-xAs/GaAs/Alx... Heterostructures", Phys. Rev. Ltrs. 33(14), 827(1974).

39. Mendez, E. E., et al., "Observation of Superlattice Effects on the Electronic Bands of Multilayer Heterostructures", Phys. Rev. Ltrs. 46 (18), 1230(1981).

40. Osbourn, G. C., "InxGa1-xAs/InyGa1-yAs Strained Layer Superlattices: A Proposal for Useful, New Electronic Materials", Phys. Rev. B (27) Nr. 8, 5126(1983).

41. Schirber, J. E., et al., "Light Hole Conduction in InGaAs/GaAs Strained Layer Superlattices", Appl. Phys. Ltrs. 46 (2), 187(1985).

42. Dingle, R., "Confined Carrier States in Ultrathin Semiconductor Heterostructures", in Advances in Solid State Physics, Vol XV, 21, (Ed) H. J. Queisser (Pergamon Press, Braunschweig, 1975).

43. Ryan, J. F., et al., "Time-Resolved Photoluminescence of Two - Dimensional Hot Carriers in GaAs/AlGaAs Heterostructures", Phys. Rev. Ltrs. 53 (19), 1841(1984).

44. Schulman, J. N. and Y.-C. Chang, "Band Mixing in Semiconductor Superlattices", Phys. Rev. B 31 (4), 2056(1985).

45. Jones, E. D., H. Ackermann, J. E. Schirber, et al., "Magneto-Optic Determination of the Light- Hole Effective Masses in InGaAs/GaAs Strained Layer Superlattices", Solid State Commun. 55 (6), 525(1985).

46. Jones, E. D., H. Ackermann, J. E. Schirber, et al., "Magneto-Optic Determinations of the Pressure-Dependence of the Band-Gap Energies

and Effective Masses in Strained Layer Superlattices", Appl. Phys. Ltrs. 47 (5), 492(1985).

47. Sakaki, H. et al., "Light Emission form Zero-Dimensional Excitons - Photoluminescence for Quantum Wells in Strong Magnetic Fields", Appl. Phys. Ltrs. 46 (1), 83(1985).

48. Bassani, F. and G Pastori-Parravicini, Electronic States and Optical Transitions in Solids, (Pergamon Press, Oxford, 1975).

49. Smith, R. A., Wave Mechanics of Crystalline Solids, (Chapman & Hall, Ltd., London, 1961).

50. Yariv, A., Quantum Electronics, (John Wiley & Sons, NY, 1975).

51. Loudon, R., The Quantum Theory of Light, (Clarendon Press, Oxford, 1978).

52. Alonso, M. and H. Valk, Quantum Mechanics: Principles and Applications, (Addison-Wesley, Reading, MA, 1973).

END
FILMED

5-86

DTIC